Report No. 163 / UILU-93-4021

The Effect of Particle Size on the Thermomechanical Fatigue of Metal Matrix Composites

by
William Walker Van Arsdell

A report of
MATERIALS ENGINEERING — MECHANICAL BEHAVIOR
College of Engineering, University of Illinois at Urbana-Champaign
August 1993

ACKNOWLEDGMENTS

This work was sponsored by Mitsubishi Motors Corporation, Kyoto, Japan. The assistance of Mr. Moriyuki Mushiake, of Mitsubishi Motors Corporation, is appreciated.

My advisor, Professor Huseyin Sehitoglu, is acknowledged for his assistance and guidance over the past two years. His efforts to maintain lines of communication during his appointment at the National Science Foundation in Washington, D.C., have been greatly appreciated.

The contributions of my colleagues at the University of Illinois have been invaluable. Without such diversions this work would have been completed long ago.

I am very grateful for the encouragement and support which my family has provided throughout my education. Despite any false impressions which I may have left as an adolescent, I have always shared their respect for education.

TABLE OF CONTENTS

LIST OF TABLES

LIST OF FIGURES

NOMENCLATURE

d = particle diameter

V_f = particle volume fraction

λ^G = geometric slip distance

D = grain size

σ_y = composite yield strength

$\sigma_{y,m}$ = matrix yield strength

σ_u = composite ultimate strength

σ = strengthening due to particle induced grain refinement

σ_q = strengthening due to dislocations generated upon quenching

G = shear modulus of the matrix

γ = shear strain

b = Burger's vector for the matrix

$\Delta\alpha$ = difference in coefficient of thermal expansion between matrix and reinforcement

ΔT = temperature over which composite is quenched

ρ^t = thermally induced dislocation density

ρG = geometrically necessary dislocation density

Ky = slope of Hall - Petch model

$\Delta\varepsilon_{mech}$ = mechanical strain range

1. INTRODUCTION

Metal matrix composites (MMCs) with discontinuous reinforcement have received a great deal of attention from researchers because of their high specific strength, high specific modulus, lower coefficient of thermal expansion, near isotropic properties, and reasonable cost (1-2). Particulate reinforced MMCs are attractive candidates for replacing metals in many high temperature applications, and it has been predicted that the commercial use of these materials will increase dramatically over the next decade (2). Despite the need to understand the high temperature isothermal fatigue (IF) and thermomechanical fatigue (TMF) behavior of particulate reinforced MMCs, most research to date has been limited to monotonic deformation studies. And although particle size has been shown to have a significant effect on the monotonic (3-6) and room temperature IF (7) behavior of particulate reinforced composites, the author is unaware of any research on the particulate size effect on the high temperature IF or TMF behavior of MMCs. The objective of this research was to investigate the particle size effect on the monotonic tension, high temperature IF and TMF behavior of a 2024 aluminum alloy reinforced with 0%, 10% and 30% by volume of 2μm and 30μm silicon carbide particles (SiC_p).

2. BACKGROUND

The ability to tailor MMCs to meet particular engineering requirements by adjusting variables such as volume fraction, particulate size and particulate shape has drawn much attention from engineers and researchers in the past decade. However, before engineers can optimize their use of MMCs, we must understand the relationship between these parameters and the thermomechanical behavior of the composite.

Much is known about the monotonic tensile behavior of discontinuously reinforced MMCs, however, very little effort has been devoted to understanding the cyclic and high temperature behavior of this very important class of materials. It has been recognized that the monotonic behavior of particulate reinforced MMCs is dependent on reinforcement volume fraction, size, and shape as well as matrix microstructure, the character of the matrix/reinforcement interface, and the level of reinforcement clustering (4, 8-10). Likewise, the limited research conducted suggests that the cyclic and high temperature behavior of discontinuously reinforced MMCs is determined by these same variables. However, little detailed work has been conducted to identify the quantitative nature of those relationships.

In the following section, the effect of particle size on the monotonic tensile behavior of discontinuously reinforced MMCs will be discussed in detail. In subsequent sections, the current level of understanding of the effect of particle size on fatigue crack initiation, fatigue crack growth, and the high temperature behavior of discontinuously reinforced MMCs will be presented.

2.1 The Particle Size Effect on Monotonic Behavior

Many researchers have observed that particulate reinforced MMCs exhibit higher flow strength and ultimate strength than their monolithic counterparts. This observed increase in ultimate strength has been explained by Ashby (11) in terms of geometrically necessary dislocations. Humphreys and Miller (5, 12) have rationalized the observed increase in flow stress in terms of particle induced grain refinement, and geometrically necessary dislocations generated during thermal processing. Since Ashby's work laid the foundations for the work of Humphreys and Miller, it will be helpful to begin by discussing Ashby's concept of geometrically necessary dislocations.

Ashby proposed that in a plastically non-homogeneous material, strain gradients are imposed on the material by the variations in elastic modulus between different microstructural constituents. Geometrically necessary dislocations are then generated by gradients in plastic strain between these microstructural constituents. In contrast, statistically stored dislocations are defined as those which result from chance encounters between dislocations which prevent their further movement.

When a hard second phase, such as SiC particles, is dispersed in a soft matrix, gradients in deformation will be produced upon loading (either thermal or mechanical). The hard SiC particles will not deform as much as the matrix away from the particle. In order to maintain compatibility, the matrix adjacent to the particles must be constrained by the particle. Hence, deformation gradients within the matrix result from the introduction of a rigid second phase. Such gradients of deformation result in the production of the so called geometrically

necessary dislocations. The macroscopic ramifications of such behavior is a significantly increased rate of work hardening.

It can be shown that the constraint offered by this rigid second phase is related to it's size and distribution. For a given volume fraction of reinforcement, smaller, more closely spaced particles result in a higher level of constraint. In other words, decreasing particle size would be expected to increase the rate of work hardening. This trend has been observed experimentally by several investigators (3-5).

Three broad categories of theories which attempt to model second phase effects have evolved: a) continuum plasticity based theories, b) dislocation mechanics based theories, and c) more general theories which combine concepts from both continuum and dislocation mechanics. Both continuum and dislocation mechanics based theories argue that only volume fraction is important, while the general theories comprehend the effects of both volume fraction and particle size.

Continuum plasticity models, such as the shear lag and Eshelby type models (6), are based on the assumption that a volume of material, no matter how small, will deform by crystallographic slip if a high enough stress is applied. Therefore, matrix flow will occur around a particle as long as the applied stress exceeds the flow stress. Essentially, what is assumed is that plastic flow is limited to the fraction of the material occupied by the relatively soft matrix. The weakness of continuum based theory is twofold (11): a) on a microscale the material is not a continuum, and b) the work hardening of the two phase materials depends not only on the applied strain, but on local strain gradients.

Dislocation mechanics based theories, such as those proposed by Orowan (13), Fisher, Hart and Pry (14) and Tanaka and Mori (15) explain particulate strengthening by assuming that no matrix flow can occur around the particles. Particles are modeled as impenetrable barriers to dislocation movements. In essence, what is assumed is that all slip occurs on the primary slip system, with no secondary slip taking place. The primary weakness of this theory results from the fact that secondary slip will occur provided stresses reach a critical value.

The more general models try to include the strengths of both the continuum and dislocation approaches. These combined models predict that up to a certain stress level, no matrix flow will occur around the particles, yet at some critical stress, secondary slip systems will be activated and the matrix will flow around the particles. It is the ability to comprehend this transition from dislocation mechanics based behavior to continuum mechanics based behavior that has made this general approach a success.

Two major tasks are involved in modeling the rate of work hardening of a particulate strengthened material using the combined model (11): a) the dislocation structure must be related to the applied strain, then b) the contribution of this dislocation structure to the rate of work hardening must be determined.

Ashby has shown that the dislocation density (number of loops per unit volume) is given by (11):

$$\rho^{G} = 4\gamma/b\lambda^{G}$$

Where the geometric slip distance, λ^G, can be related to volume fraction and particle size by,

$$\lambda^G = d/2V_f$$

Therefore, the geometrically necessary dislocation density can be expressed as,

$$\rho^G = 8\gamma V_f/bd \qquad (2.1)$$

It follows that as particle size decreases the number of geometrically necessary dislocations, and the resulting particulate strengthening, will increase.

This particle size effect is explained via the ease with which dislocations are generated at the matrix/reinforcement interface. Orowan dislocation loops are those loops formed when a dislocation on the primary slip system is trapped by the particle (13). In the combined model, geometrically necessary dislocations are created when the Orowan dislocation loops become unstable. In other words, when the stress required to generate a new dislocation is lower than the stress needed to restrain the Orowan loop (11). Since the highest stress tends to occur at the matrix/reinforcement interface, dislocations are generated at this point. Smaller particles require greater stress to generate new dislocations at the interface, thus, increasing the rate of work hardening.

Ashby (11) has shown that the number of geometrically necessary dislocations outweighs the number of statistically necessary dislocations when $\lambda^G \leq 50$ μm and $\gamma < 20\%$. Since $\lambda^G_{max} = [30\ \mu m/2(0.30)] = 50\ \mu m$ in this research, it follows

that the effects of geometrically necessary dislocations should dominate the work hardening behavior of our materials. Ashby has suggested that the flow stress for a particulate strengthened material should be given by (11):

$$\sigma = \sigma_{y,m} + C_1 G(V_f b\gamma/d)^{1/2} \tag{2.2}$$

It should also be noted that thermal cycling can introduce a significant amount of plastic deformation in the matrix surrounding the reinforcement (16). As a result of the large difference in the thermal coefficient of expansion for the two constituents, geometrically necessary dislocation are generated during simple heating or cooling. Humphreys and Miller (5) have suggested that during thermal processing, such as quenching, a significant number of geometrically necessary dislocations are generated in MMCs reinforced with ceramic particles. Miller and Humphreys have proposed a relationship for the increase in flow stress which results from these thermally induced dislocations (5):

$$\sigma_q = Gb(\rho^t)^{1/2} \tag{2.3}$$

where the thermally induced dislocation density, ρ^t, is given by (5):

$$\rho^t = 12\Delta T\Delta\alpha V_f/bd \tag{2.4}$$

This hypothesis was supported by the experimental results presented in (5).

Another possible mechanism by which the particle size affects the flow stress of particulate reinforced MMCs is through grain refinement (5, 12). During

processing or application, recrystallization may take place if the composite is held at the recrystallization temperature for a sufficient time. It has been hypothesized that during recrystallization a new grain will nucleate at each particle. Thus, particle size and grain size should be directly related by the following relationship (5):

$$D = d[(1-V_f)/V_f]^{1/3} \tag{2.5}$$

The Hall-Petch relation can then be used to predict the increase in flow stress due to grain refinement:

$$\sigma_g = KyD^{-1/2} = Ky\ \{[(1-V_f)/V_f]^{1/3}\}^{-1/2}\ d^{-1/2} \tag{2.6}$$

Miller and Humphreys (5) observed that large particles tended to nucleate more then one grain, and small particles sometimes failed to act as seeds for nucleation. That is, composites with large microstructures (40 μm) had a finer grain structure than predicted, and the smaller particles (7 μm) tended to have courser grain structures then predicted. Non the less, there was a definite relation between particle size and grain size.

Damage Mechanisms

It has been shown that high tensile stresses can be developed across the matrix/reinforcement interface, and that high triaxial stress states exist in the matrix near the particles (14, 17). It follows that particle fracture or interfacial failure may result from the high tensile stresses developed across the interface, or matrix void formation may result from the triaxial stress state present near the

reinforcement. Just such mechanisms were observed by Hunt, Brockenbrough, and Magnusen (18) by looking at sections of a tensile specimen which had undergone various degrees of deformation. This damage process has been observed to initiate in clustered regions where constraint is highest (7, 19).

Further evidence of the importance of the triaxial stress state on crack initiation under uniaxial loading has been provided by Lewandowski, Liu and Liu (20) who observed an increase in the rate of work hardening when specimens were tested in compression or under hydrostatic pressure. The increased ductility and rate of work hardening were attributed to the suppression of matrix void formation and particle cracking.

Lloyd (21) investigated the evolution of damage in particulate reinforced MMCs by testing specimens which had been prestrained and resolutionized. It was observed that for pre-strains of up to 5.5%, the composite ductility could be entirely regained by resolutionizing the specimens. From this work, Lloyd concluded that damage mechanisms for strains of up to 5.5% were related to dislocation generation, movement and storage. Beyond 5.5% prestrain, ductility could not be entirely regained by resolutionizing, thus, it was concluded that at these strain levels non recoverable damage mechanisms such as void formation, debonding and particle cracking become important.

A particle size effect on particle fracture and void formation has been observed by several investigators. The propensity for particle fracture increases as the mean particle diameter increases (3, 8, 9, 19, 21), and voids form preferentially at larger particles (3). Therefore, in cases where the failure mechanism involves

some degree of particle cracking or void formation, particle size would be expected to be an important factor.

2.2 The Particle Size Effect on Fatigue Crack Initiation

Many researchers have noted that the fatigue performance of discontinuously reinforced composites is superior to that of their monolithic counterparts when compared on the basis of applied stress (7, 22-3). It is further noted that this improvement in fatigue performance is most pronounced at low and intermediate stress levels (i.e. long life fatigue). The classic argument for this phenomena centers around the lower strains, and more importantly the lower plastic strains, required to develop a given stress in the composite material.

Conversely, when the fatigue performance is compared on the basis of total strain range, the discontinuously reinforced MMC's consistently exhibit inferior fatigue performances compared to their unreinforced counterparts (7, 22-3). Such differences are most apparent in the high strain, short life regime. This is attributed to the composites higher elastic modulus which results in a larger portion of the total strain being plastic in nature. In addition, due to the strain localization near particles, the local damage is often much higher in the composite than in the unreinforced material for a given plastic strain range.

There is one important exception to the above generalization regarding the relative strain-life performance of MMCs. In the out-of-phase TMF data presented by Karayaka and Sehitoglu (1), the composites exhibited superior behavior to that of the unreinforced material even when compared on the basis of strain.

Several investigators have observed that the fatigue life of a composite, under stress controlled conditions, increases as the volume fraction is increased. This is attributed to the decrease in strain which results from the higher modulus of elasticity and rate of work hardening.

Another variable which can be adjusted in the aim of obtaining desirable fatigue properties is the size of the reinforcement. Continuum theory suggests that only volume fraction is important, and that the size and shape of the discontinuous reinforcement is irrelevant. Dislocation based theories dispute this, and suggest that both size and shape have an important relationship to strength. The relationship between monotonic tensile properties and particle size has been well established through experimental investigation, however, the relationship between particle size and cyclic behavior is not well understood. Several studies have addressed the effect of particle size on the room temperature fatigue performance of SiCp reinforced composites. Holcolm (7) showed that the fatigue behavior of a 2124-T6 aluminum reinforced with SiC particles was improved by reducing the mean particulate diameter from 35 μm to 3 μm. Similar observations were made by Hall, Jones and Sachdev (24) in their study of a 6061-T6 aluminum reinforced with SiC particles with mean diameters ranging from 5 μm to 19 μm. The author is aware of no work done on the particle size effect on the high temperature isothermal fatigue or thermomechanical fatigue behavior of Al/SiCp MMCs.

The above size effect is attributed to several factors (2):

a) decreasing the particle size acts to increase resistance to slip

b) large particles have been found to crack more easily than small particles

c) voids have been found to form preferentially at larger particles

d) smaller particles may refine the grain structure

Crack initiation has been found to occur within the composite at fractured particles, the particle/matrix interface, or in the matrix near clustered regions (25). These observations can be explained using the arguments presented in the previous section.

It should be noted that while the elastic portion of the stress fields generated by geometrically necessary dislocations do not affect monotonic strength, they may play an important role in fatigue (5).

2.3 The Particle Size Effect on Fatigue Crack Growth

The particle size effect on crack growth can be explained by considering three phenomena: crack closure, crack tip trapping, and particle fracture (26). Crack closure phenomena are only important at low load ratios where crack closure is significant. At low load ratios, the rougher the fracture surface, the more crack closure will occur. Of course, as crack closure increases, the growth rate decreases, since the effective stress intensity range, ΔK_{eff}, decreases. Since crack propagation tends to be restricted to the matrix or along interfacial regions, larger particles result in a rougher crack profile and increased crack closure.

Crack tip trapping occurs at low ΔK when the crack tip reaches a particle and can not advance beyond the particle matrix interface region. Shang and Ritchie (26) have predicted that larger particles should be more effective at trapping cracks.

Particle fracture would be expected to reduce propagation life by providing a more direct propagation path. Larger particles have been shown to be more likely to crack than smaller particles, hence, a particle size effect can be envisioned here as well.

At low load ratios crack closure effects dominate, and experimental results suggest that the near threshold behavior for low load ratio conditions is improved by using larger particles. At high load ratios, particle fracture considerations dominate, and smaller particles improve near threshold behavior.

2.4 The Particle Size Effect at High Temperatures

In theory, particle strengthening is drastically reduced at high temperatures due to diffusive reactions which mobilize dislocations (11). Observations have indicated that geometrically necessary dislocations are much more easily mobilized by diffusion than statistically stored dislocations. Indeed, the conditions for diffusion of these geometrically necessary dislocations are favorable in the sense that a) the high stresses at the interface provide a large driving force, b) the diffusion paths are short, and c) the matrix/reinforcement interface provides a high diffusivity path. It is interesting to note that smaller particles provide smaller diffusion paths and higher local stresses. Therefore, particulate strengthening at high temperatures may diminish faster for materials reinforced with smaller particles.

3. MATERIAL AND EXPERIMENTAL PROCEDURE

3.1 Material

The material being studied is a 2024 aluminum alloy reinforced with 0%, 10% and 30% SiC_p. Two different particle diameters were examined, d = 2 μm and d= 30 μm. The material was supplied by Kobe Steel of Japan and was produced using powder metallurgy techniques. The 15 mm diameter bar stock provided by Kobe Steel was produced by extruding powder metallurgy ingots at 400 °C and an extrusion ratio of 17:1. The test specimens were circular in cross section with a diameter of 7.62 mm (0.300 in), and a gage length of 25.4 mm (1 in).

The chemical composition of the alloy studied was: 4.35 % Cu, 1.54 % Mg, 0.59 % Mn, 0.19 % Fe, 0.13 % Si, 0.032 % Zr, , and 0.030 % Cr. This material is different than the MMC studied by Karayaka and Sehitoglu (1). The particle distribution within the two composite materials reinforced with 30% SiCp is shown in figures 3.1 and 3.2. The relatively homogeneous distribution of reinforcement illustrated by figures 3.1 and 3.2 is indicative of all portions of the microstructure observed in this study. That is, no significant clustering was observed in any of the 10% or 30% reinforced composites.

3.2 Experimental Equipment

Testing was conducted using a 100 kN Instron servo-hydraulic test machine. Specimens were heated using a Lepel induction heater. Early tests were conducted using a 2.5 kW heater, while more recent tests were performed with a 15 kW heater. The isothermal fatigue and thermomechanical fatigue tests were

conducted using a computer based control package developed by Instron Corporation.

Data was collected and stored using the IBM PS/2 computer on a logarithmic basis. That is, multiples of 10^n cycles were collected (e.g. 1, 2, 3, ..., 9, 10, 20, 30, ..., 90, 100, 200, 300, ..., 1000,...,10000,...). At least 200 data points were collected per cycle. Data was manipulated and plotted after transferring data files to a Macintosh computer.

Strain was measured using an MTS high temperature extensometer with a 25.4 mm gage length and a strain range of ± 15%. The extensometer used quartz rods which were grinded to a point and held in contact with the specimen using a spring loaded mounting bracket. This type of extensometer proved effective for all in-phase TMF and IF experiments, however, an alternative technique was required for out-of-phase TMF tests. When out-of-phase TMF experiments were performed using quartz rods with pointed ends, crack initiation occurred at the point where the rod contacted the specimen. To eliminate this problem, extensometer rods with a knife edge were used for all out-of-phase TMF experiments. While conducting monotonic tensile tests, diametral strain was recorded using a high temperature MTS extensometer with quartz rods.

Temperature was remotely measured using a Raytek non-contact infrared pyrometer. In order to use the infrared pyrometer, the shoulder of the specimens had to be painted black to obtain an acceptably high emissivity. The temperature distribution within the gage length, and the relationship between gage length

temperature and shoulder temperature was determined using thermocouples. The temperature distribution within the gage length was uniform to within 5 °C.

3.3 Experimental Procedure

In thermomechanical fatigue testing, both total strain and temperature are varied simultaneously. Therefore, the total strain has both thermal and mechanical components. In order to control the mechanical strain, the relationship between temperature, total strain and mechanical strain must be identified. This was done by: a) cycling the temperature at zero load and recording the thermal strain as a function of temperature, and b) adding thermal strain to the desired mechanical strain to obtain the required total strain control signal. In addition, a post-processor in the TMF software subtracts the thermal strain from the feedback signal to provide a record of mechanical strain.

Two types of TMF tests were performed, in-phase TMF (TMF IP) and out-of-phase TMF (TMF OP). TMF IP tests are defined as strain controlled tests in which the maximum strain (tensile) coincides with the maximum temperature. Conversely, TMF OP tests are defined as strain controlled tests in which the maximum strain (tensile) coincides with the minimum temperature. Figure 3.3 illustrates the thermo-mechanical phase relations for TMF IP, TMF OP and IF experiments. By looking at TMF IP and TMF OP results, insight can be gained into a wide variety of complex thermomechanical loading histories.

Monotonic tensile experiments were performed at room temperature, 200 °C and 300 °C, and at a strain rate of 10^{-4} 1/sec. The IF and TMF experiments were conducted under fully reversed strain control conditions, at various strain

amplitudes, and at a strain rate on the order of 10^{-4} 1/sec. IF lives were established at 300 °C, while TMF IP and TMF OP experiments were performed with a minimum temperature of 100 °C and a maximum temperature of 300 °C.

The low frequency of the tests performed was the result of the limits imposed by the heating and cooling rates of the material tested. The relatively poor magnetic coupling and low convective cooling rate of the composite tested limited the period of the thermal cycle to no less than 100 seconds.

4. EXPERIMENTAL RESULTS

4.1 Monotonic Tensile Experiments

Monotonic tensile experiments were performed at 20 °C, 200 °C, and 300°C on all MMCs (Vf = 10% and 30%, and d = 2 μm and 30 μm) and the unreinforced matrix material. Figures 4.1 - 4.3 illustrate the monotonic tensile behavior of all materials at 20 °C, 200 °C, and 300 °C, respectively. Figures 4.4 - 4.8 illustrate the effect of temperature changes on the monotonic tensile behavior of each material. Elastic modulus, yield strength, ultimate strength, and true fracture strain are reported in Table 4.1.

The modulus of elasticity and ductility showed little dependence on the particulate size. For the MMCs reinforced with 30% SiCp, the ultimate and yield strengths were significantly higher when reinforced with the smaller (2 μm) particles (figure 4.9). Interestingly, for the MMCs reinforced with 10% SiCp, the ultimate and yield strengths were either: a) unaffected by particle size, or b) slightly higher when reinforced with the larger (30 μm) particles. All materials showed dramatic reductions in strength at 300 °C as compared to 20 °C and 200°C values.

4.2 Isothermal Fatigue Experiments

IF experiments were conducted on two MMCs (Vf = 30% with d = 2 μm and 30μm) at 300 °C, under fully reversed (R = -1) strain control conditions, and at a strain rate of approximately 10^{-4} 1/sec. The cyclic stress-strain response of the unreinforced material was measured, however, no life data was obtained. Figure 4.10 is a strain-life curve for the IF tests which shows the fatigue life, in cycles, as

a function of the applied strain. Figure 4.11 is a stress-life curve for the IF tests which shows the fatigue life, in cycles, as a function of the stress range observed during the first cycle of each strain controlled test.

Based on both applied strain and first cycle stress, fatigue lives obtained for the MMC reinforced with 2 μm particles were greater than those observed for the MMC reinforced with 30 μm particles. The IF cyclic stress-strain response of the two MMCs reinforced with 30% SiCp and the unreinforced material is illustrated in figure 4.12. All three materials cyclically softened, however, the level of softening was much higher for the unreinforced material than for the composite materials.

4.3 Thermomechanical Fatigue Experiments

As discussed in the previous chapter, TMF experiments were conducted by cycling both temperature and mechanical strain at the same time. The thermal expansion properties of the materials under study are therefore of great importance. Figure 4.13 illustrates the thermal strains induced in the two 30% volume fraction MMCs and the unreinforced material when subjected to zero load, thermal cycling between 100 °C and 300 °C. As expected, the coefficient of thermal expansion for the composite material is significantly lower than that of the monolithic aluminum specimen. It is also clear that particle size has very little influence on the composites coefficient of thermal expansion.

In-Phase Thermomechanical Fatigue

TMF IP experiments were conducted on two MMCs (Vf = 30% with d = 2 μm and 30 μm) between 100 °C and 300 °C, under fully reversed (R = -1) strain

control conditions, and at a strain rate of approximately 10^{-4} 1/sec. The cyclic stress-strain response of the unreinforced material under TMF IP loading was measured, however, no life data was obtained. Figure 4.14 is a strain-life curve for the TMF IP tests which shows the life, in cycles, as a function of mechanical strain. Figure 4.15 is a stress-life curve for the TMF IP tests which shows the life, in cycles, as a function of the stress range observed during the first cycle of each strain controlled test.

Based on both mechanical strain and first cycle stress, fatigue lives obtained for the MMC reinforced with 2 μm particles were greater than those observed for the MMC reinforced with 30 μm particles. The TMF IP cyclic stress-strain response of the two MMCs reinforced with 30% SiCp and the unreinforced material is illustrated in figure 4.16. All three materials cyclically softened, however, the level of softening was higher for the unreinforced material than for the two composite materials. Note the significant particle size effect on the hysteresis loops of figure 4.16. In addition, it is interesting to note that for the same mechanical strain range, the TMF IP lives were lower than the IF lives.

Out-of-Phase Thermomechanical Fatigue

TMF OP experiments were conducted on two MMCs (Vf = 30% with d = 2 μm and 30 μm) and the unreinforced material between 100 °C and 300 °C, under fully reversed (R = -1) strain control conditions, and at a strain rate of approximately 10^{-4} 1/sec. Figure 4.17 is a strain-life curve for the TMF OP tests which shows the life, in cycles, as a function of mechanical strain. Figure 4.18 is a stress-life curve for the TMF OP tests which shows the life, in cycles, as a

function of the stress range observed during the first cycle of each strain controlled test.

Based on mechanical strain, for $\Delta\varepsilon_{mech} < 0.6\%$, lives obtained for the MMC reinforced with 2 μm particles were greater than those observed for the MMC reinforced with 30 μm particles. While for $\Delta\varepsilon_{mech} > 0.6\%$, the lives obtained for the MMC reinforced with 30 μm particles were greater than those observed for the MMC reinforced with 2 μm particles. Based on first cycle stress, lives obtained for the MMC reinforced with 2 μm particles were always greater than those observed for the MMC reinforced with 30 μm particles. The composite behavior was inferior to that of the unreinforced material based on mechanical strain, but superior when based on first cycle stress range.

The TMF OP cyclic stress-strain response of the two MMCs reinforced with 30% SiCp and the unreinforced material is illustrated in figure 4.19. All three materials cyclically softened. Note the significant particle size effect on the hysteresis loops of figure 4.19. In addition, it is interesting to note that for the same mechanical strain range, the TMF OP lives were lower than the IF lives.

Figure 4.20 is a comparison of the TMF IP and TMF OP behavior of the two MMCs studied. It can be seen that, with the exception of low life tests run on the 2 μm MMC, for the same first cycle stress and particle size, TMF OP loading results in a longer life than the TMF IP loading. For the 2 μm MMC, high stress (low life) TMF IP loading results in a longer life than the TMF OP loading .

4.4 Metallographic Examination

The fatigued specimens were longitudinally sectioned in such a way as to allow for observation of the crack path. The specimen was then polished using a diamond paste, etched with dilute Keller's reagent, and viewed using a scanning electron microscope. Great care had to be exercised in order to avoid overetching or underetching.

Figures 4.21 and 4.22 illustrate the crack path within a specimen reinforced with 30% of 2 μm SiCp. Figures 4.23 and 4.24 illustrate the crack path within a specimen reinforced with 30% of 30 μm SiCp. All crack growth appears to have been confined to the matrix. No sign of particle cracking or preferential crack propagation along the matrix/particle interface was identified. The observed crack growth in the matrix regions is consistent with the findings reported in an earlier study on MMCs (1).

4.5 Discussion

As discussed in section 2.1, Miller and Humphreys (5) have proposed that the increase in flow strength in particulate reinforced MMCs is the result of particle induced grain refinement and geometrically necessary dislocations generated during material processing. Particles are assumed to act as nuclei for grain formation during recrystallization. Therefore, for a given volume fraction, smaller particles result in a finer grain structure. The Hall-Petch relationship can be used to relate the strengthening due to grain refinement to particle diameter (equation 2.6). In addition, it is argued that geometrically necessary dislocations generated during thermal processing further increase the yield strength of the composite. These thermally induced dislocations result from the constraint

offered by the low thermal expansion coefficient SiC particles. Ashby's (11) ideas regarding geometrically necessary dislocations can be used to relate this additional increase in flow strength to particle size (equation 2.6).

Equations 2.3 and 2.6 suggest that if these hypothesis are correct, than the increase in flow strength of the composite as compared to its monolithic counterpart should be dependent on $d^{-1/2}$. Figure 4.25 shows the relationship between $(\sigma_y - \sigma_{y,m})$ and $d^{-1/2}$ for the materials studied in this research and in references 4-6. The relatively linear relationship exhibited by each individual set of data presented in figure 4.25 supports the hypothesis of grain refinement and thermally induced dislocation strengthening in particulate reinforced MMCs.

Ashby argued that the rate of work hardening of a plastically non-homogeneous material should be governed by the generation of geometrically necessary dislocations (11). As discussed in section 2.1, geometrically necessary dislocations are generated in a plastically non-homogeneous material when it is subjected to a stress sufficient to activate secondary slip systems. Dislocations which have been immobilized by rigid SiC particles are than free to move around the particles via these secondary slip systems. The work hardening associated with the generation of geometrically necessary dislocations has been shown to be proportional to $(V_f/d)^{-1/2}$. Figure 4.26 shows the relationship between $(\sigma_u - \sigma_y)$ and $(V_f/d)^{-1/2}$ for the materials studied in this research project and in references 3-5. The relatively linear relationship exhibited by each individual set of data presented in figure 4.26 supports the hypothesis that geometrically necessary dislocations are responsible for the increase in work hardening in particulate reinforced MMCs.

Among the most interesting observations of this study is the strong effect of particulate size on the cyclic stress-strain response of MMCs (figures 4.16 and 4.19). At first it may be surprising that the IF stress-strain response (figure 4.12) does not exhibit the same particle size dependence as the TMF IP and TMF OP stress-strain behavior. However, this lack of particle size dependence is consistent with the high temperature behavior of the TMF and monotonic experiments. Close examination of figures 4.16 and 4.19 will reveal that at 300°C, the behavior of all three materials is very similar. To illustrate this point, the IF, TMF IP and TMF OP stress-strain behavior of the MMC reinforced with 30% of the 2 μm particles is shown in figure 4.27. In addition, examination of figures 4.25 and 4.26 indicates that at 300 °C, very little increase in either flow stress or work hardening is realized by the addition of particles.

All materials were observed to cyclically soften during IF, TMF IP and TMF OP experiments. Figure 4.28 (a) illustrates the cyclic softening trend for the MMC reinforced with 2 μm particles. Figure 4.28 (b) illustrates the cyclic softening behavior of the MMC reinforced with 30 μm particles. Softening is more pronounced for the MMC reinforced with 30 μm particles than for the MMC reinforced with 2 μm particles. In addition, the TMF IP and TMF OP tests exhibited more softening than the IF experiments. As illustrated in figure 4.28, the stress range for TMF OP loading was consistently higher than the stress range for TMF IP loading.

Also of significant importance is the observation that MMCs reinforced with small particles consistently have IF, TMF IP and TMF OP behavior which is superior to that of MMCs reinforced with larger particles (figures 4.11, 4.15, 4.18).

These results are consistent with the room temperature IF results presented by (7, 24).

The observed confinement of the crack path to the matrix material is consistent with the findings of Lewandowski , Liu and Hunt (8) who reported that weak matrices, such as those which would be expected at high temperatures, promote matrix damage mechanisms rather than particle cracking. Karayaka and Sehitoglu also observed crack propagation in the matrix (1).

5. CONCLUSIONS

1. The 2024 aluminum reinforced with 2 μm particles had superior mechanical properties than the MMC reinforced with 30 μm particles.

2. A significant particle size effect was observed on TMF stress-strain response.

3. For the same mechanical strain range, the TMF IP and TMF OP lives (T_{min} = 100 °C, T_{max} = 300 °C) were consistently lower than the IF lives at 300 °C.

4. For the same first cycle stress, the TMF IP lives were consistently lower than the TMF OP lives.

5. Crack growth was observed to occur predominately in the matrix regions for both MMCs.

6. At high temperatures (300 °C), the particulate induced increases in flow strength and rate of work hardening are significantly reduced.

TABLES

Table 4.1: Monotonic tensile behavior of Al2024 reinforced with SiC particles

Property	Temperature (°C)	Unreinforced	d = 2 μm V_f = 10 %	d = 30 μm V_f = 10 %	d = 2 μm V_f = 30 %	d = 30 μm V_f = 30 %
Elastic Modulus (GPa)	20	74.1	84.5	86.7	107	111
	200	68.9	75.1	76.5	102	101
	300	46.5	58.4	53.0	85.8	80.5
0.2% Yield Strength (MPa)	20	244	259	276	389	283
	200	223	247	260	405	300
	300	49.6	58.3	79.2	84.4	73.9
Ultimate Strength (MPa)	20	374	404	393	545	362
	200	289	282	301	467	345
	300	53.7	62.8	89.8	96.2	79.4
True Fracture Strain (%)	20	22.9	12.5	13.5	3.19	2.83
	200	53.6	26.0	13.2	4.03	6.39
	300	265	117	61.2	24.0	25.1

FIGURES

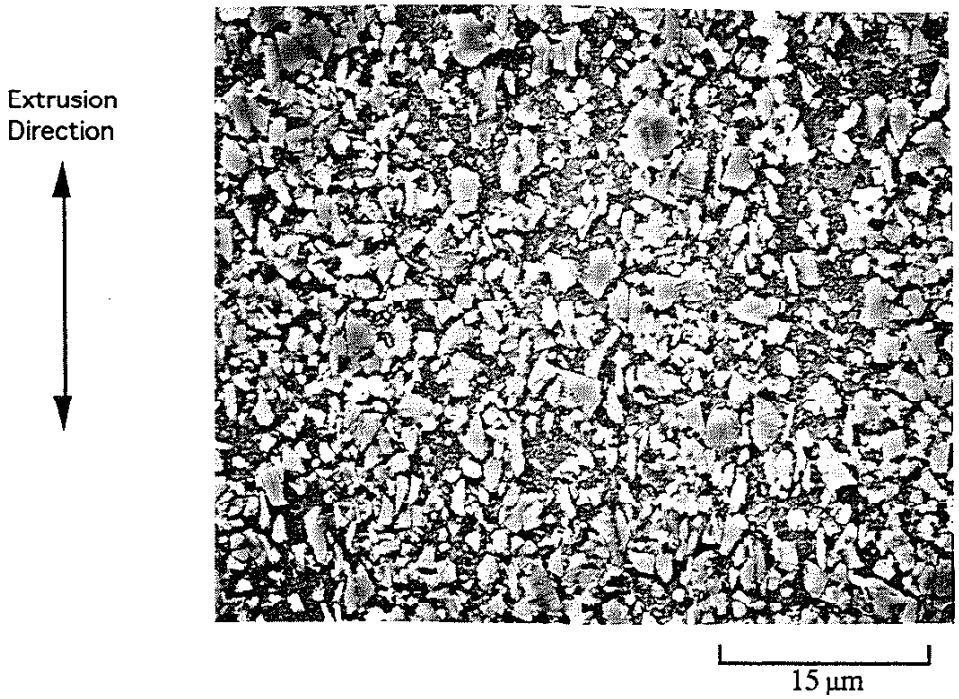

Figure 3.1: Particle distribution in Al2024 reinforced with 30% of 2 µm SiCp.

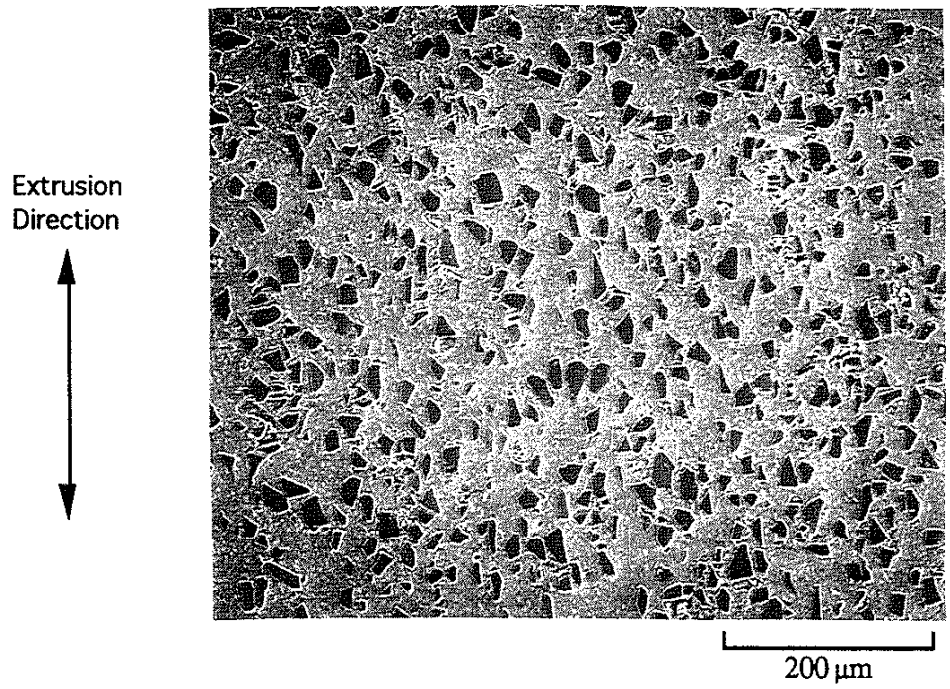

Figure 3.2: Particle distribution in Al2024 reinforced with 30% of 30 µm SiCp.

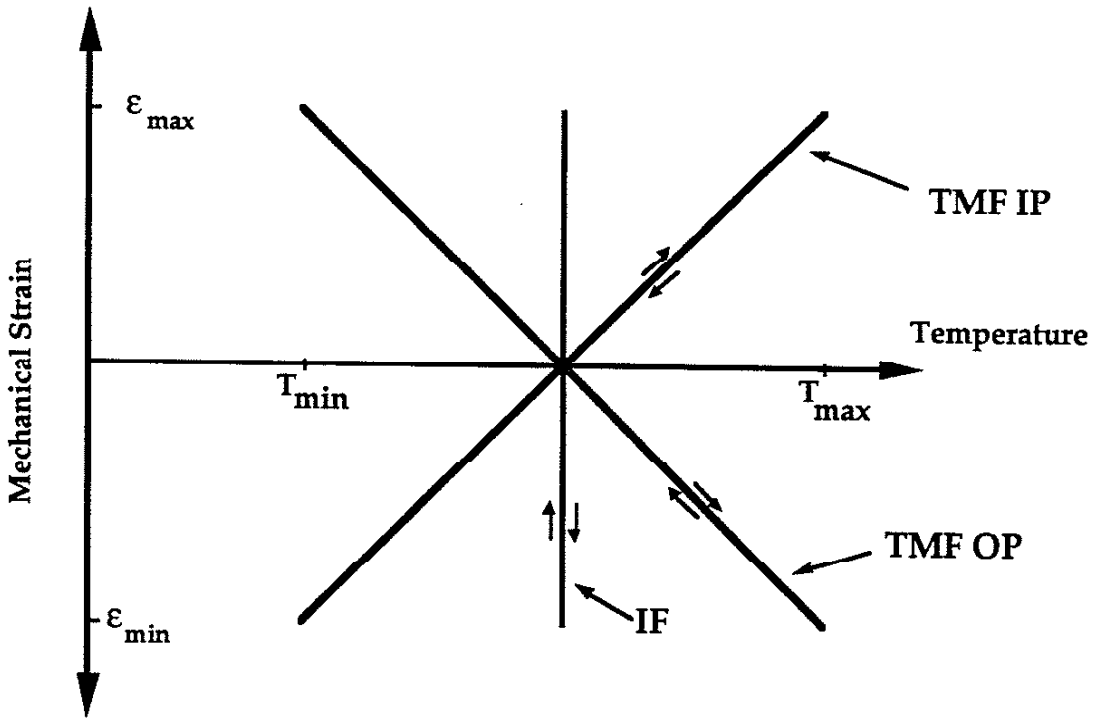

Figure 3.3: Schematic of mechancial strain-temperature variation in TMF In-Phase, TMF Out-of-Phase and isothermal fatigue loading

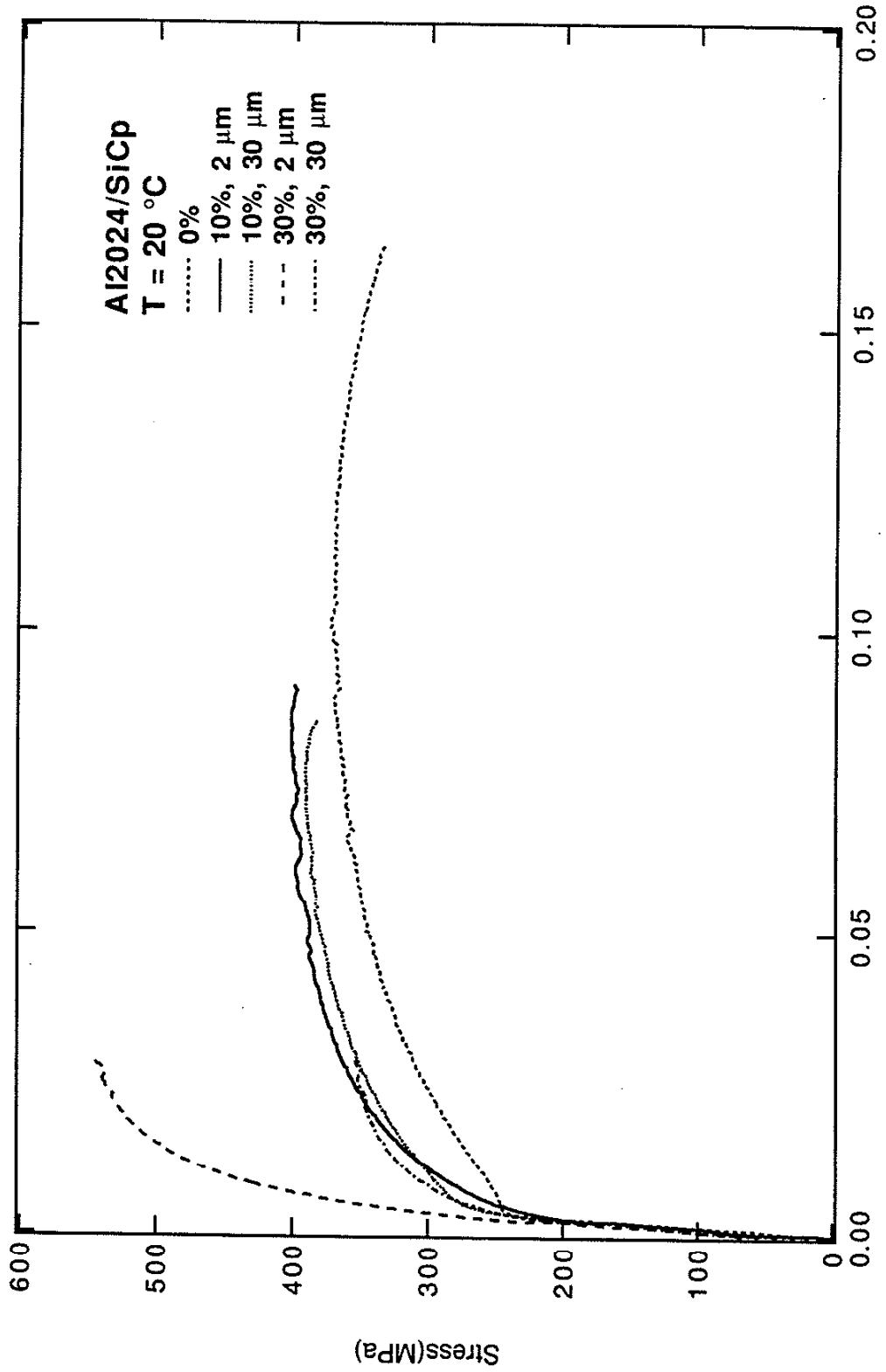

Figure 4.1: Monotonic tensile behavior of Al2024/SiCp at 20 °C

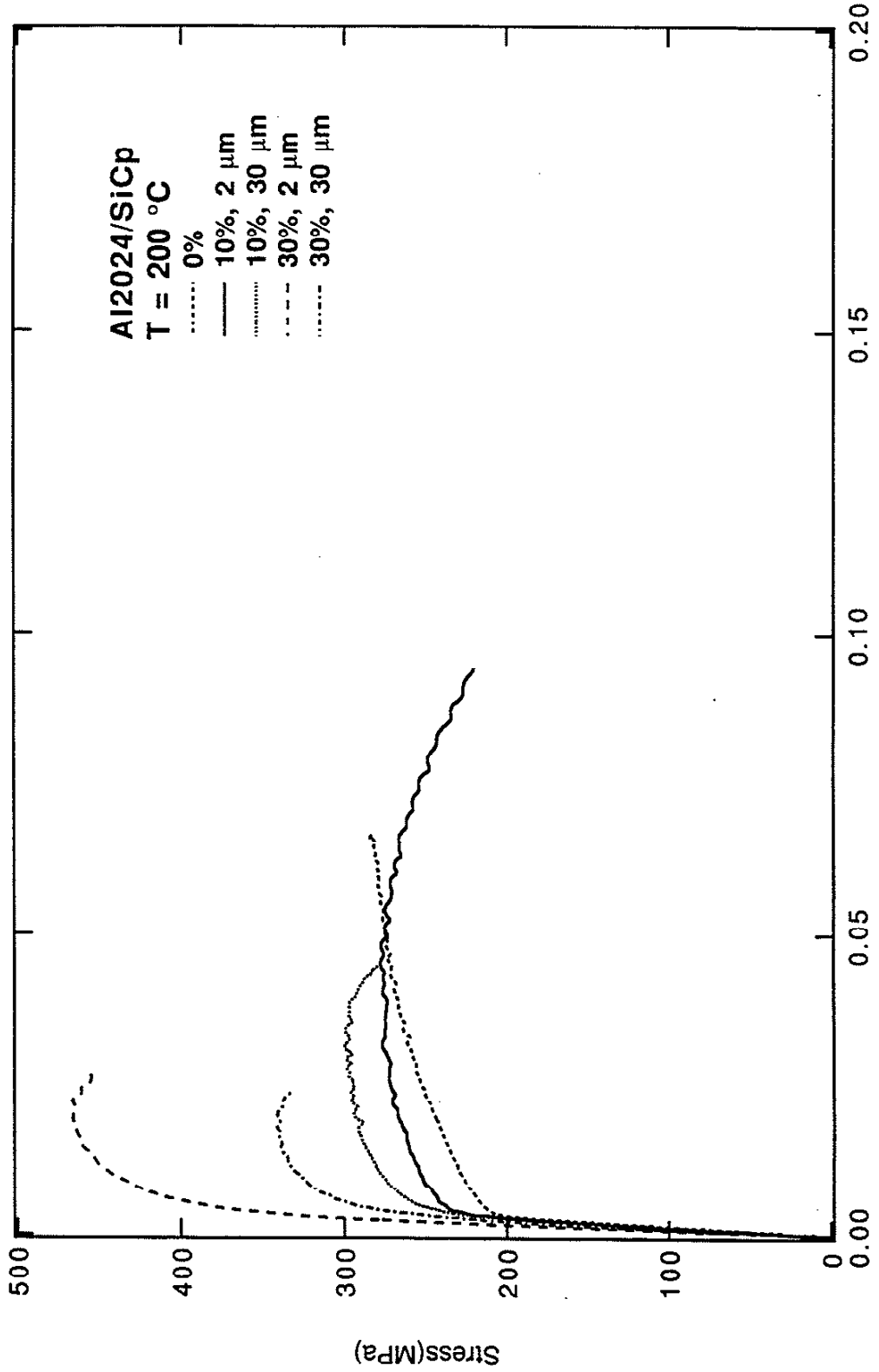

Figure 4.2: Monotonic tensile behavior of Al2024/SiCp at 200 °C

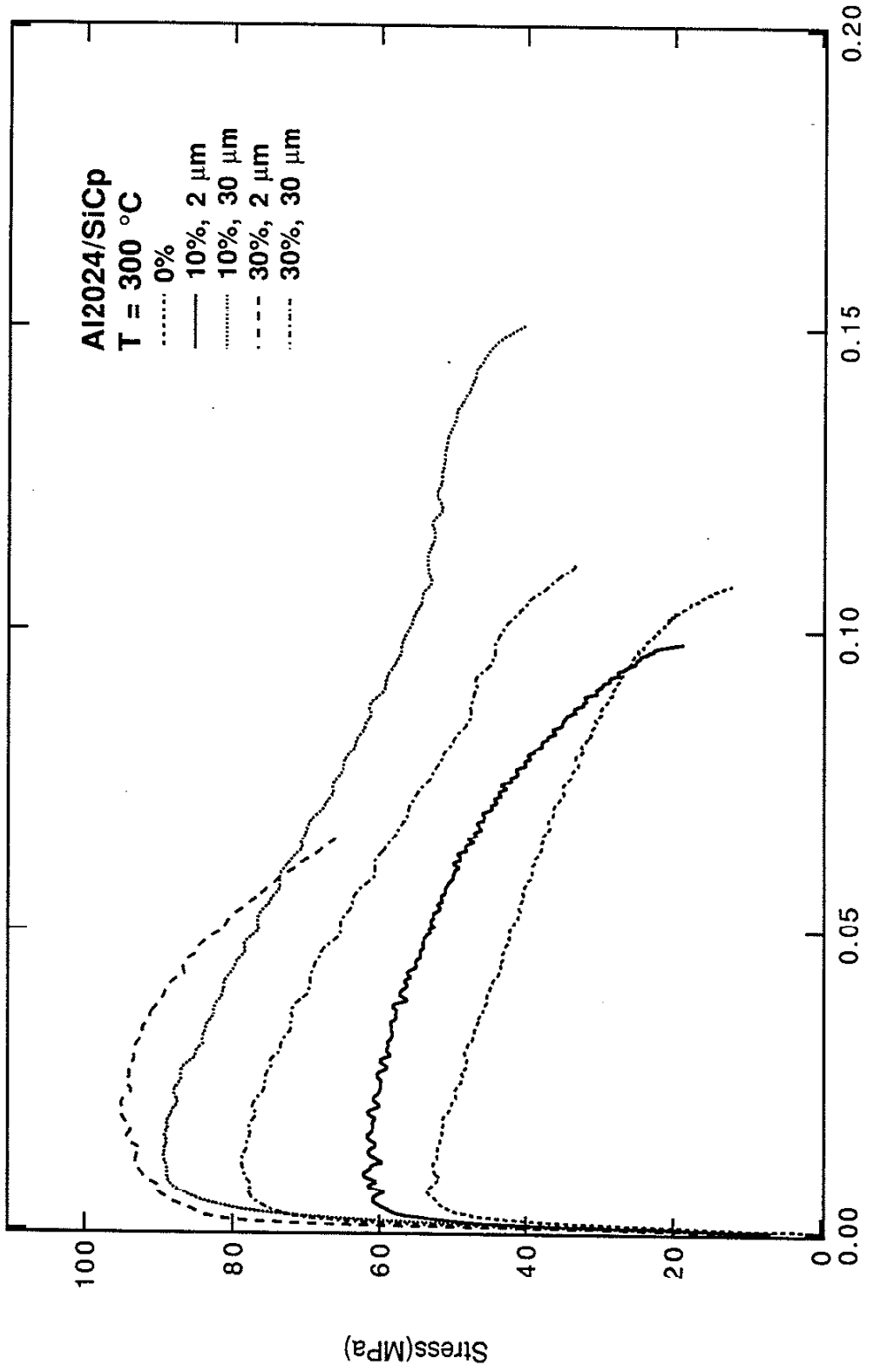

Figure 4.3: Monotonic tensile behavior of Al2024/SiCp at 300 °C

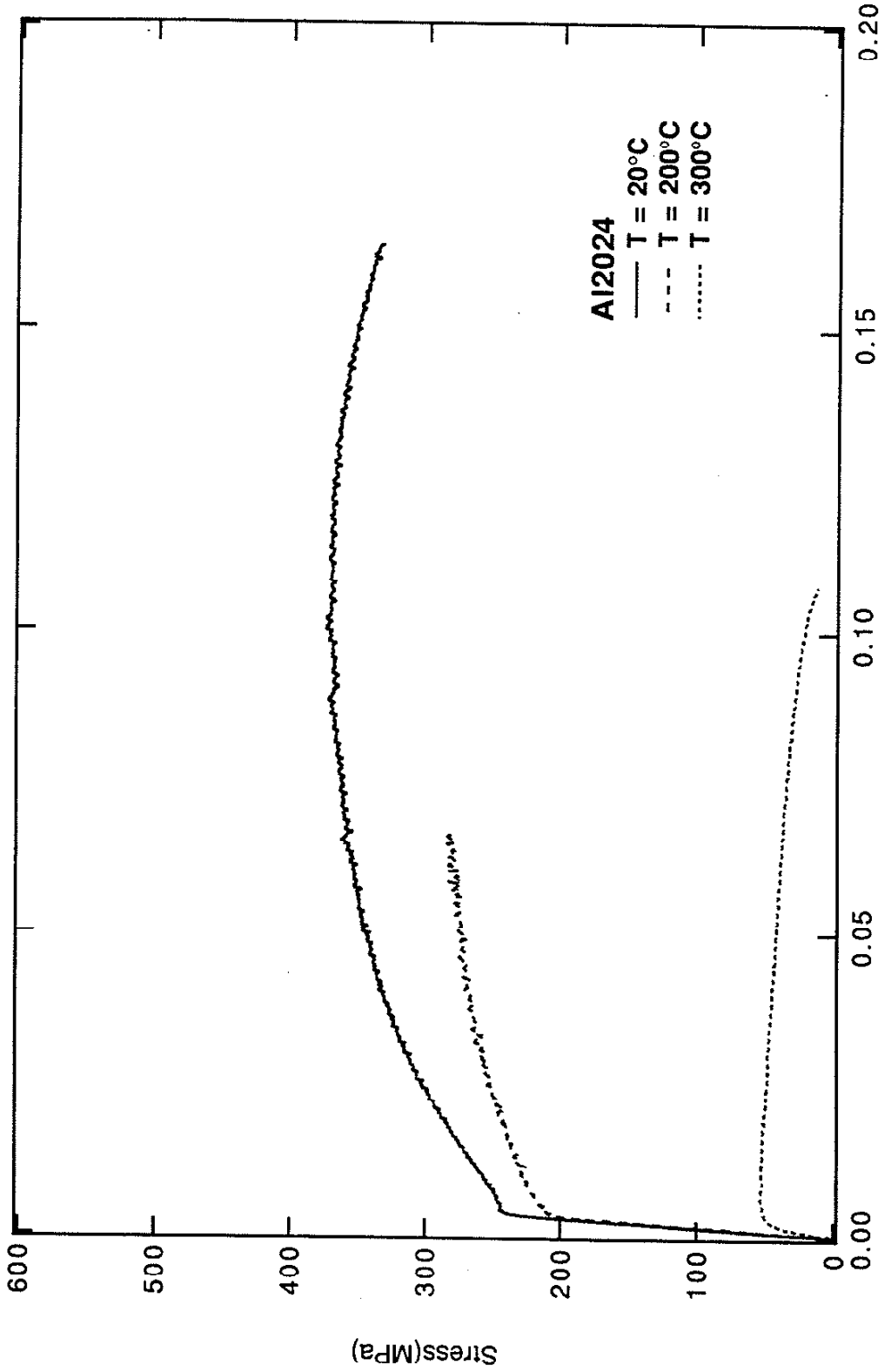

Figure 4.4: Monotonic tensile behavior of Al2024/0% SiCp

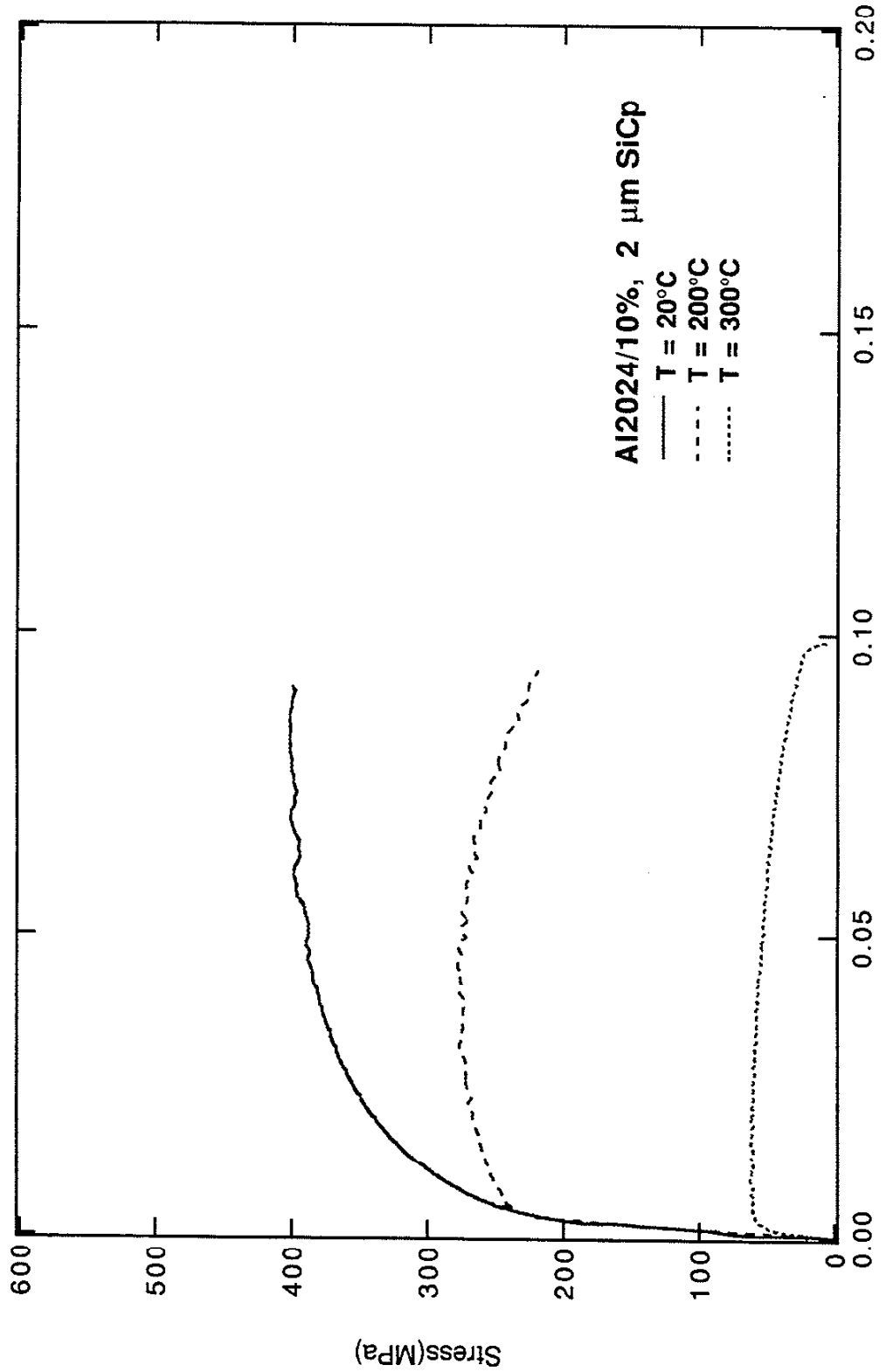

Figure 4.5: Monotonic tensile behavior of Al2024/10%, 2μm SiCp

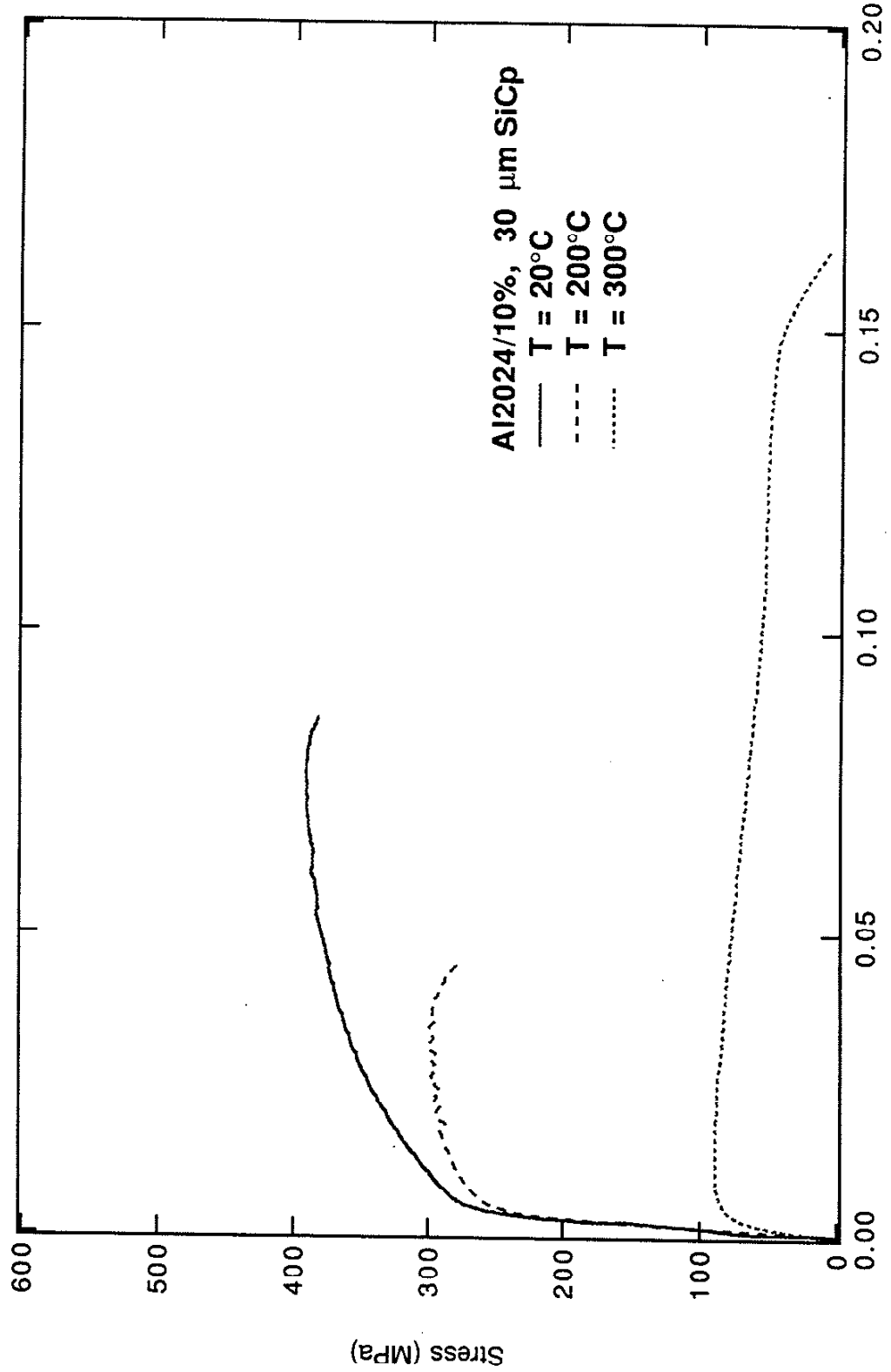

Figure 4.6: Monotonic tensile behavior of Al2024/10%, 30μm SiCp

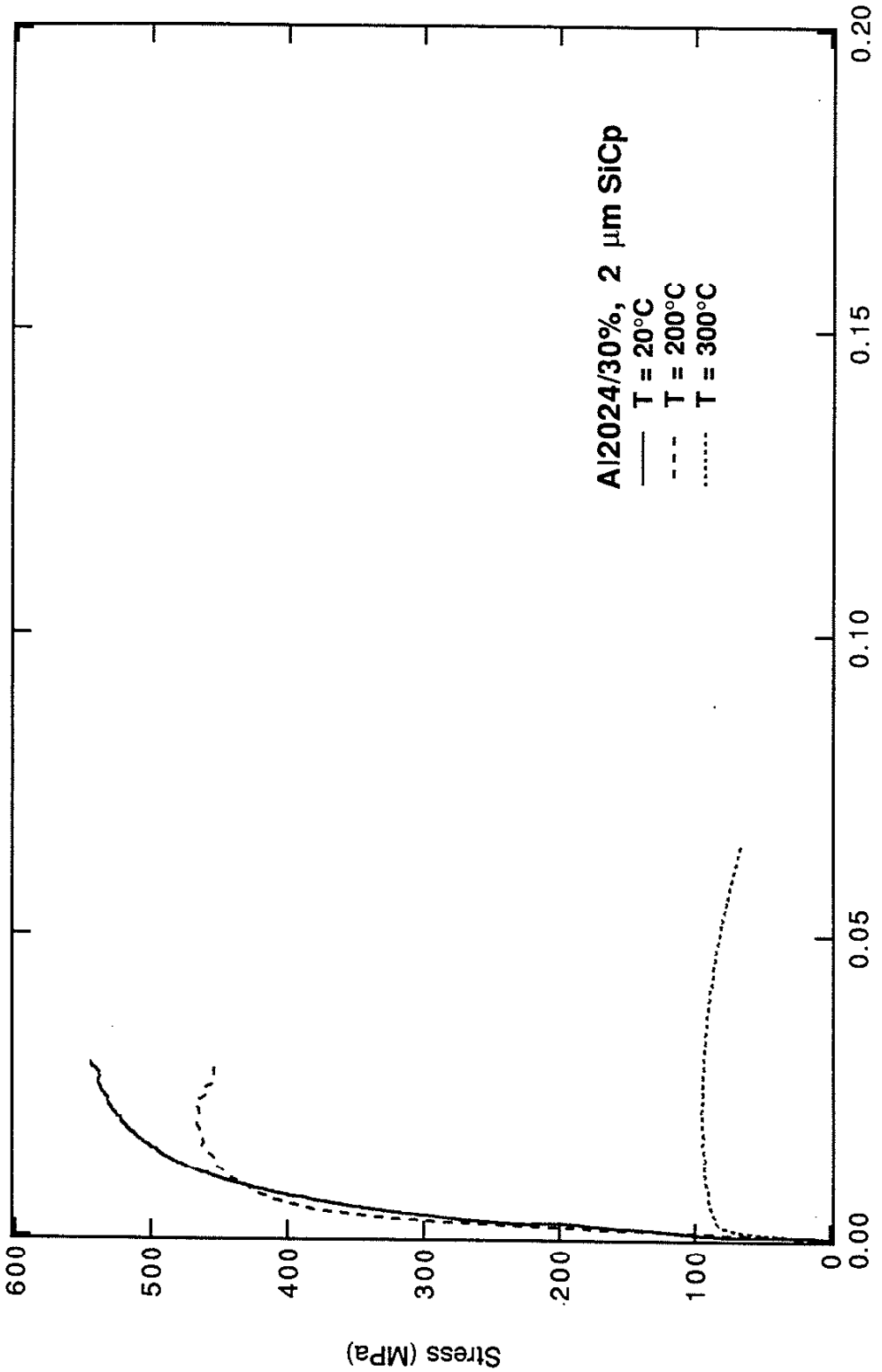

Figure 4.7: Monotonic tensile behavior of Al2024/30%, 2μm SiCp

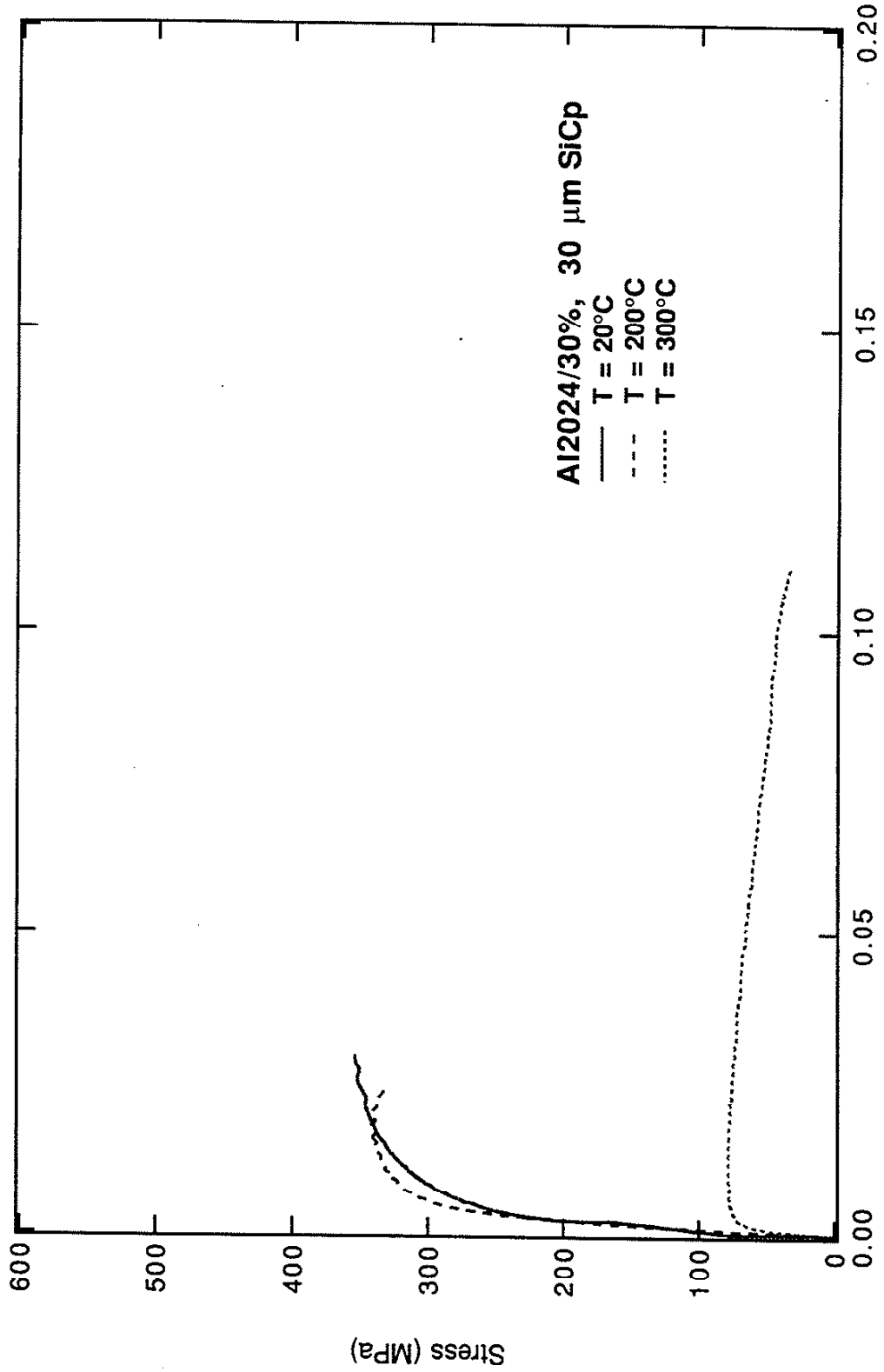

Figure 4.8: Monotonic tensile behavior of Al2024/30%, 30μm SiCp

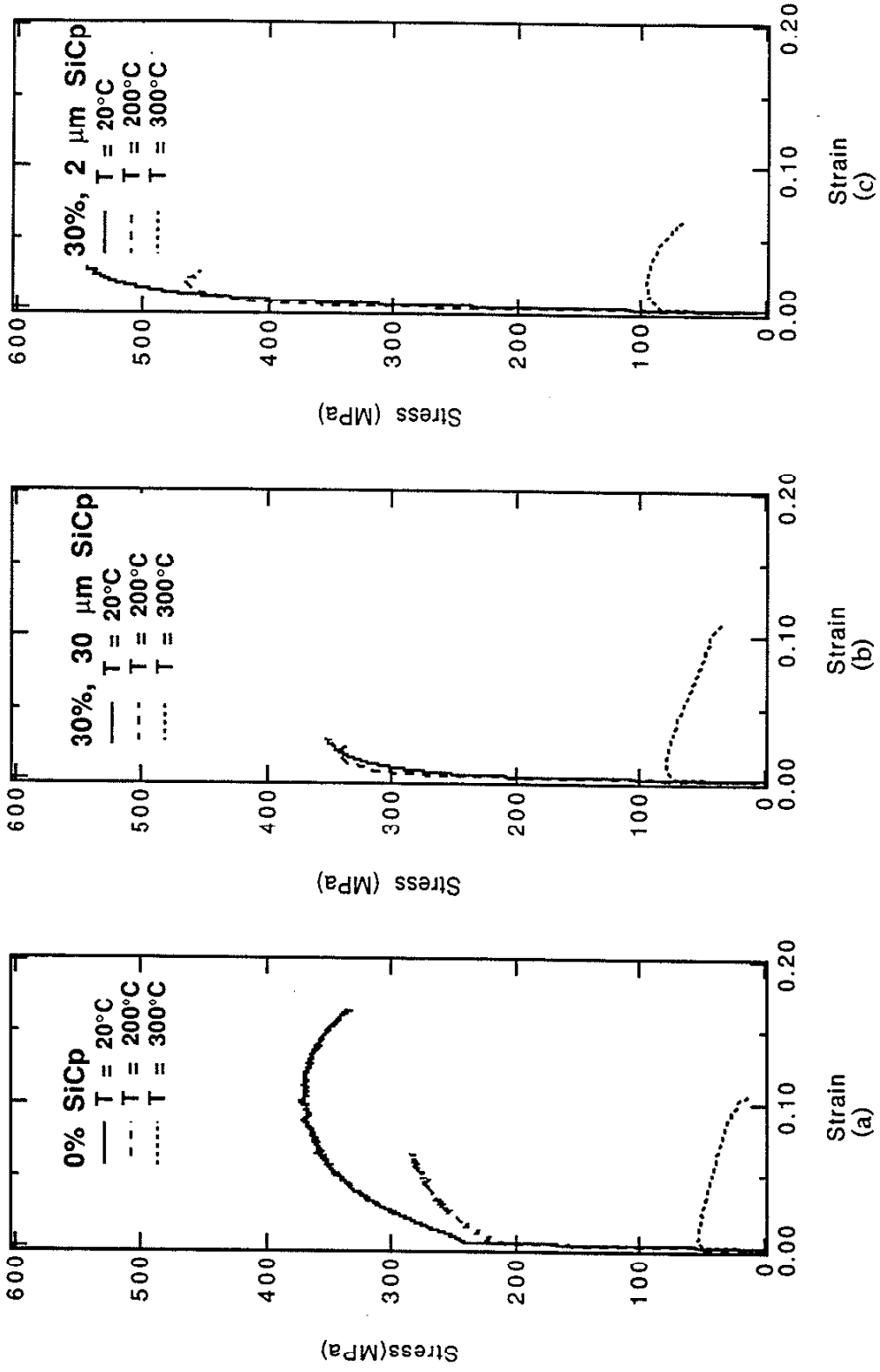

Figure 4.9: Monotonic stress-strain behavior of (a) Al2024, (b) Al2024/30%, 30 μm, and (c) Al 2024/30%, 2 μm.

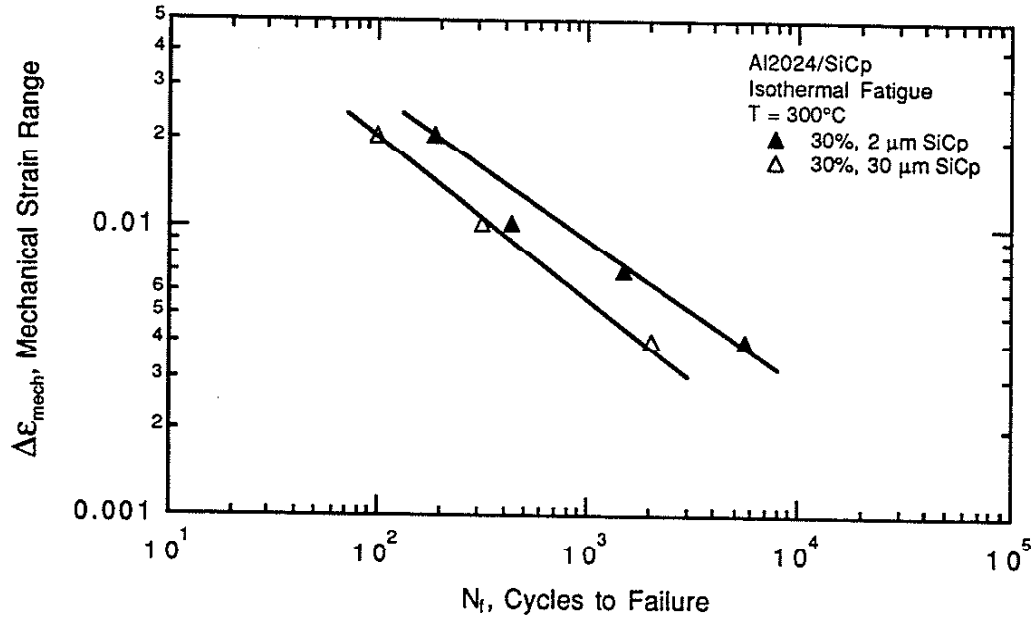

Figure 4.10: Isothermal fatigue behavior of 2024 aluminum reinforced with SiC particles

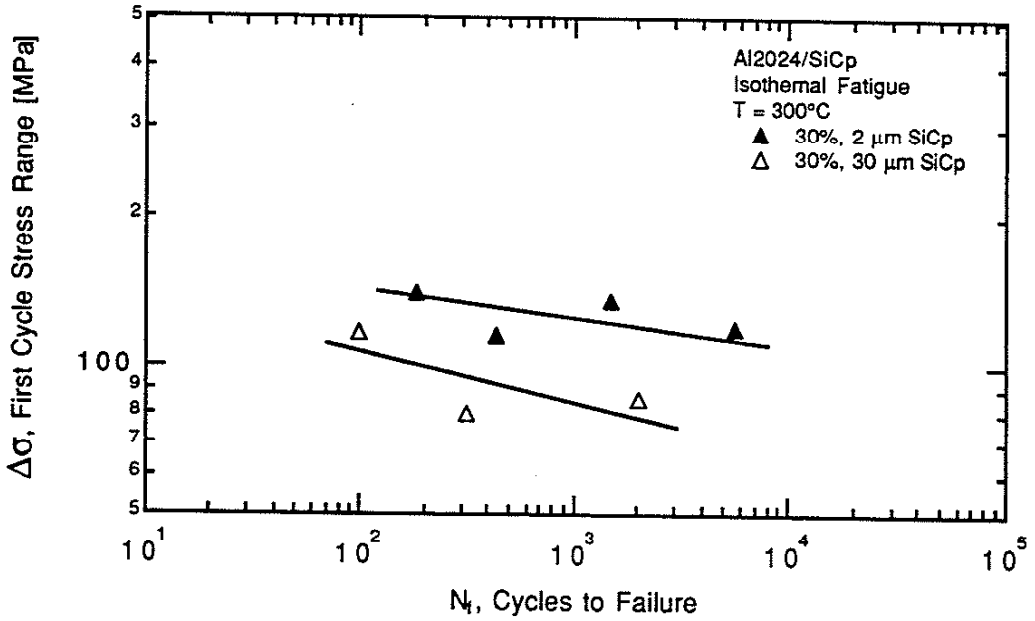

Figure 4.11: Isothermal fatigue behavior of 2024 aluminum reinforced with SiC particles

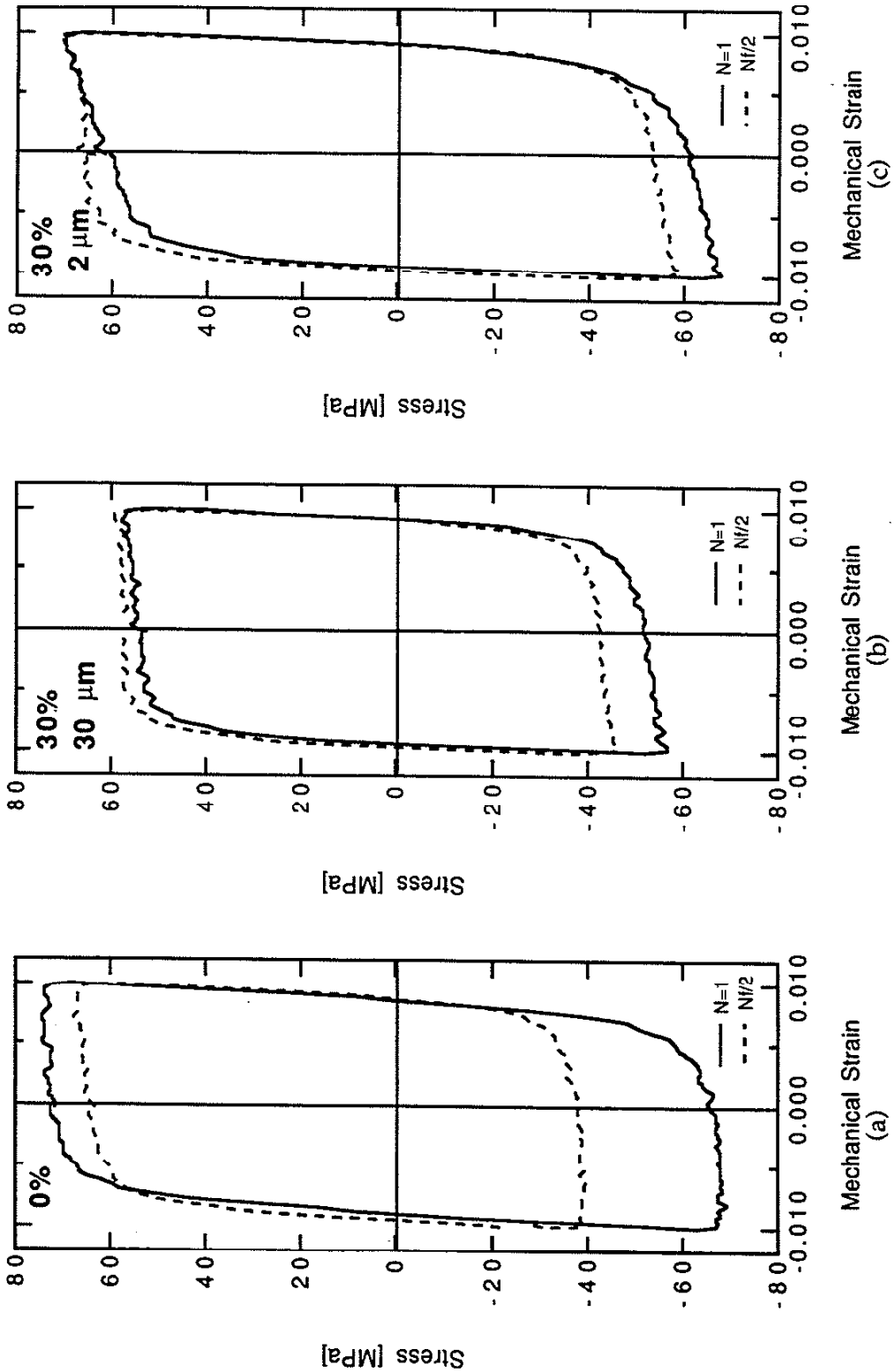

Figure 4.12: Stress-strain behavior during isothermal fatigue at 300 °C and $\Delta\varepsilon_{mech}$ = 2% of (a) Al2024, (b) Al2024/30%, 30 µm, and (c) Al 2024/30%, 2 µm.

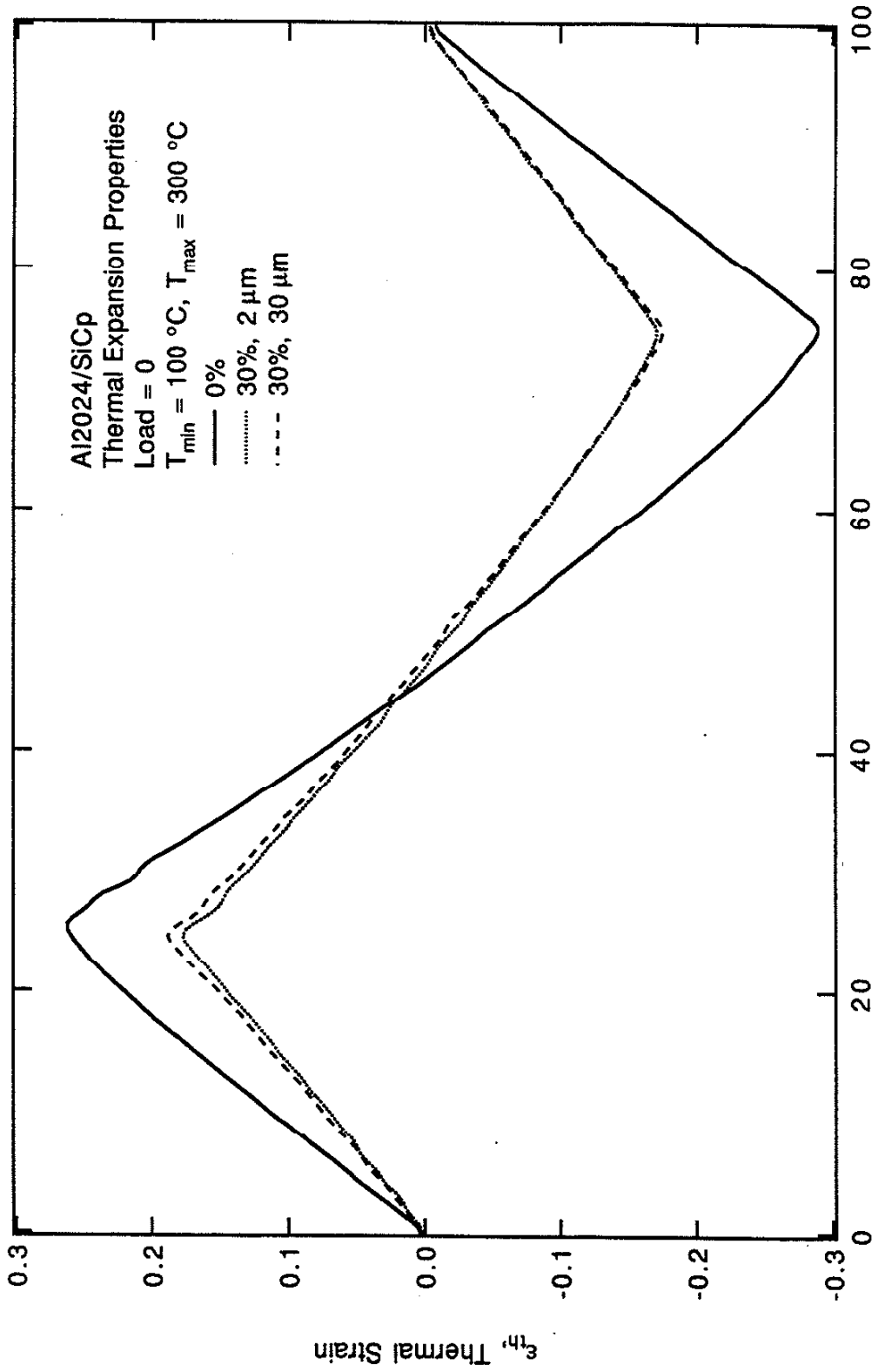

Figure 4.13: Thermal expansion properties of Al2024/SiCp

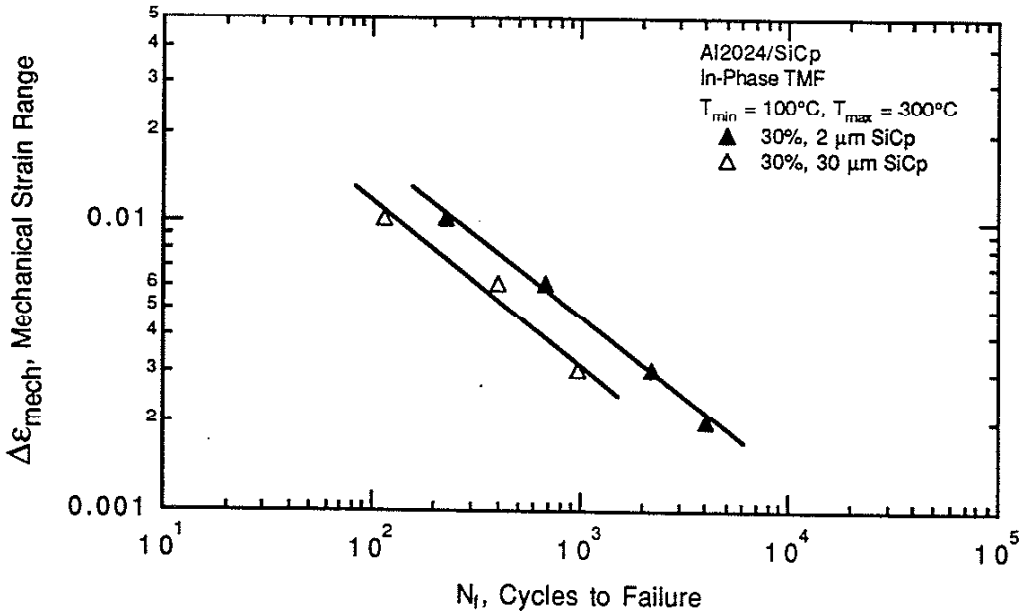

Figure 4.14: In-Phase TMF behavior of 2024 aluminum reinforced with SiC particles

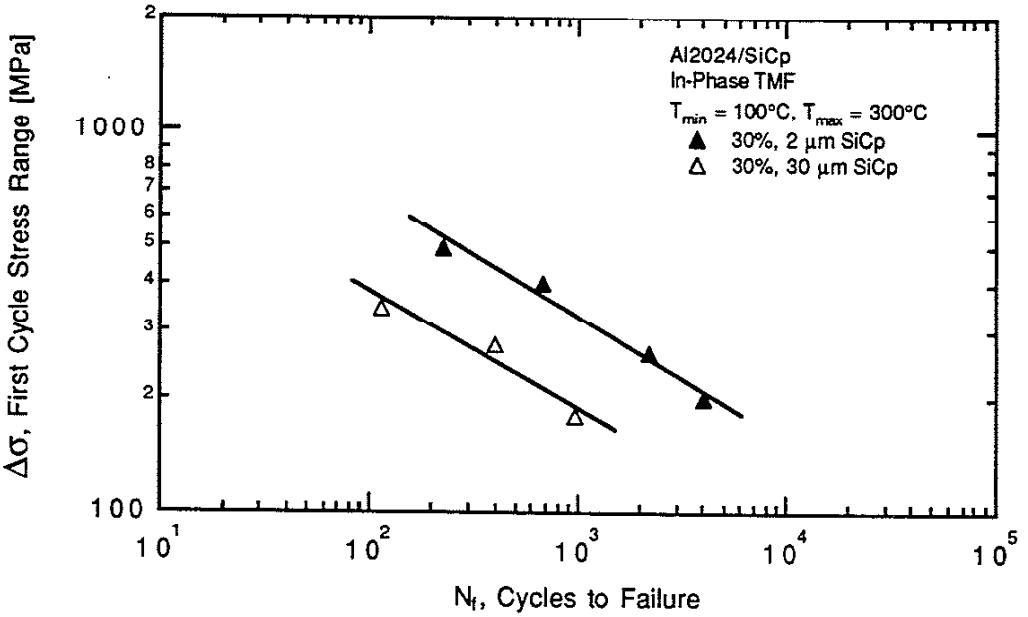

Figure 4.15: In-Phase TMF behavior of 2024 aluminum reinforced with SiC particles

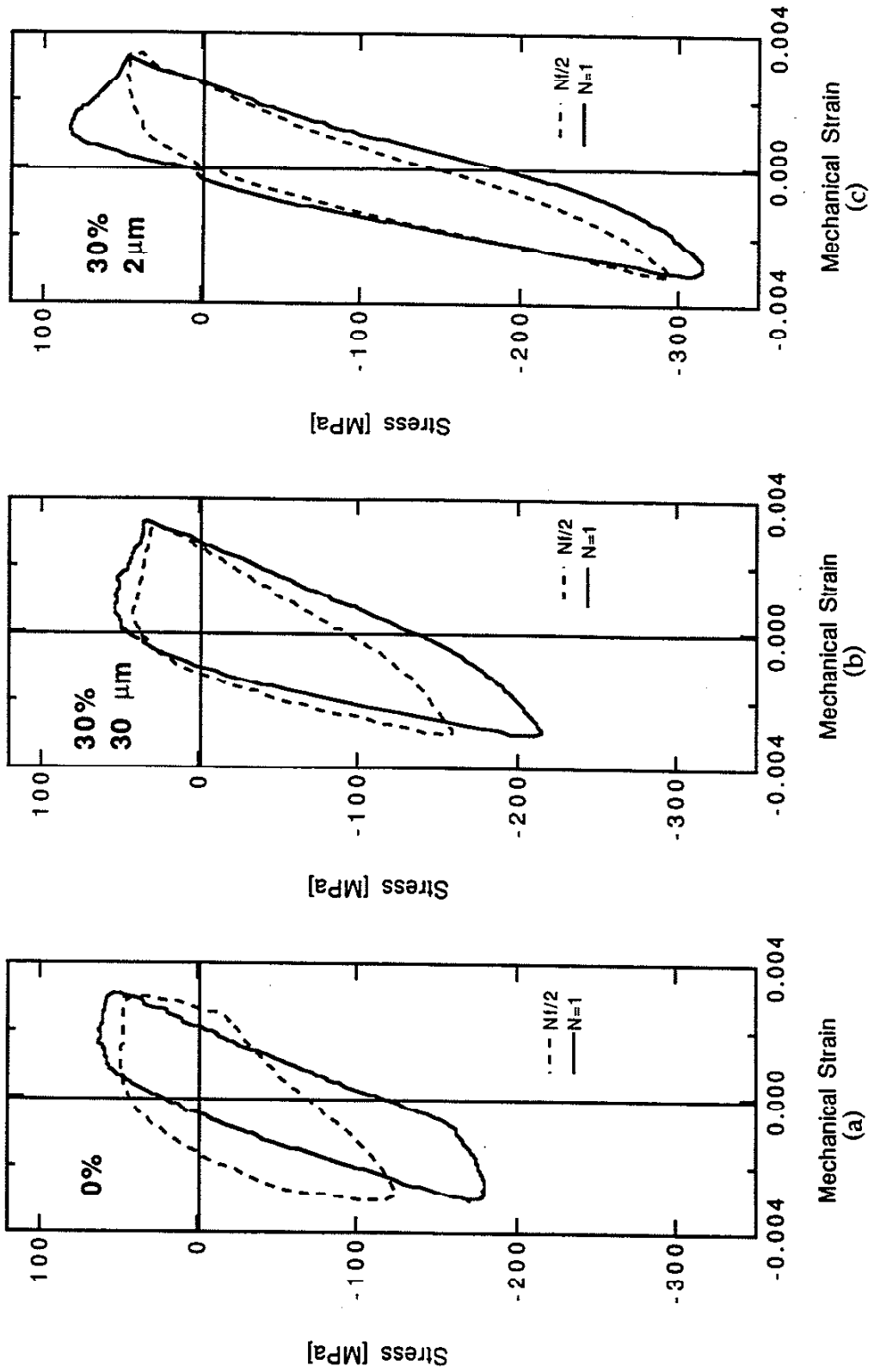

Figure 4.16: Stress-strain behavior during In-Phase TMF with T = 100 - 300 °C and $\Delta\varepsilon_{mech}$ = 0.6% of (a) Al2024, (b) Al2024/30%, 30 µm, and (c) Al 2024/30%, 2 µm.

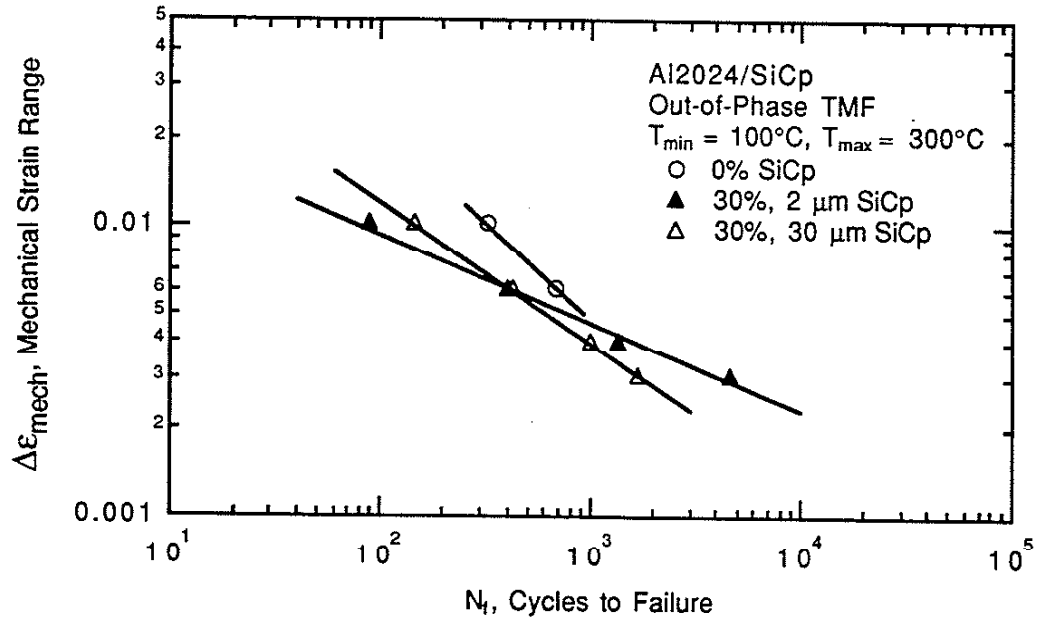

Figure 4.17: Out-of-Phase TMF behavior of 2024 aluminum reinforced with SiC particles

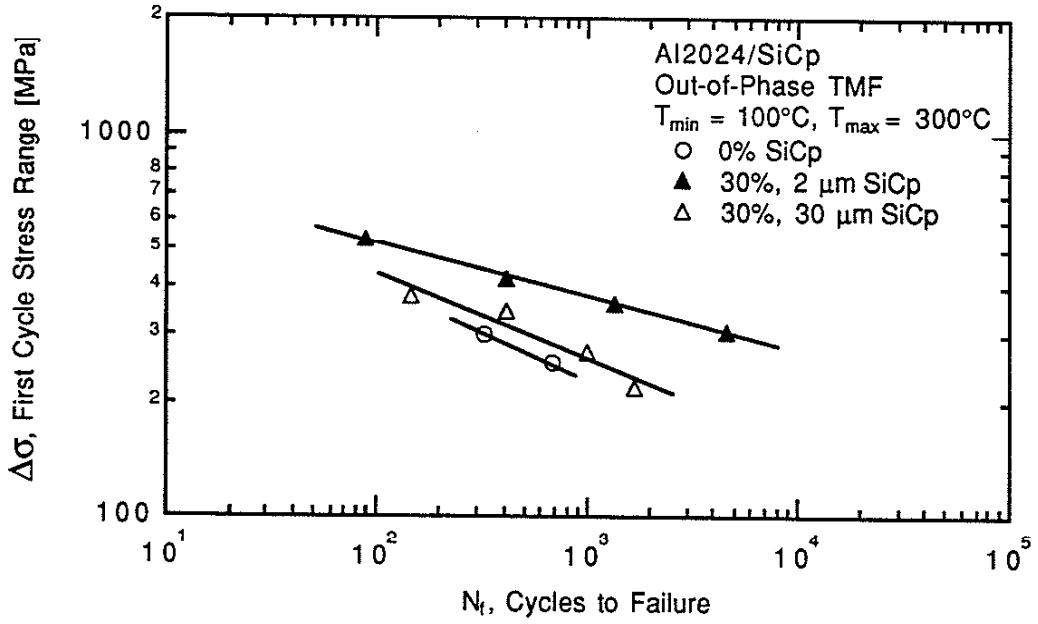

Figure 4.18: Out-of-Phase TMF behavior of 2024 aluminum reinforced with SiC particles

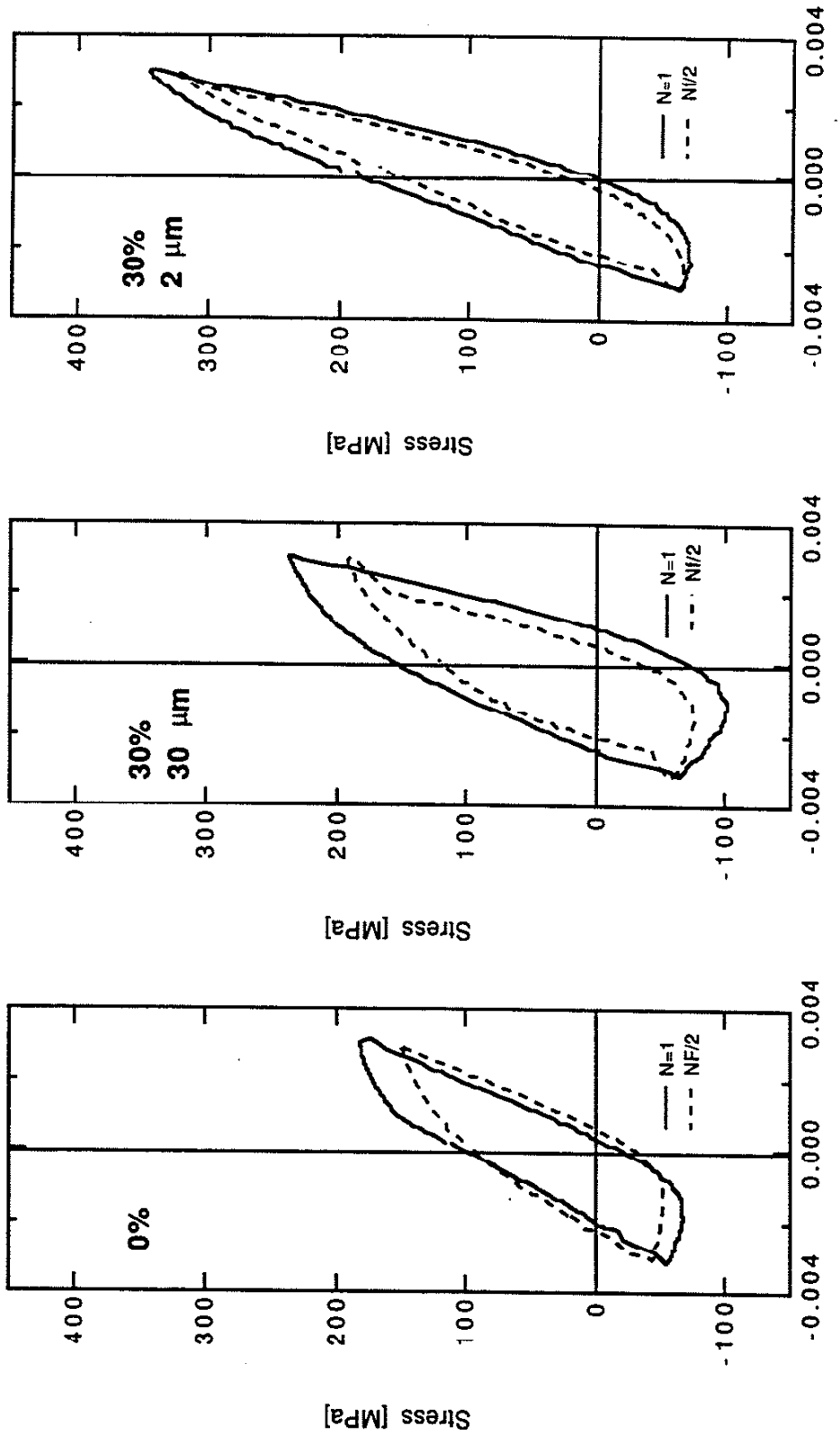

Figure 4.19: Stress-strain behavior during Out-of-Phase TMF with T = 100 - 300 °C and $\Delta\varepsilon_{mech}$ = 0.6% of (a) Al2024, (b) Al2024/30%, 30 µm, and (c) Al 2024/30%, 2 µm.

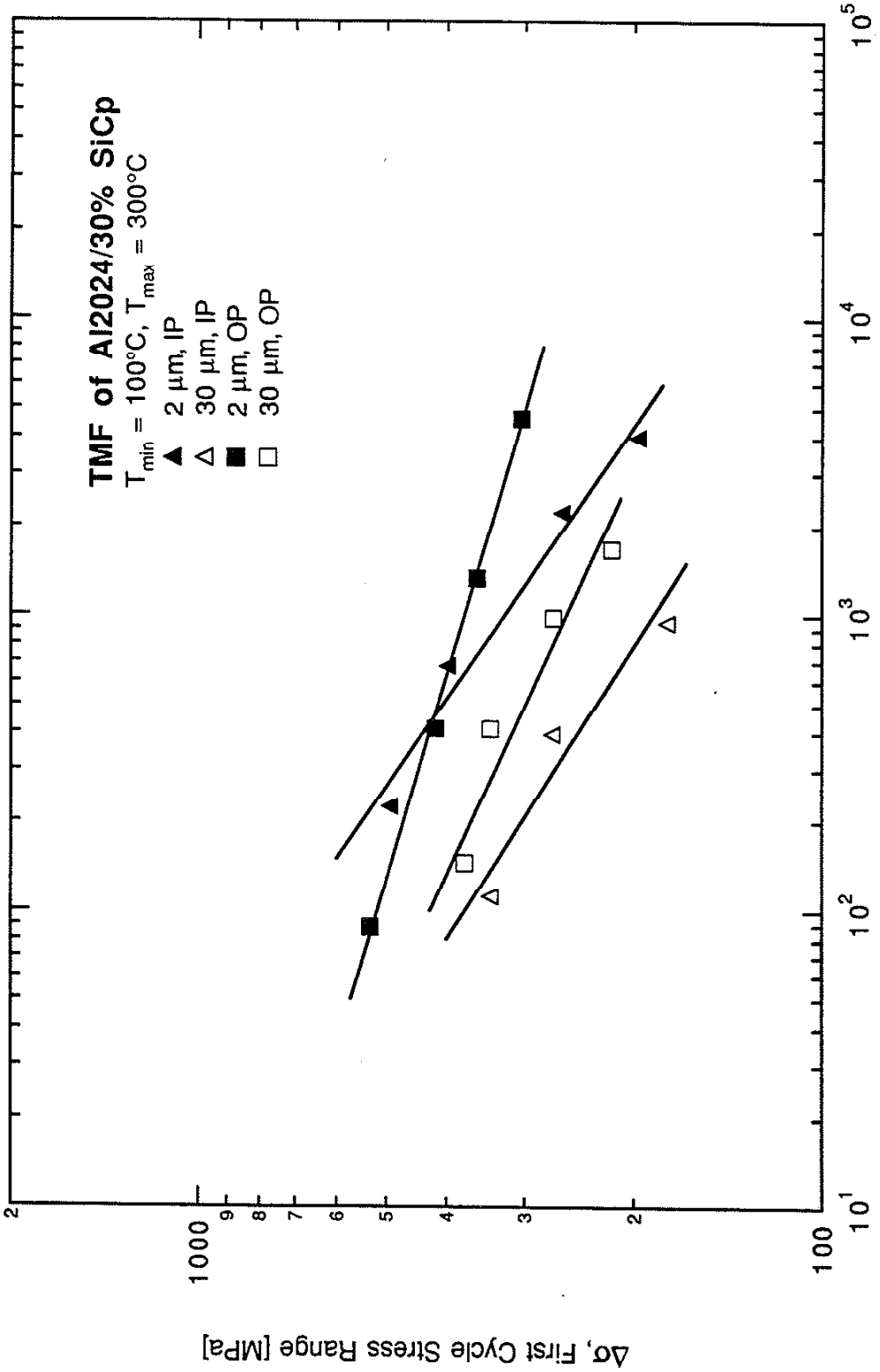

Figure 4.20: In-Phase and Out-of-Phase TMF behavior of Al2024/SiCp

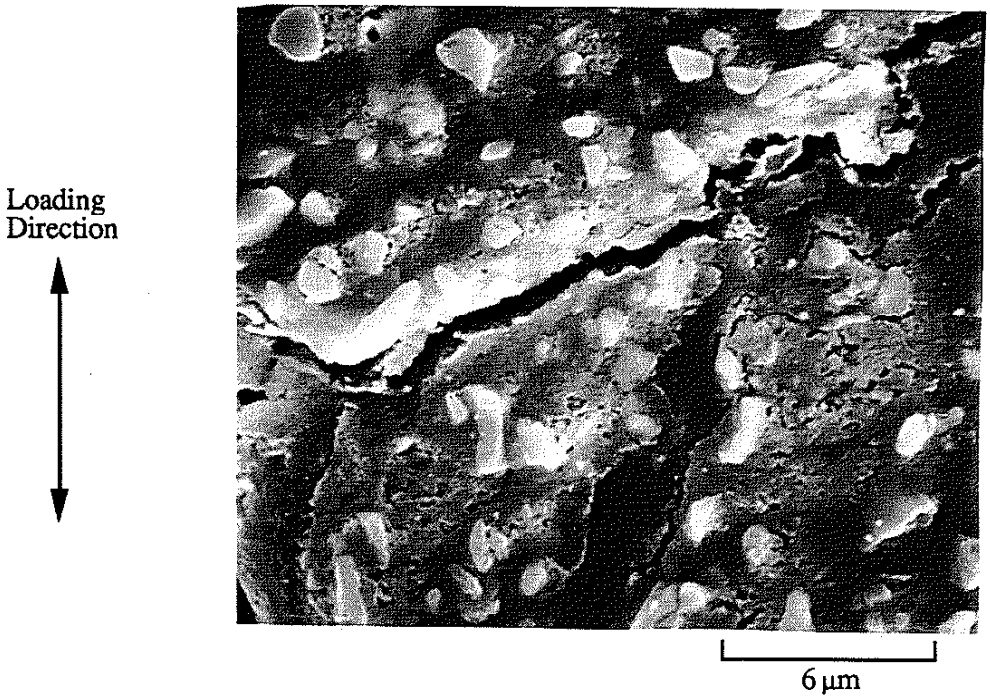

Figure 4.21: Crack growth in matrix, 2 μm particles, Isothermal Fatigue, 300 °C.

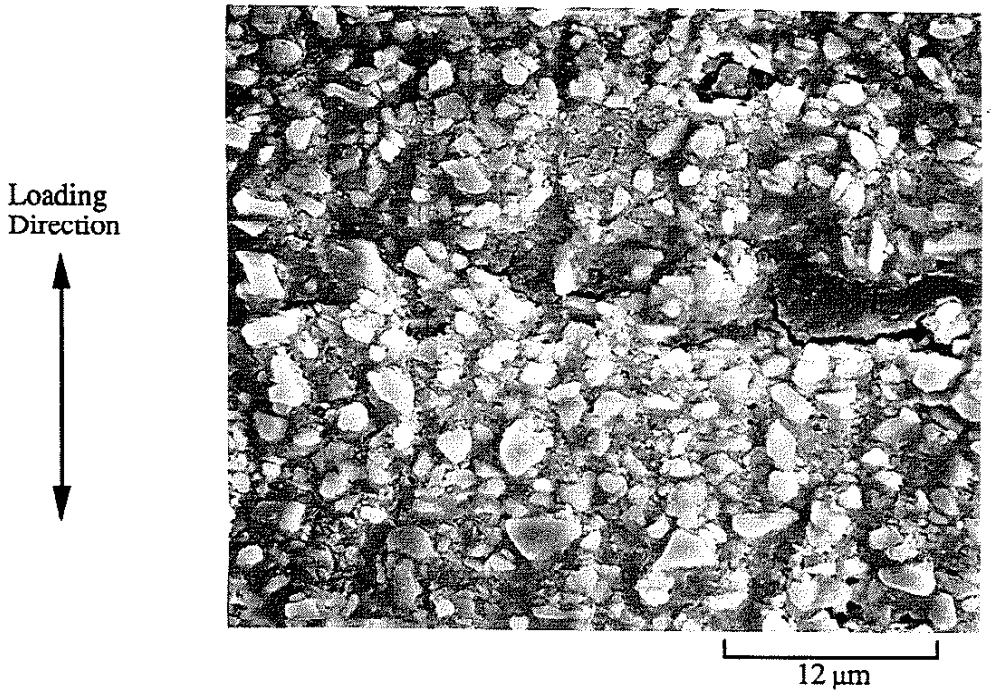

Figure 4.22: Crack growth in matrix, 2 μm particles, Isothermal Fatigue, 300 °C.

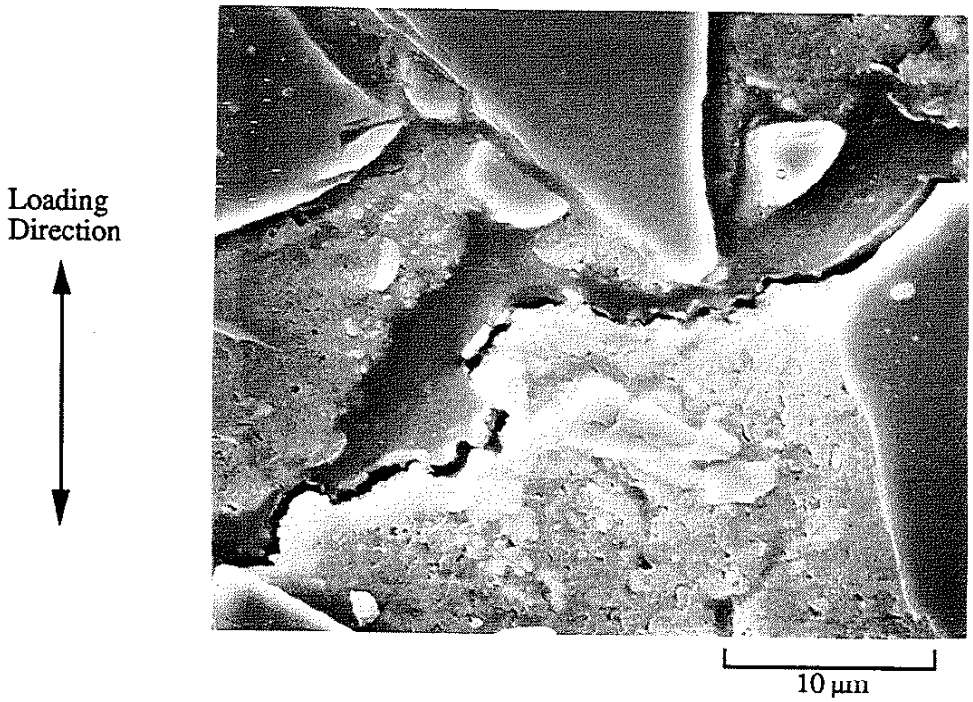

Figure 4.23: Crack growth in matrix, 30 μm particles, Isothermal Fatigue, 300 °C.

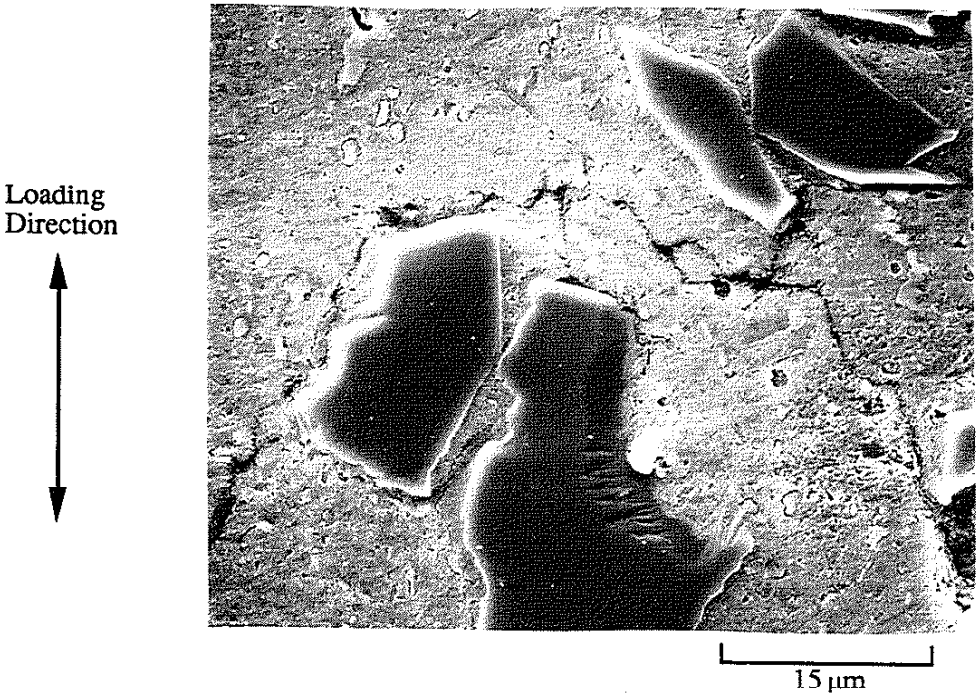

Figure 4.24: Crack growth in matrix, 30 μm particles, Isothermal Fatigue, 300 °C.

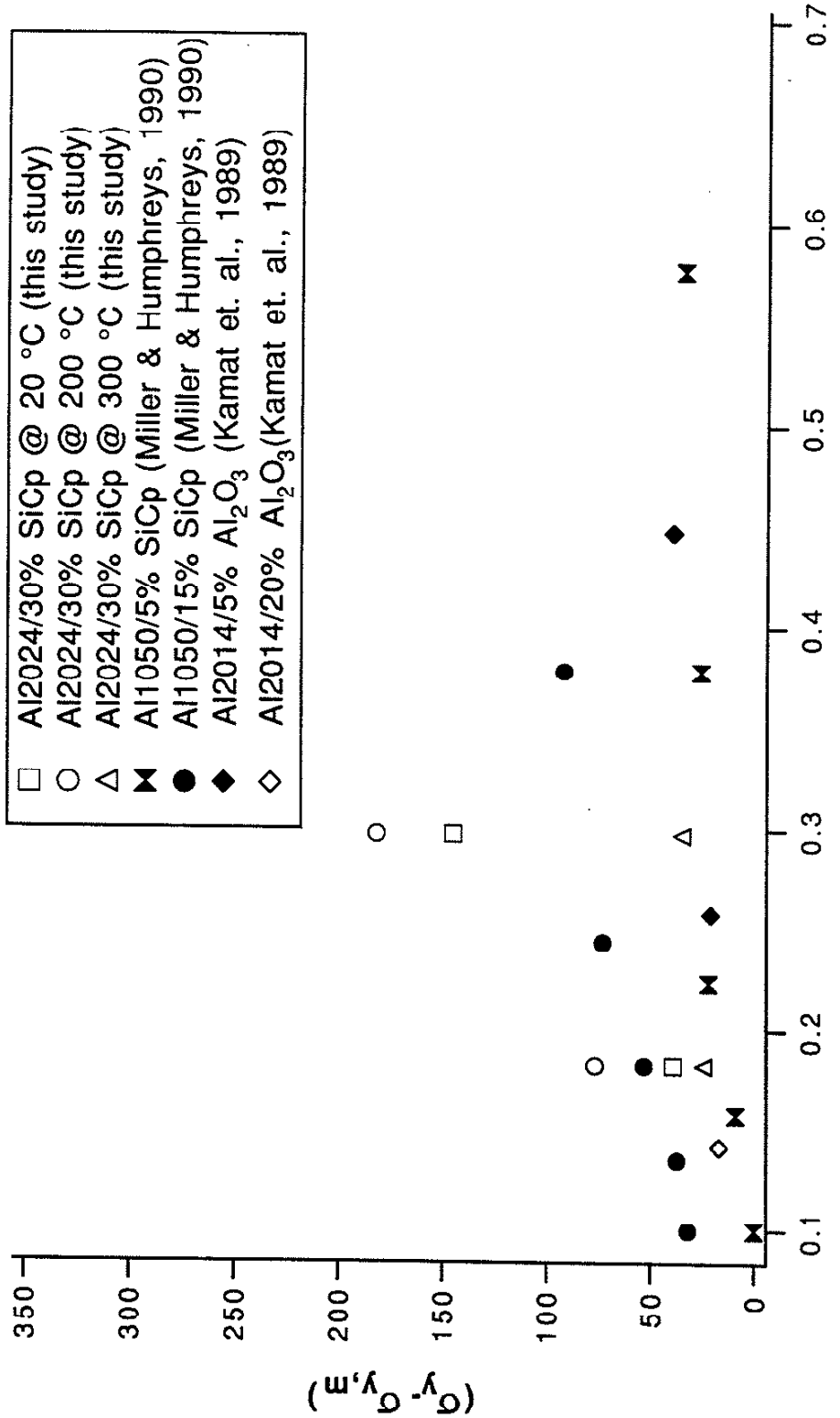

Figure 4.25: Increase in 0.2% yield strength due to particle strengthening (data from this study and references 4-6).

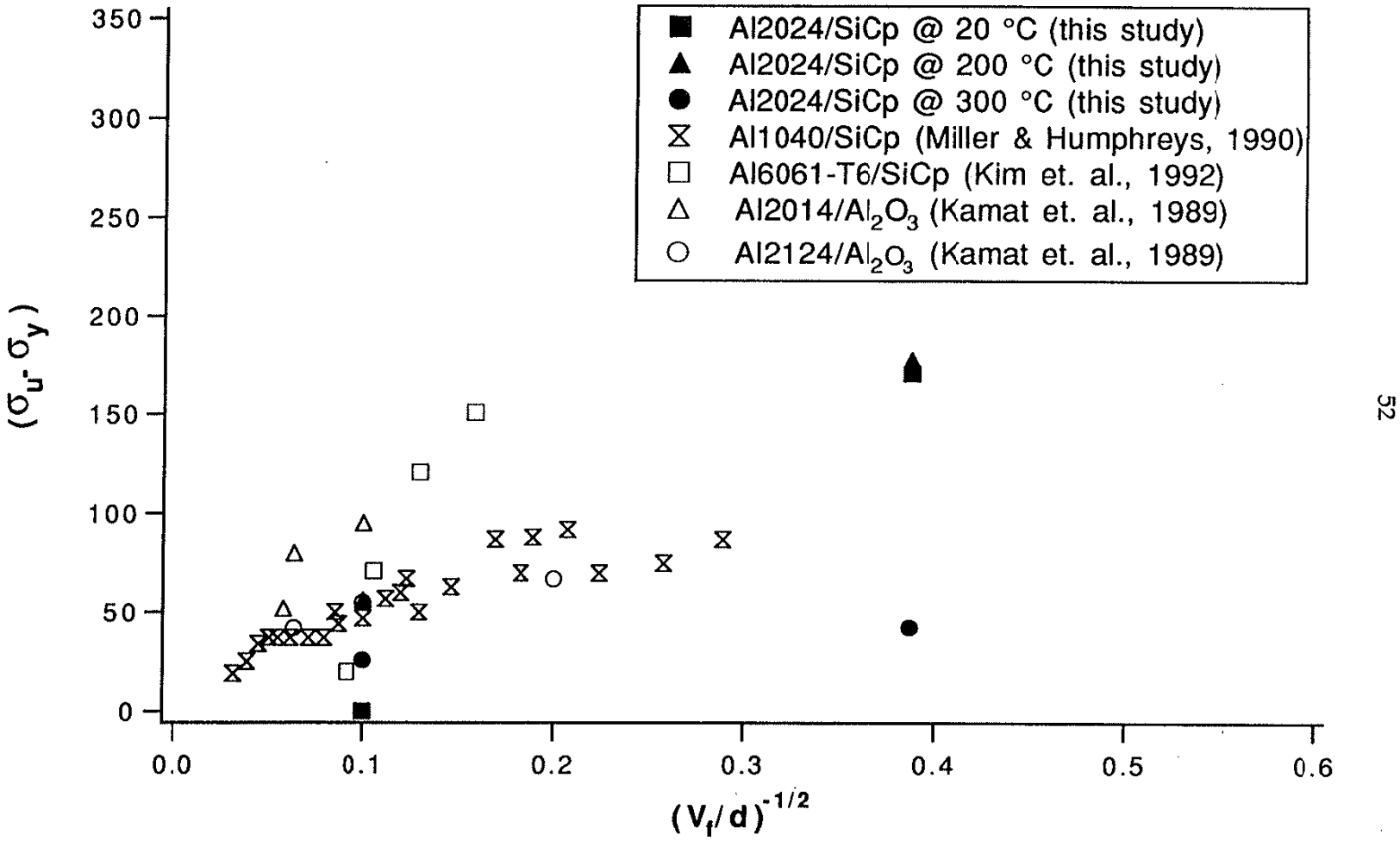

Figure 4.26: Work hardening due to particle strenghtening (data from this study and references 3-5).

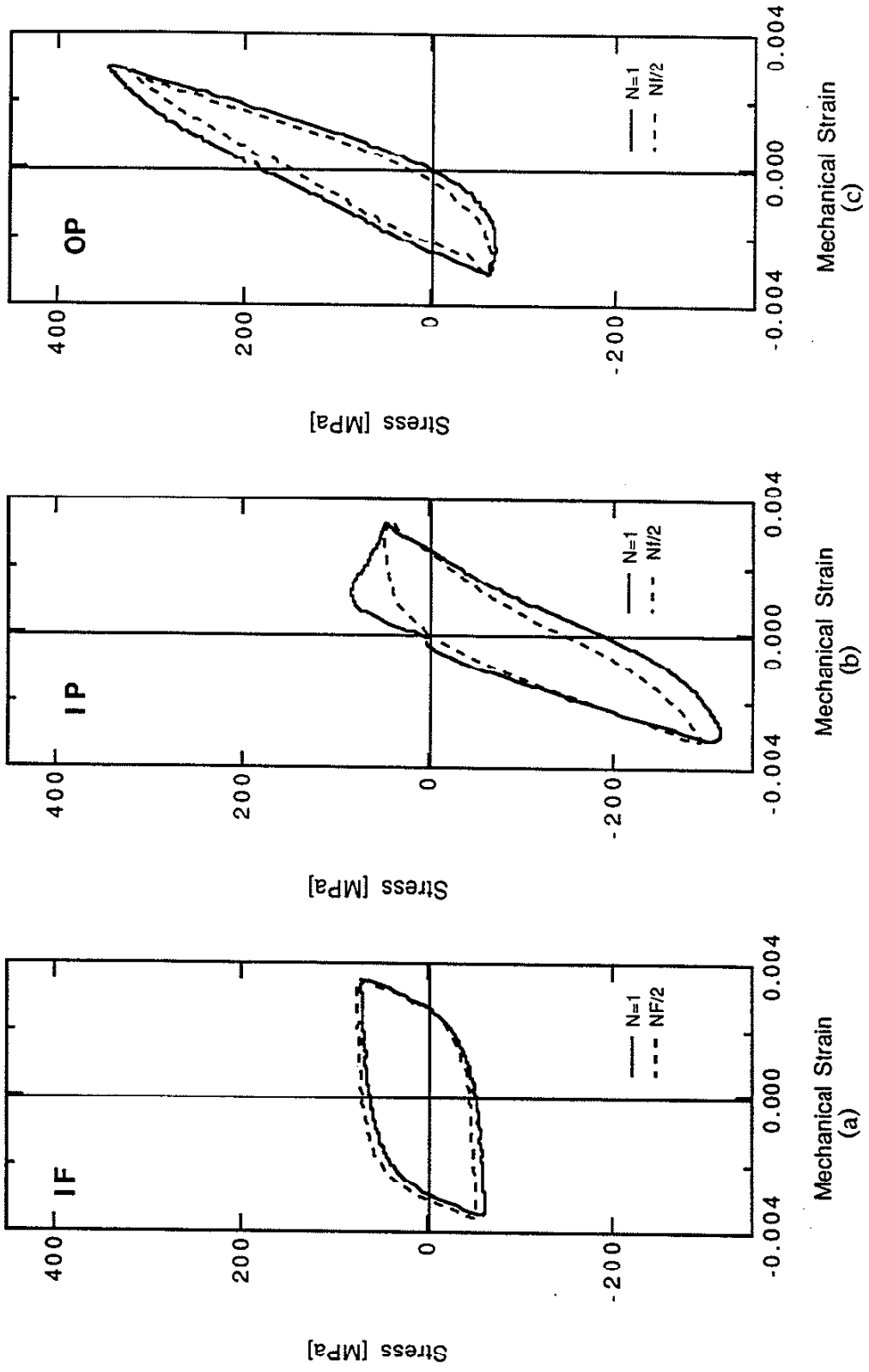

Figure 4.27: Stress-strain behavior of Al 2024/30%, 2 μm subjected to $\Delta\varepsilon_{mech}$ = 0.6% during (a) Isothermal Fatigue at T = 300 °C, (b) In-Phase TMF with T = 100 - 300 °C, and (c) Out-of-Phase TMF with T = 100 - 300 °C.

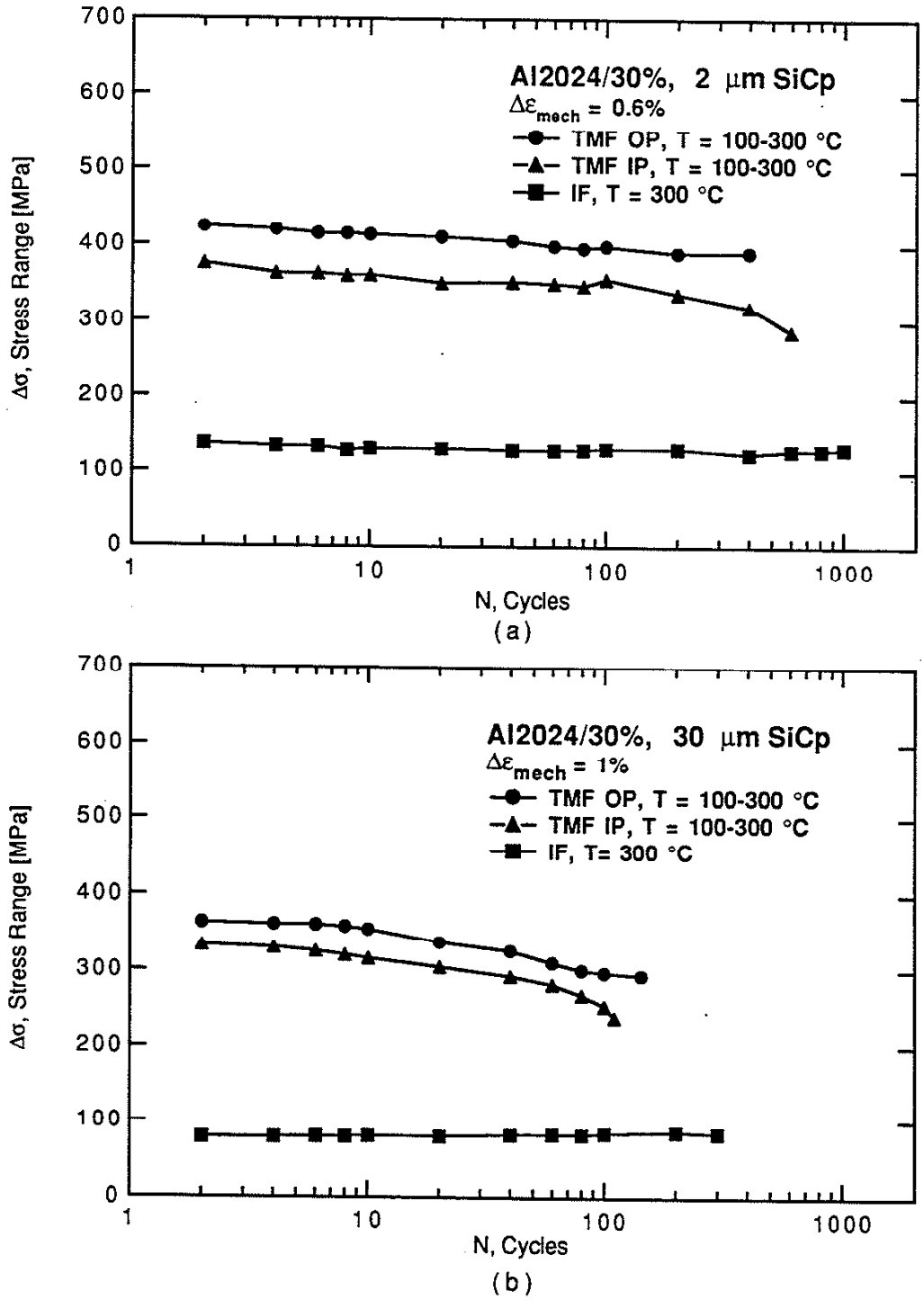

Figure 4.28: Cyclic softening behavior of (a) Al2024/30%, 2 μm SiCp and (b) Al2024/30%, 30 μm SiCp

REFERENCES

1. Karayaka, M. and Sehitoglu, S., "Thermomechanical Fatigue of Particulate-Reinforced Aluminum 2xxx-T4", Metall. Trans., Vol. 22A, pp. 697-707 (1991).
2. Allison, J. E. and J. W. Jones, "Fatigue Behavior of Discontinuously Reinforced Metal Matrix Composites," to appear in Fundamentals of Metal Matrix Composites, Betterworth-Heinmann (1993).
3. Kim, H. J., T. Kobayashi and H. S. Yoon, " Micromechanical Fracture Process of SiC-Particle-Reinforced Aluminum Alloy 6061-T6 Metal Matrix Composites," Materials Science and Engineering, A154, pp. 35-41 (1992).
4. Kamat, S. V., J. P. Hirth and R. Mehrabian, "Mechanical Properties of Particulate Reinforced Aluminum Matrix Composites," Acta Metall., Vol. 37, pp. 2395-2402 (1989).
5. Miller , W. S. and F. J. Humphreys, "Fundamental Relationships Between Microstructure and Mechanical Properties of Metal Matrix Composites," Ed. P. K. Liaw and M. Gungor, TMS, pp.517-41 (1990).
6. Aikin, R. M. and L. Christodoulou, "The Role of Equiaxed Particles on the Yield Stress of Composites," Scripta Metall., Vol. 25, pp. 9-14 (1991).
7. Holcolm, S., "The Effects of Particle Size on High Cycle Fatigue Properties of Silicon Carbide Reinforced 2124 Aluminum," M. S. Thesis, University of Southern California (1992).
8. Lewandowski, J. J., C. Liu and W. H. Hunt, "Effects of Matrix Microstructure and Particle Distribution on Fracture of an Aluminum Metal Matrix Composite," Mat. Sci. and Eng., A107, pp. 241-255 (1989).

9. LLorca, J., A. Martin, J. Ruiz and M. Elices, " Particulate Fracture During Deformation of a Spray Formed Metal Matrix Composite," Submitted to Metall. Trans. (1993).

10. Manoharan, M. and J. J. Lewandowski, " Crack Initiation and Growth Toughness of an Aluminum Metal Matrix Composite," Acta Metall., Vol. 38, pp. 489-96 (1990).

11. Ashby, M. F., "The Deformation of Plastically Non-Homogeneous Alloys," edited by A. Kelly and R. B. Nicholson, Elsevier, Amsterdam, pp. 137-193 (1971).

12. Miller, W. S. and F. J. Humphreys, "Strengthening Mechanisms in Particulate Metal Matrix Composites," Scripta Metall., Vol. 25, pp. 33-38 (1991).

13. Orowan, E., "Symposium on Internal Stresses in Metals and Alloys," p. 451, Institute of Metals (1948).

14. Fisher, J. C., E. W. Hart and R. H. Pry, " The Hardening of Metal Crystals by Precipitate Particles," Acta Metall., Vol. 1, pp. 336-339 (1953).

15. Tanaka, K. and T. Mori, The Hardening of Crystals by Non-Deforming Particles and Fibres," Acta Metall., Vol. 18, pp. 931-41 (1970).

16. Pickard, S. M., and B. Derby, " The Deformation of Particulate Reinforced Metal Matrix Composites During Temperature Cycling," Acta Metall., Vol. 38, pp. 2537-52 (1990).

17. Ruiz, J., J. LLorca and M. Elices, "Influence of the Environment on Fatigue Crack Growth in a SiC Reinforced Al Alloy," to be presented at Fatigue '93 (1993).

18. Hunt, W., J. Brockenbrough and P. Magnusen, "An Al-Si-Mg Composite Model System: Microstructural Effects on Deformation and Damage Evolution," Scripta Metall, Vol. 25, pp. 15-20 (1991).

19. Brechet, Y., J. D. Embury, S. Tao and L. Luo, "Damage Initiation in Metal Matrix Composites," Acta Metall., Vol. 39, pp. 1781-1786 (1991).

20. Lewandowski, J., D. Liu and C. Liu, "Observations on the Effects of Particulate Size and Superposed Pressure on Deformation of Metal Matrix Composites," Scripta Metall, Vol. 25, pp. 21-26 (1991).

21. Lloyd, D. J., "Aspects of Fracture in Particulate Reinforced Metal Matrix Composites," Acta Metall., Vol. 39, pp. 59-71 (1991).

22. Karayaka, M., and H. Sehitoglu, "Thermo-mechanical Fatigue of Al-SiCp Composites," Fatigue 90 (1990).

23. Sehitoglu, H. and M. Karayaka, "Prediction of Thermomechanical Fatigue Lives in Metal Matrix Composites," Metall. Trans., Vol. 23A, pp. 2029-2038 (1992).

24. Hall, J., J. W. Jones and A. Sachdev, submitted to Materials Sci. and Eng. (1992).

25. Bonnen, J. J., J. E. Allison, and J. W. Jones, "Fatigue Behavior of a 2XXX Series Aluminum Alloy Reinforced with 15 Vol Pct SiCp," Metall. Trans., Vol. 22A, pp. 1007-19 (1991).

26. Shang, J. K, and R. O. Ritchie, " On the Particle Size Dependence of Fatigue Crack Propagation Thresholds in Particulate Reinforced Aluminum Alloy Composites: Role of Crack Closure and Crack Trapping," Acta Metall., Vol. 37, pp. 2267-78 (1989).

APPENDIX A. Isothermal Fatigue Data

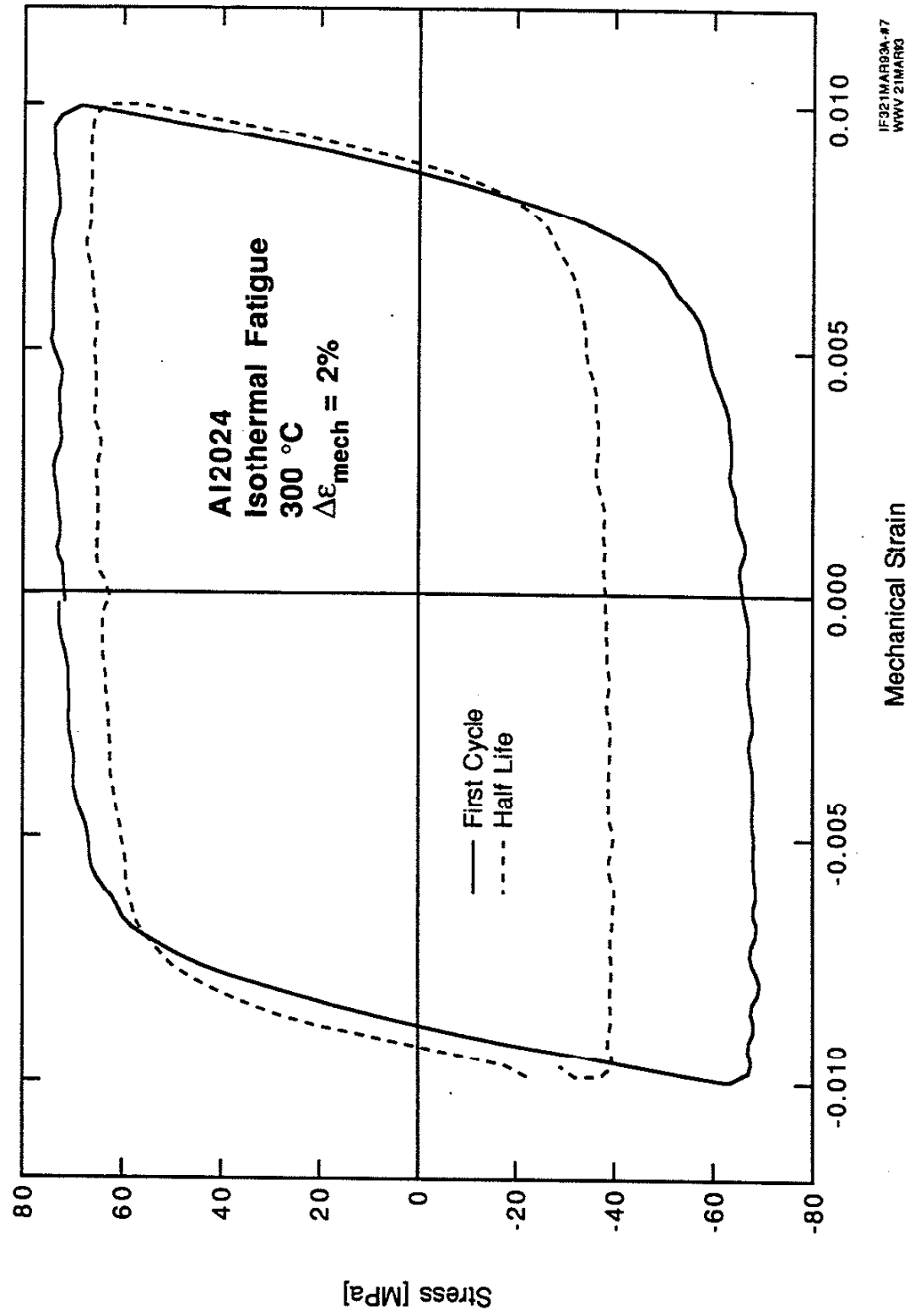

Figure A.1: Isothermal fatigue stress-strain response of Al2024

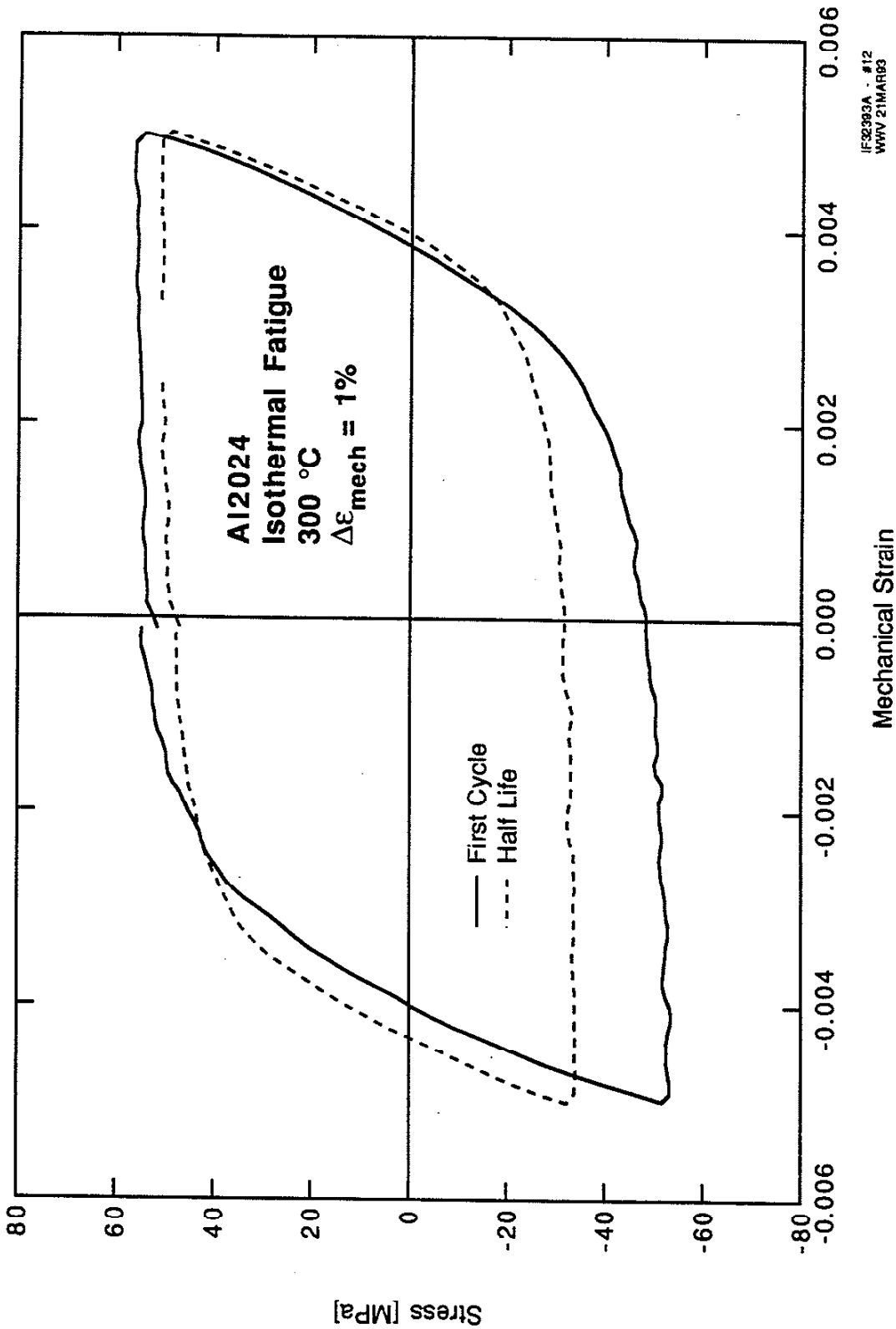

Figure A.2: Isothermal fatigue stress-strain response of Al2024

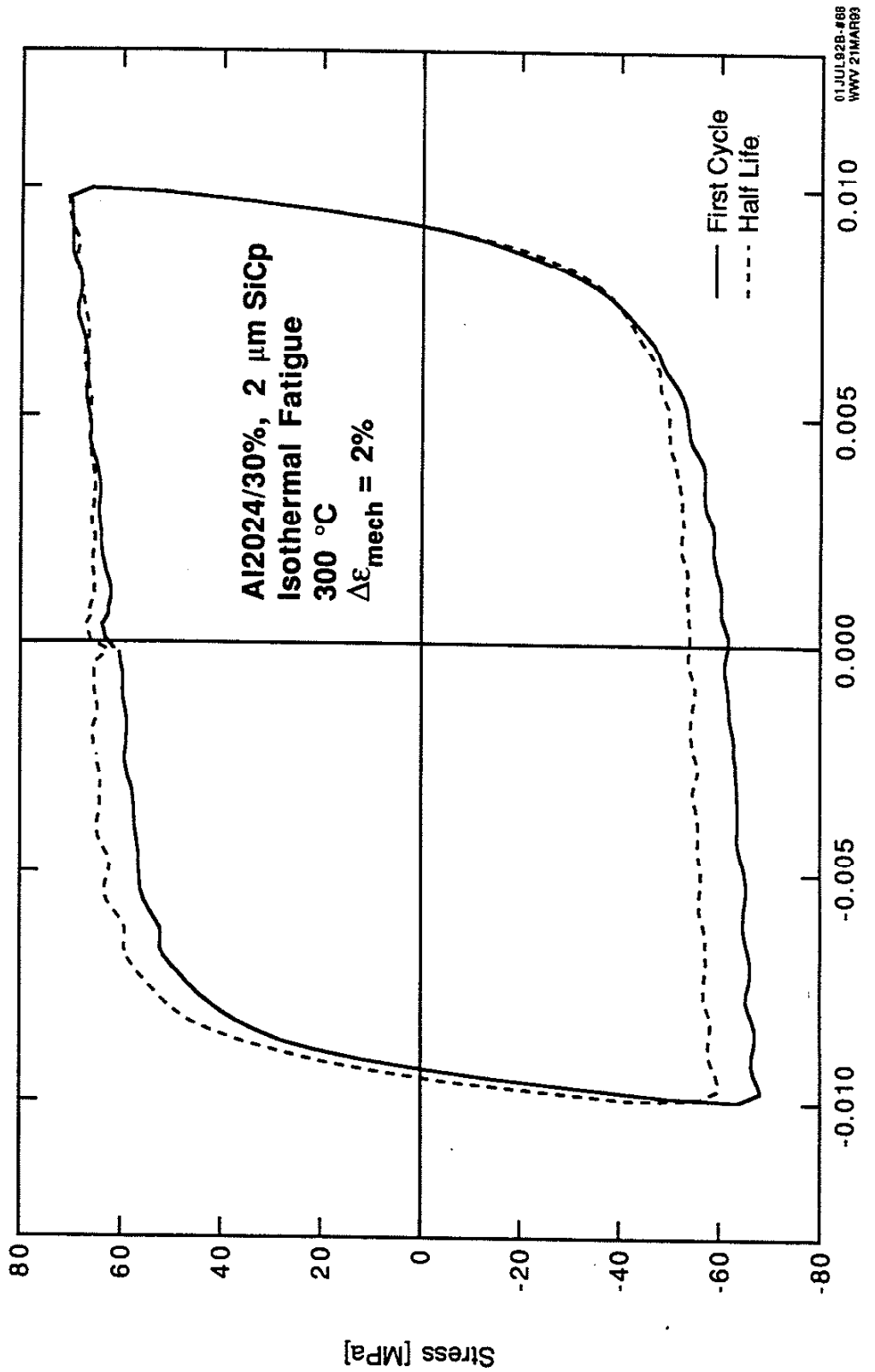

Figure A.3: Isothermal fatigue stress-strain response of Al2024/30%, 2 μm SiCp

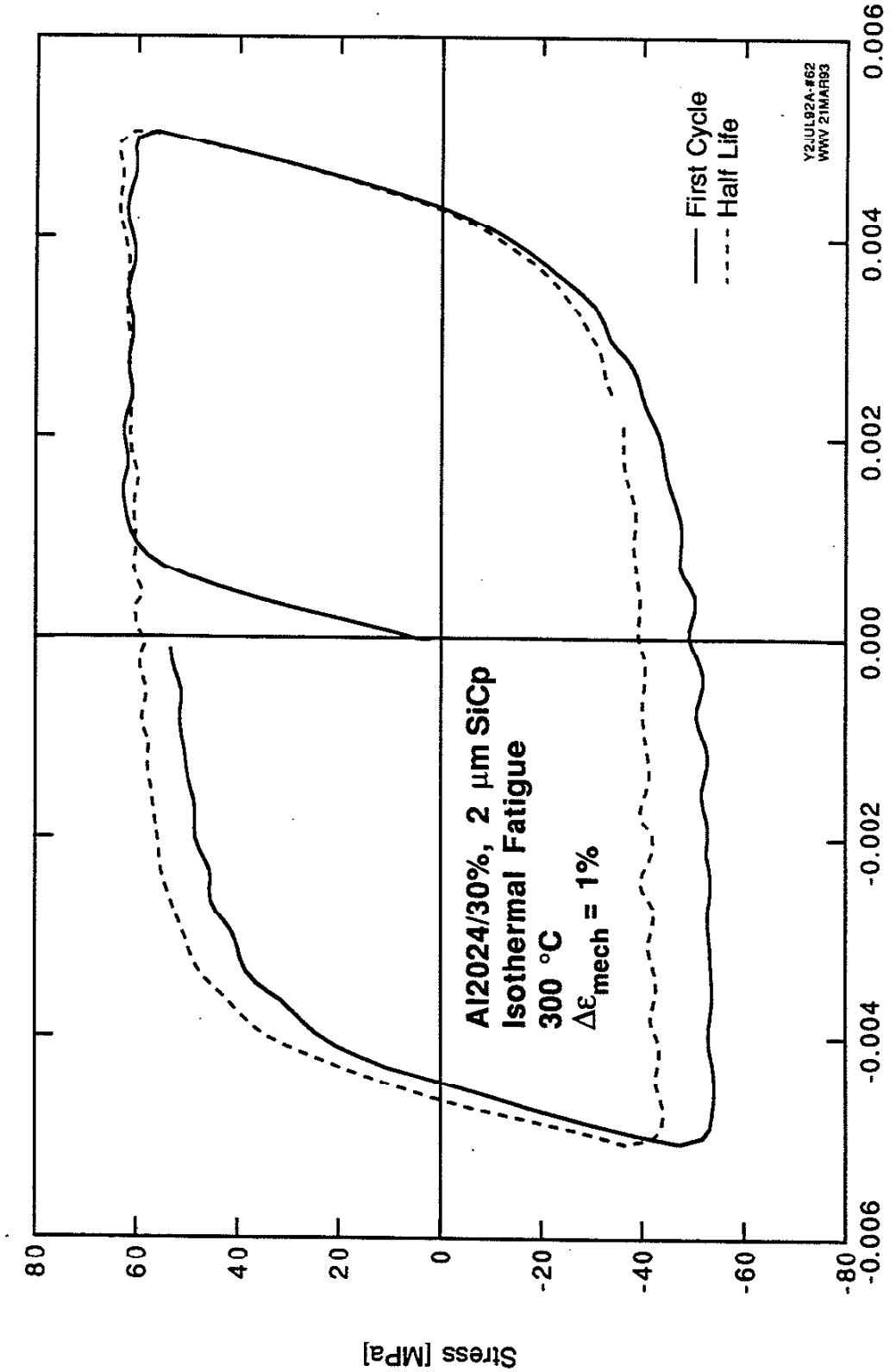

Figure A.4: Isothermal fatigue stress-strain response of Al2024/30%, 2 μm SiCp

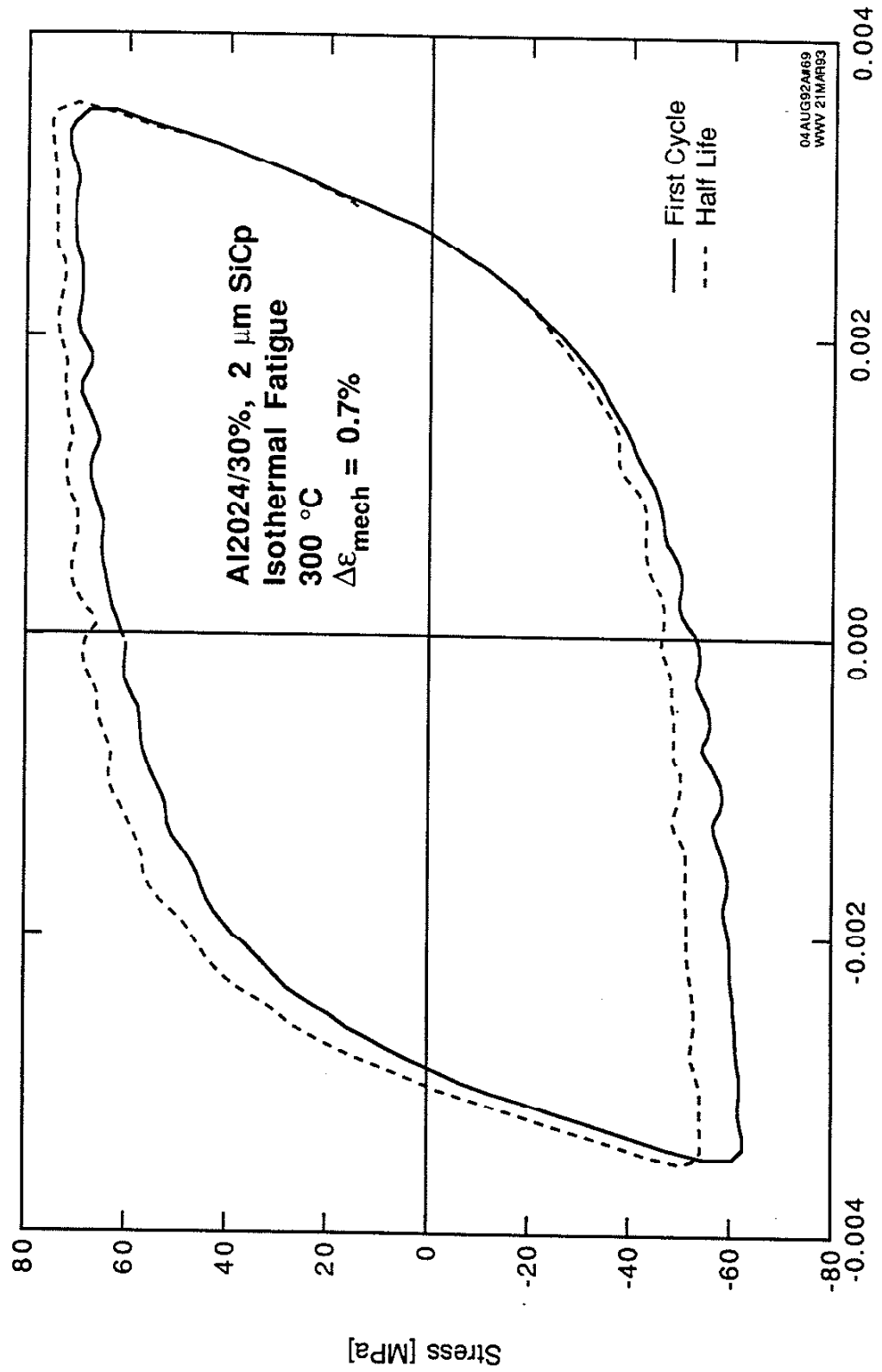

Figure A.5: Isothermal fatigue stress-strain response of Al2024/30%, 2 μm SiCp

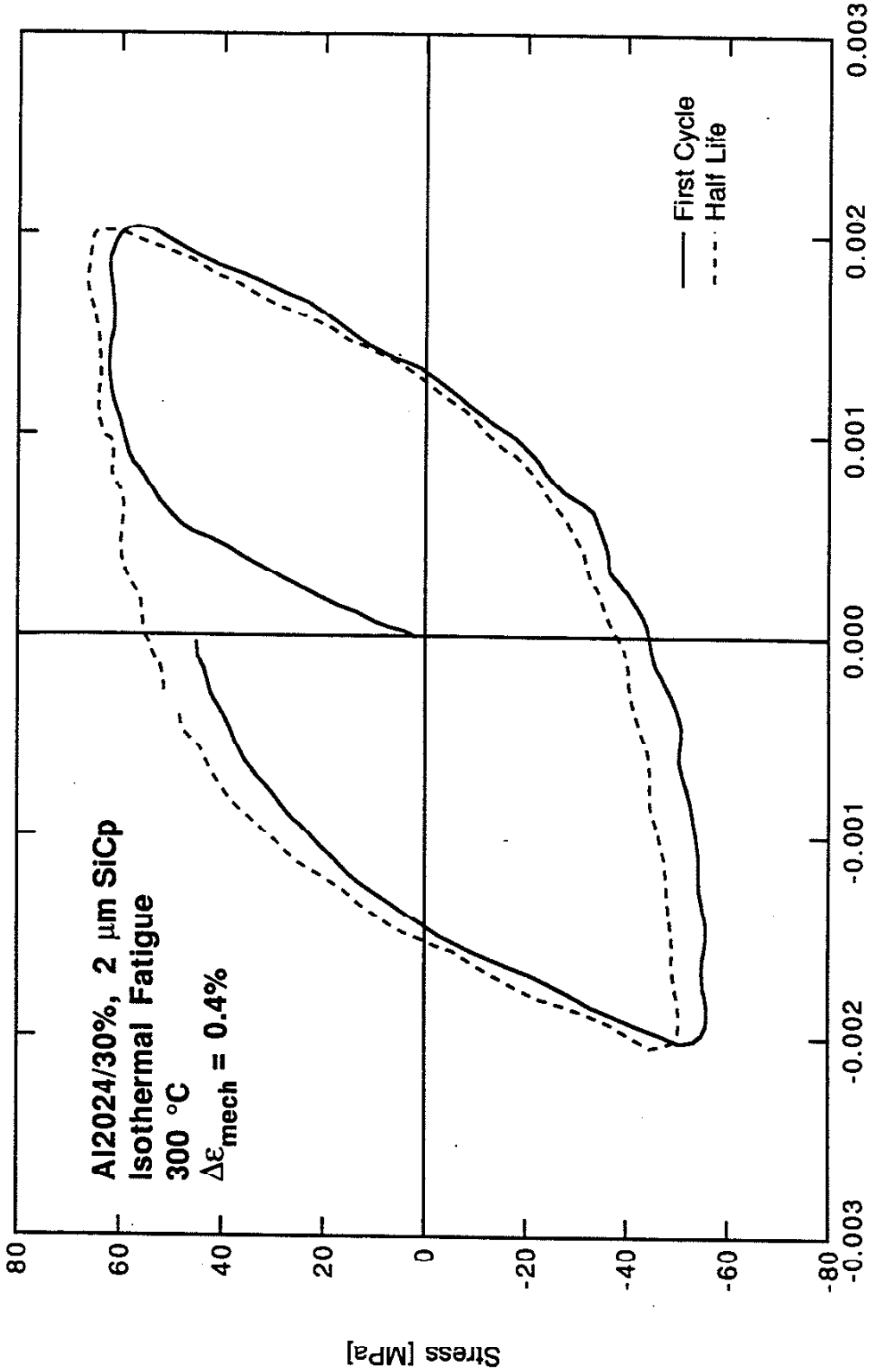

Figure A.6: Isothermal fatigue stress-strain behavior of Al2024/30%, 2 μm SiCp

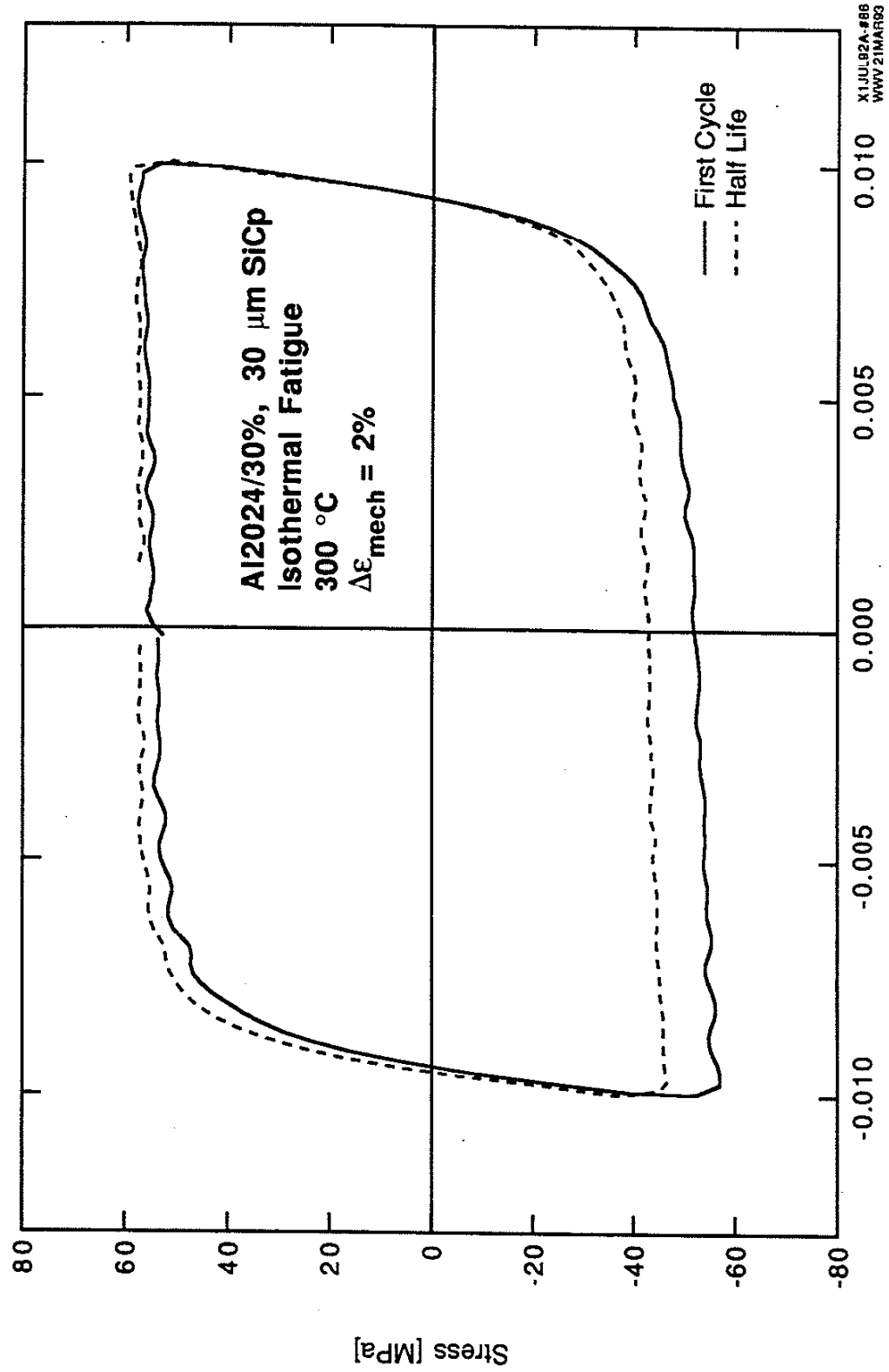

Figure A.7: Isothermal fatigue stress-strain behavior of Al2024/30%, 30 μm SiCp

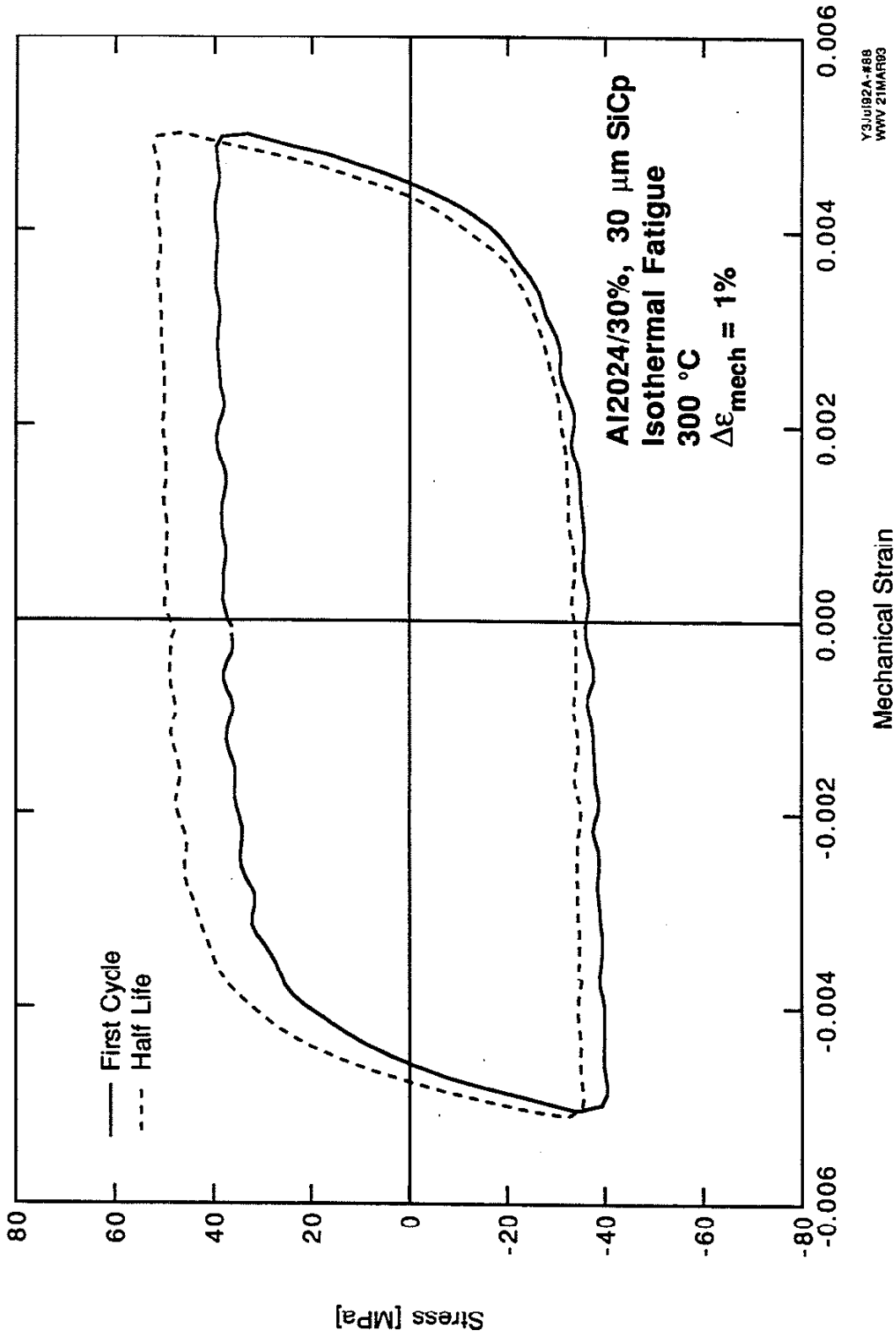

Figure A.8: Isothermal fatigue stress-strain behavior of Al2024/30%, 30 μm SiCp

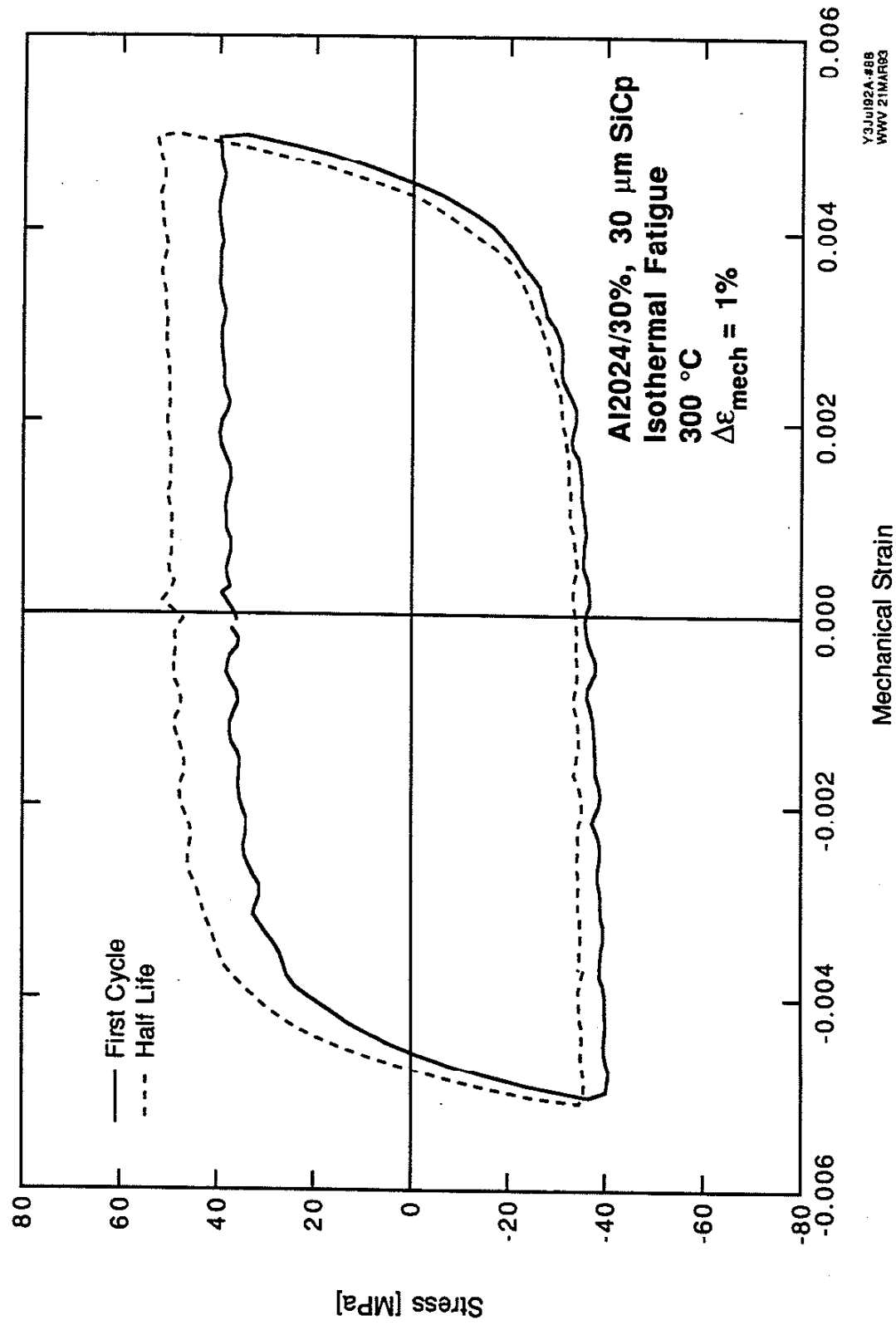

Figure A.9: Isothermal fatigue stress-strain behavior of Al2024/30%, 30 μm SiCp

APPENDIX B. Thermomechanical Fatigue Data

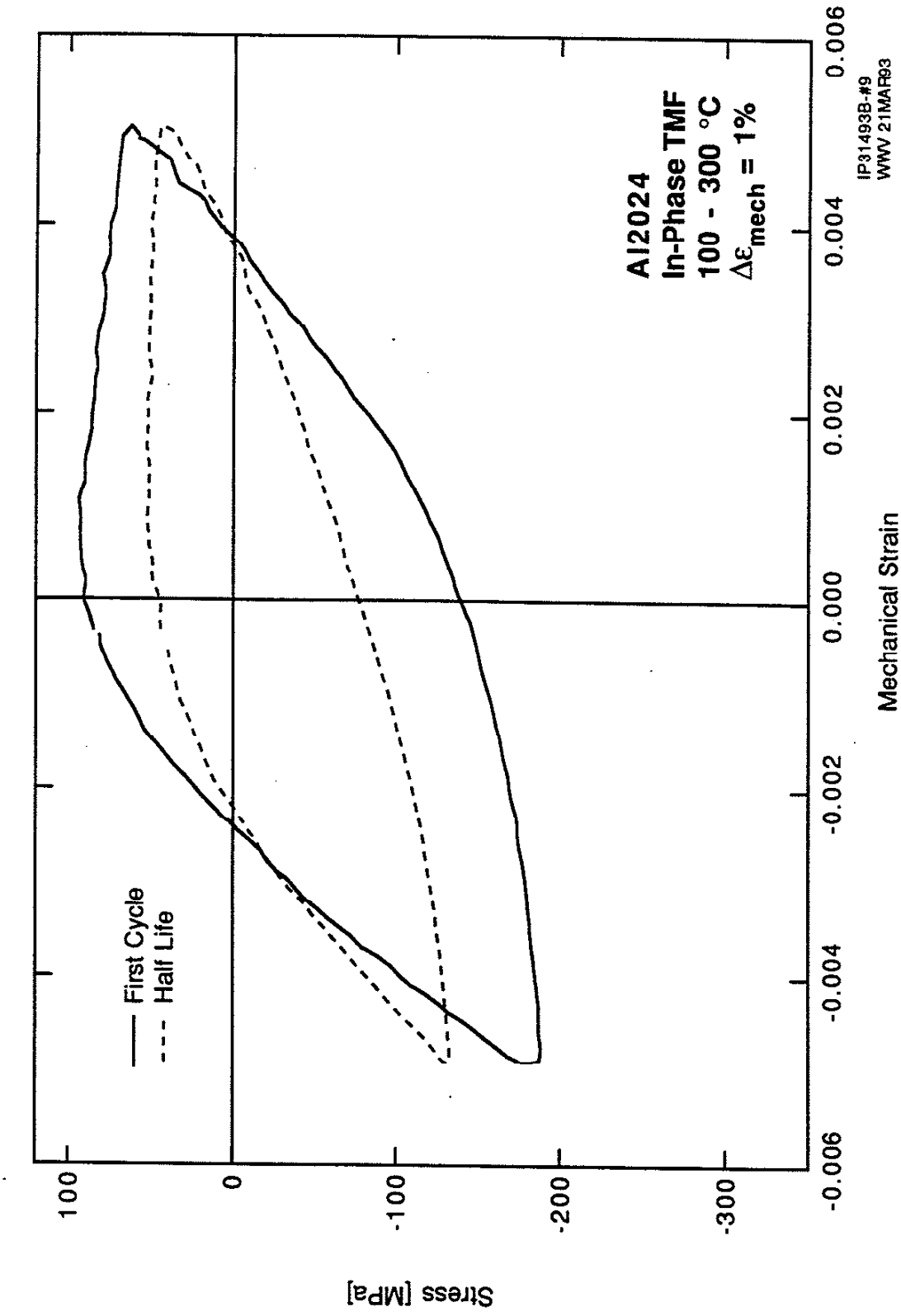

Figure B.1: In-Phase TMF stress-strain behavior of Al2024

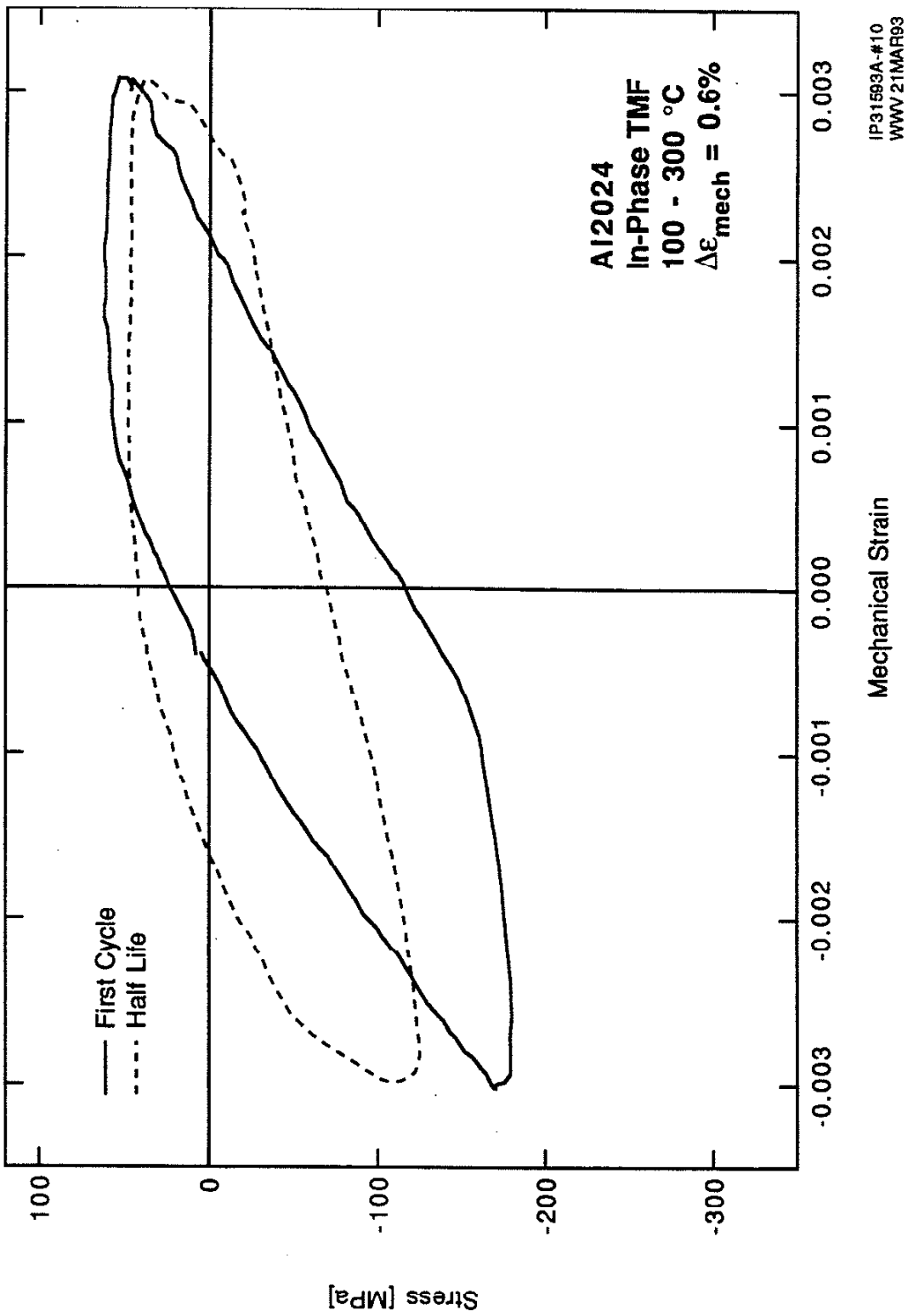

Figure B.2: In-Phase TMF stress-strain behavior of Al2024

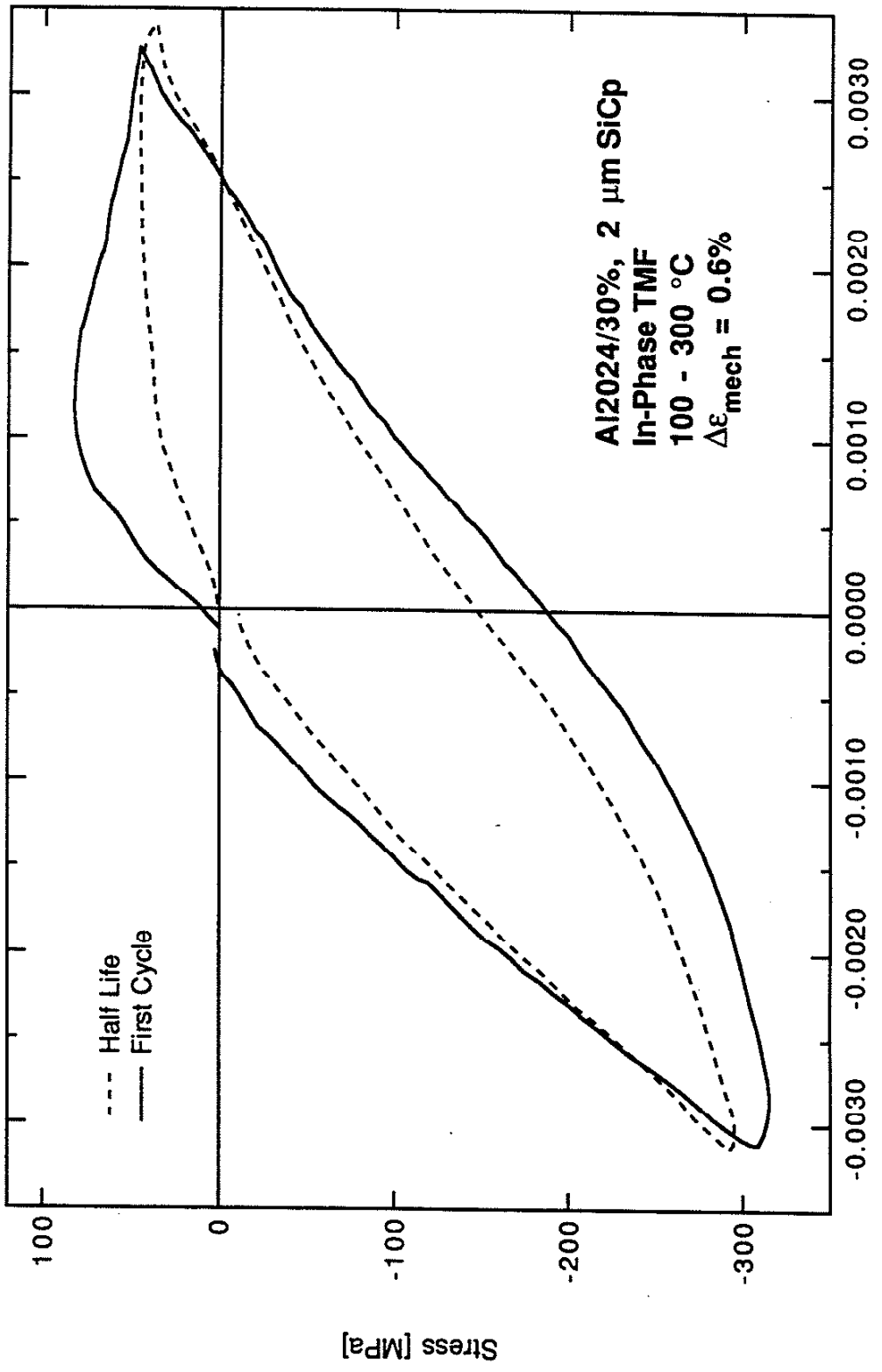

Figure B.3: In-Phase TMF stress-strain behavior of Al2024/30%, 2 μm SiCp

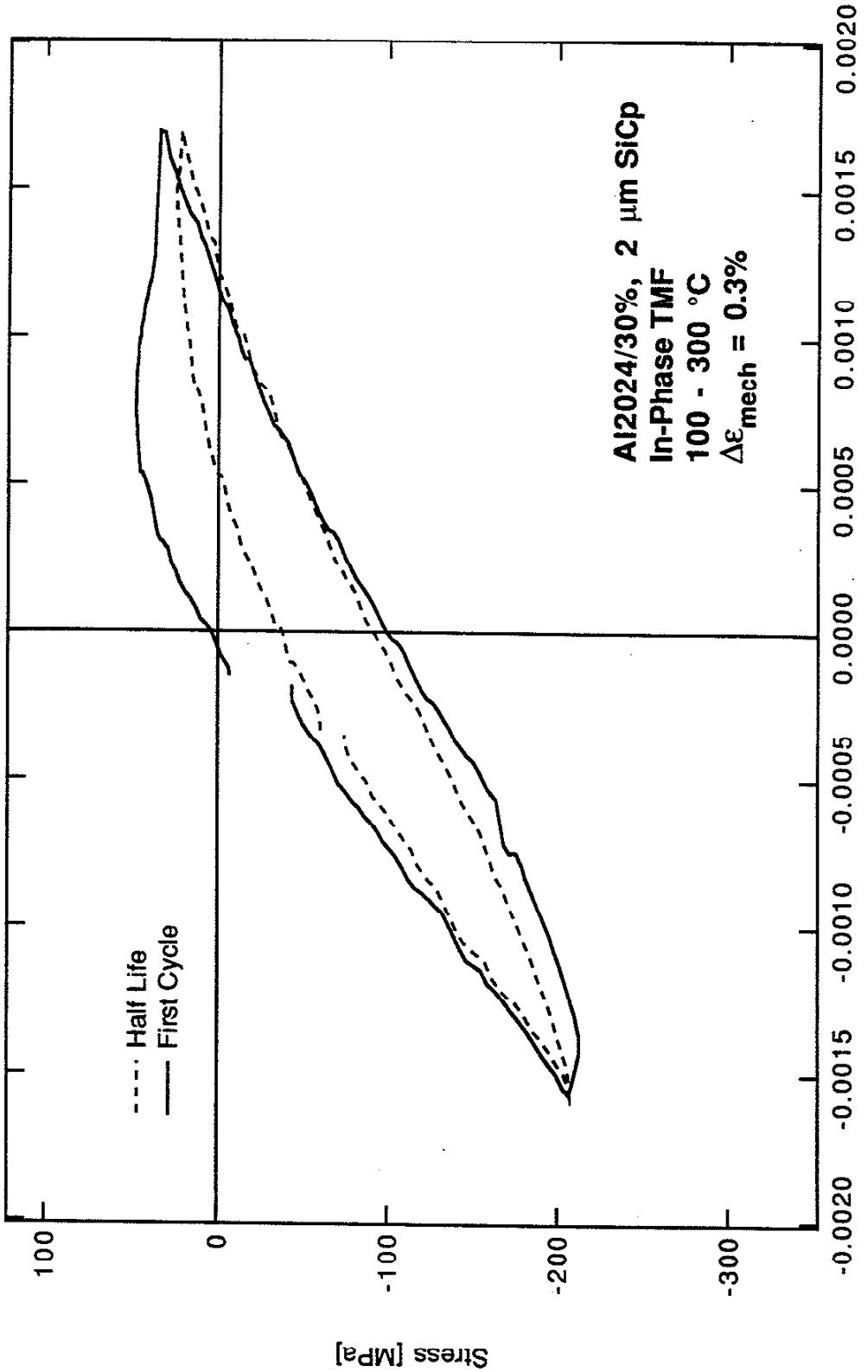

Figure B.4: In-Phase TMF stress-strain behavior of Al2024/30%, 2 μm SiCp

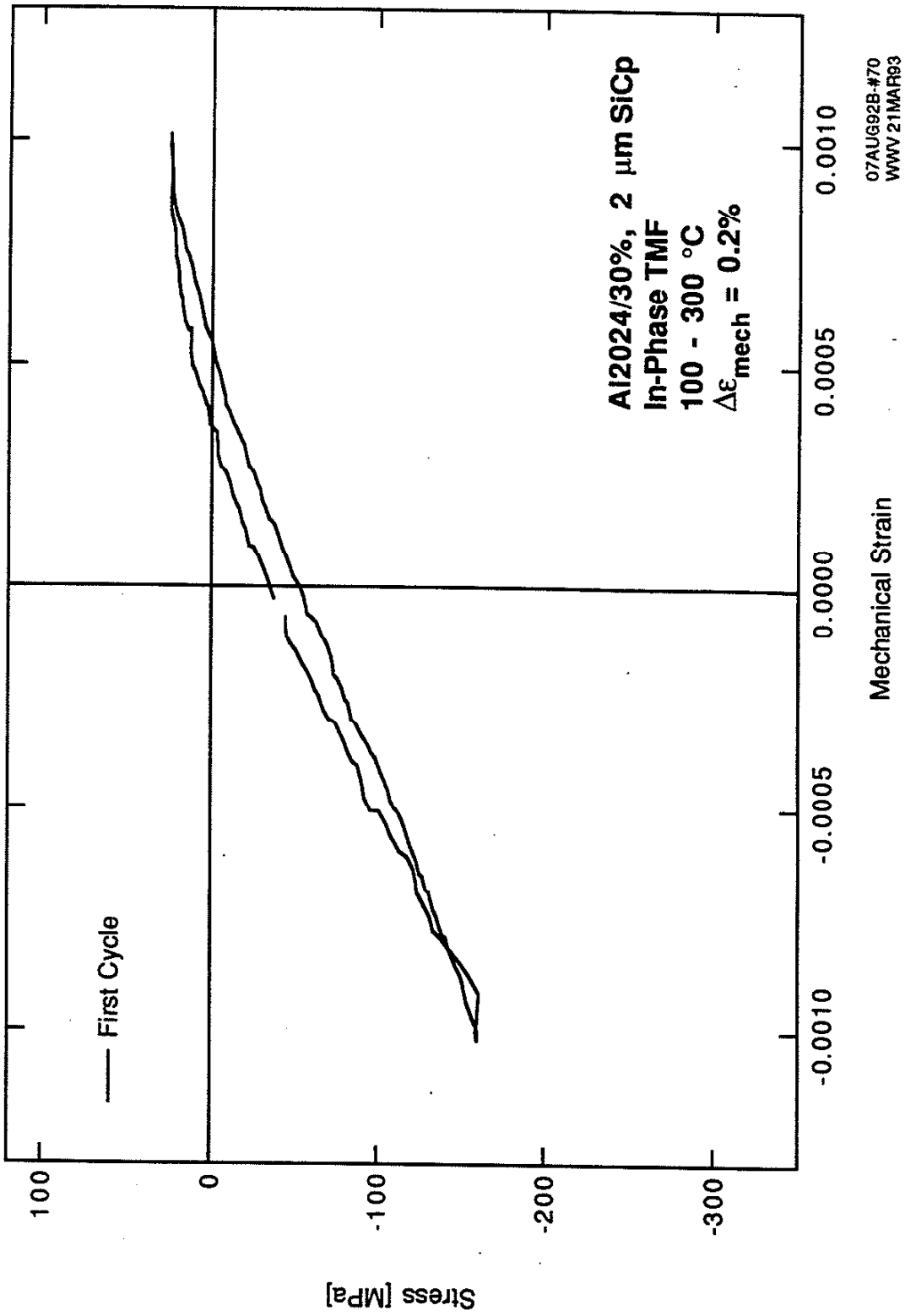

Figure B.5: In-Phase TMF stress-strain behavior of Al2024/30%, 2 μm SiCp

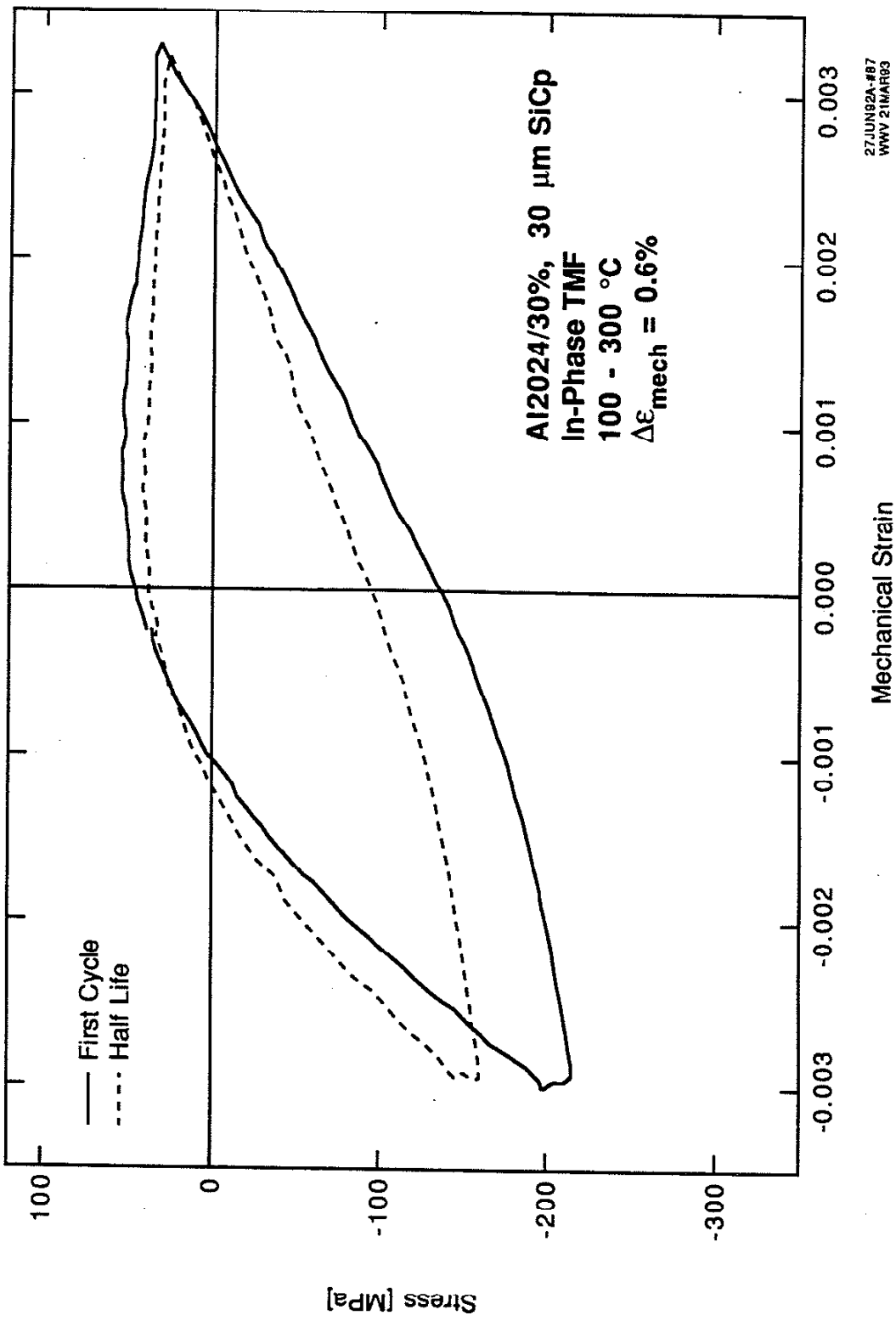

Figure B.6: In-Phase TMF stress-strain behavior of Al2024/30%, 30 μm SiCp

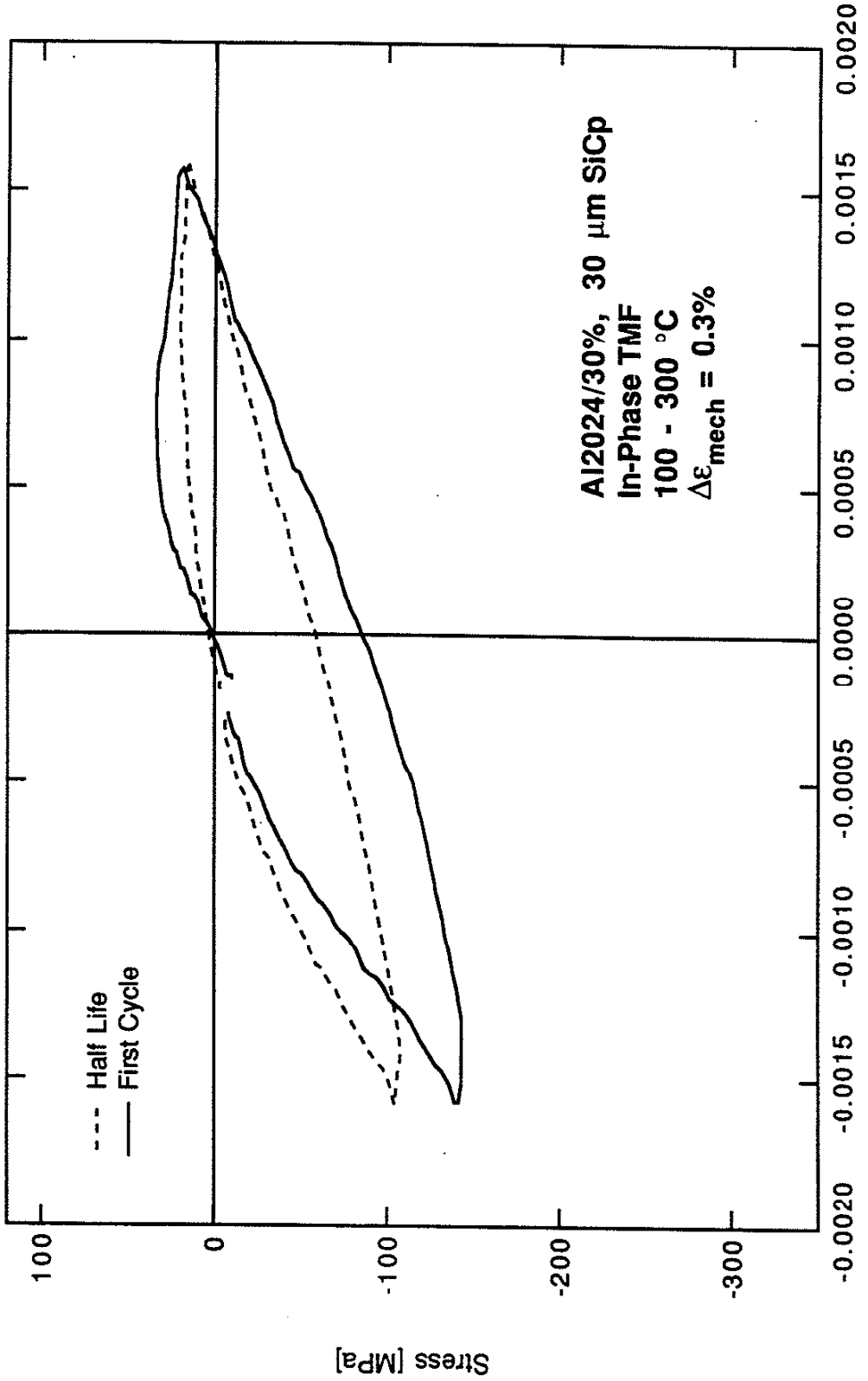

Figure B.7: In-Phase TMF stress-strain behavior of Al2024/30%, 30 μm SiCp

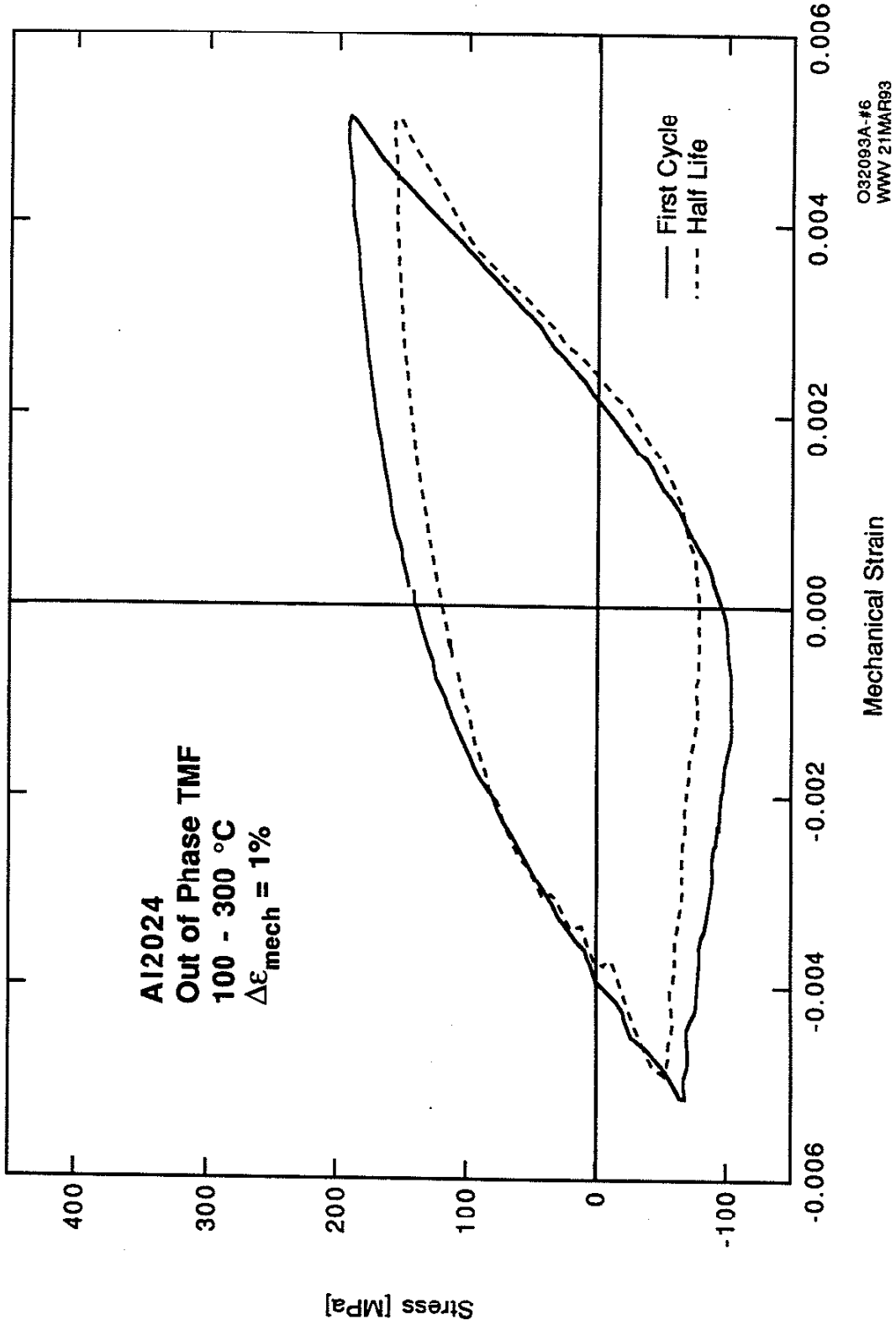

Figure B.8: Out-of-Phase TMF stress-strain behavior of Al2024

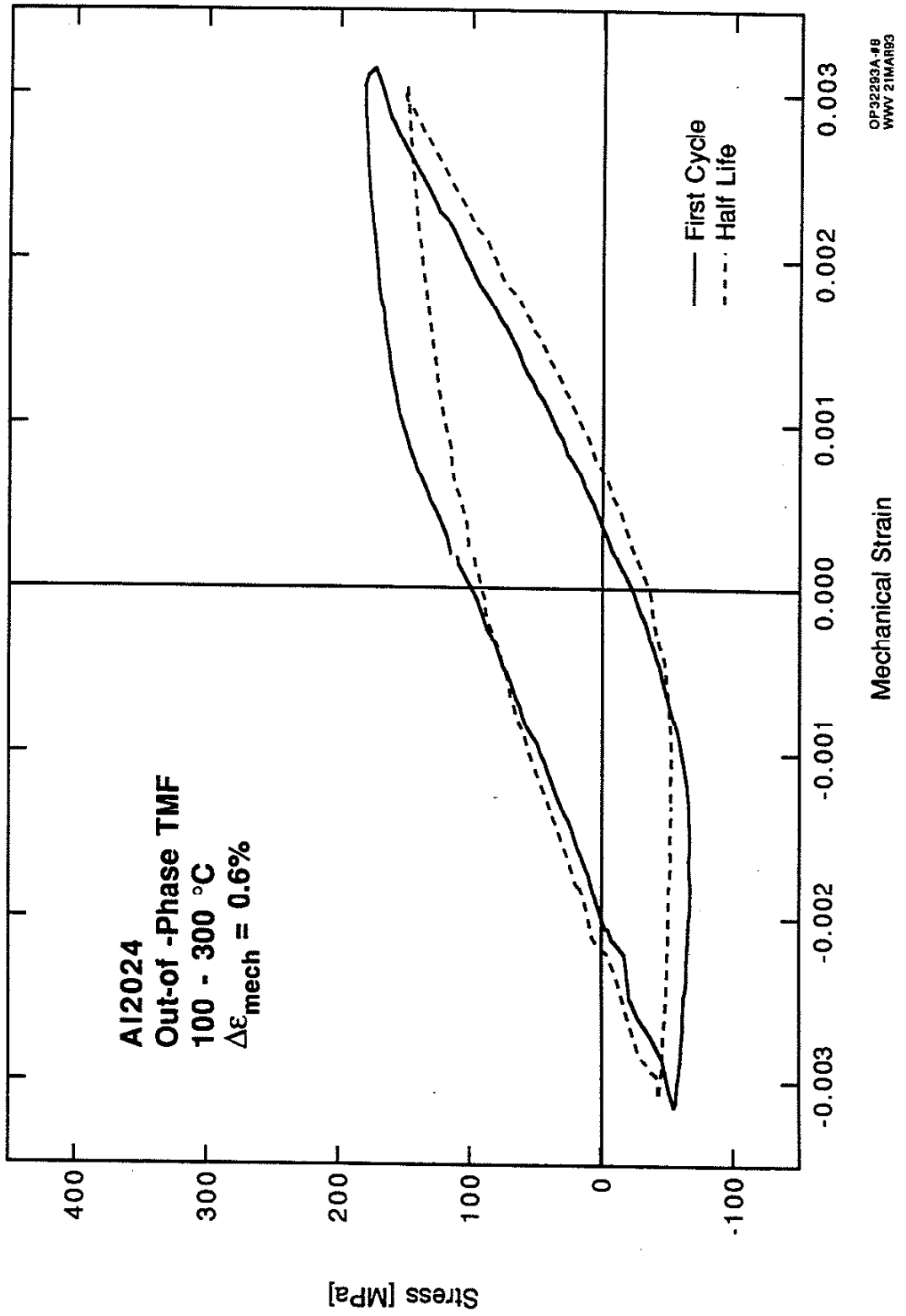

Figure B.9: Out-of-Phase TMF stress-strain behavior of Al2024

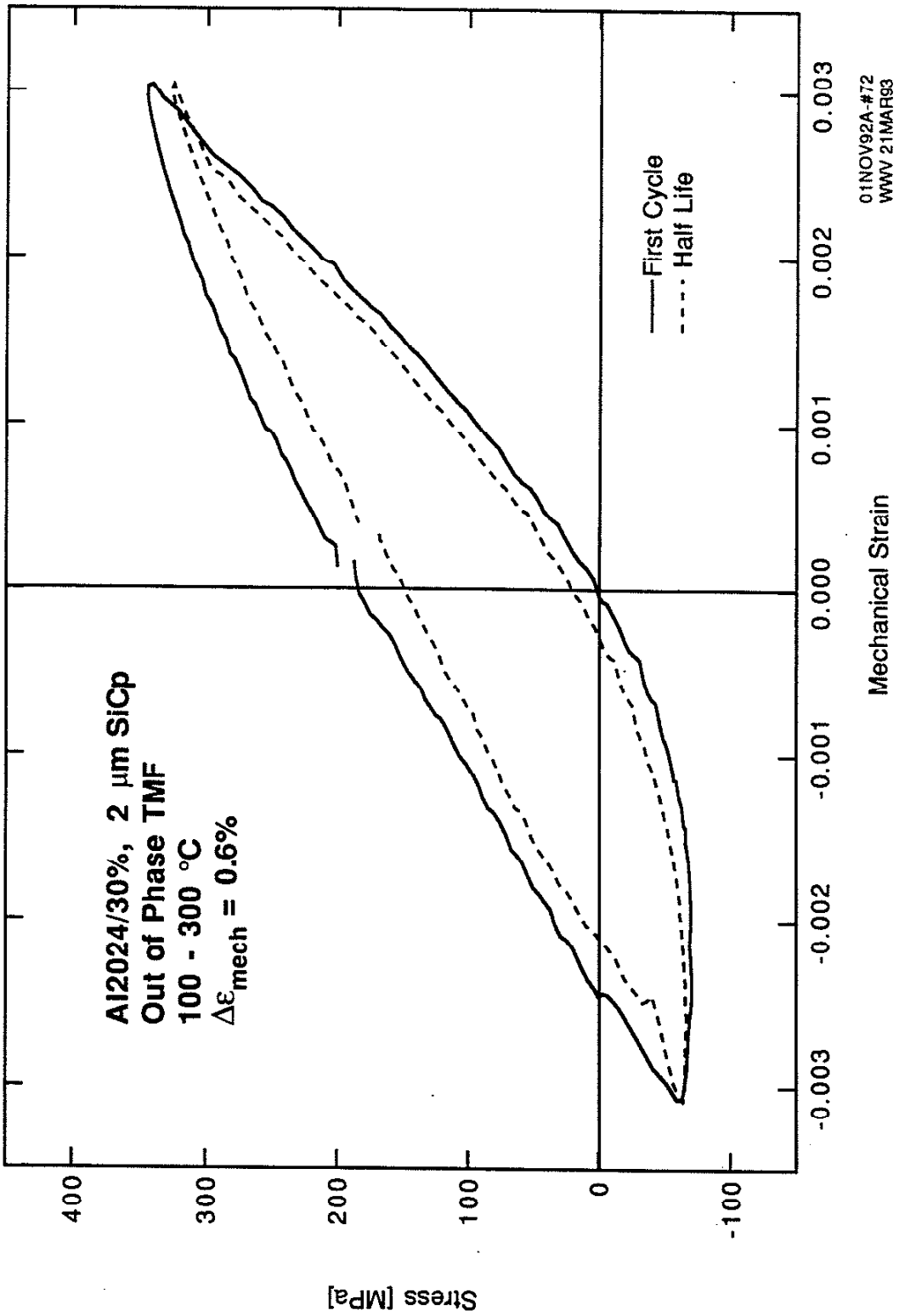

Figure B.10: Out-of-Phase TMF stress-strain behavior of Al2024/30%, 2 μm SiCp

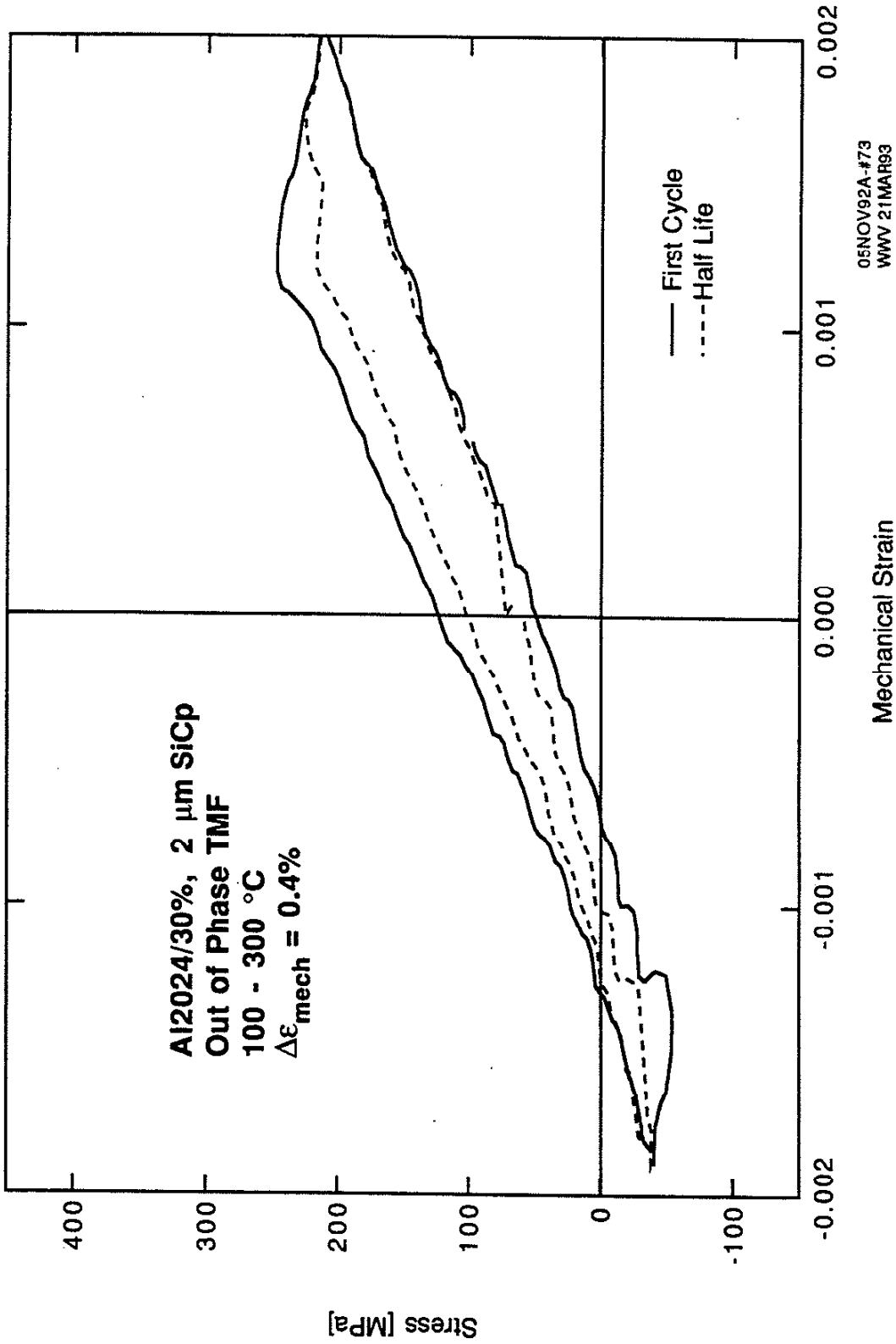

Figure B.11: Out-of-Phase TMF stress-strain behavior of Al2024/30%, 2 µm SiCp

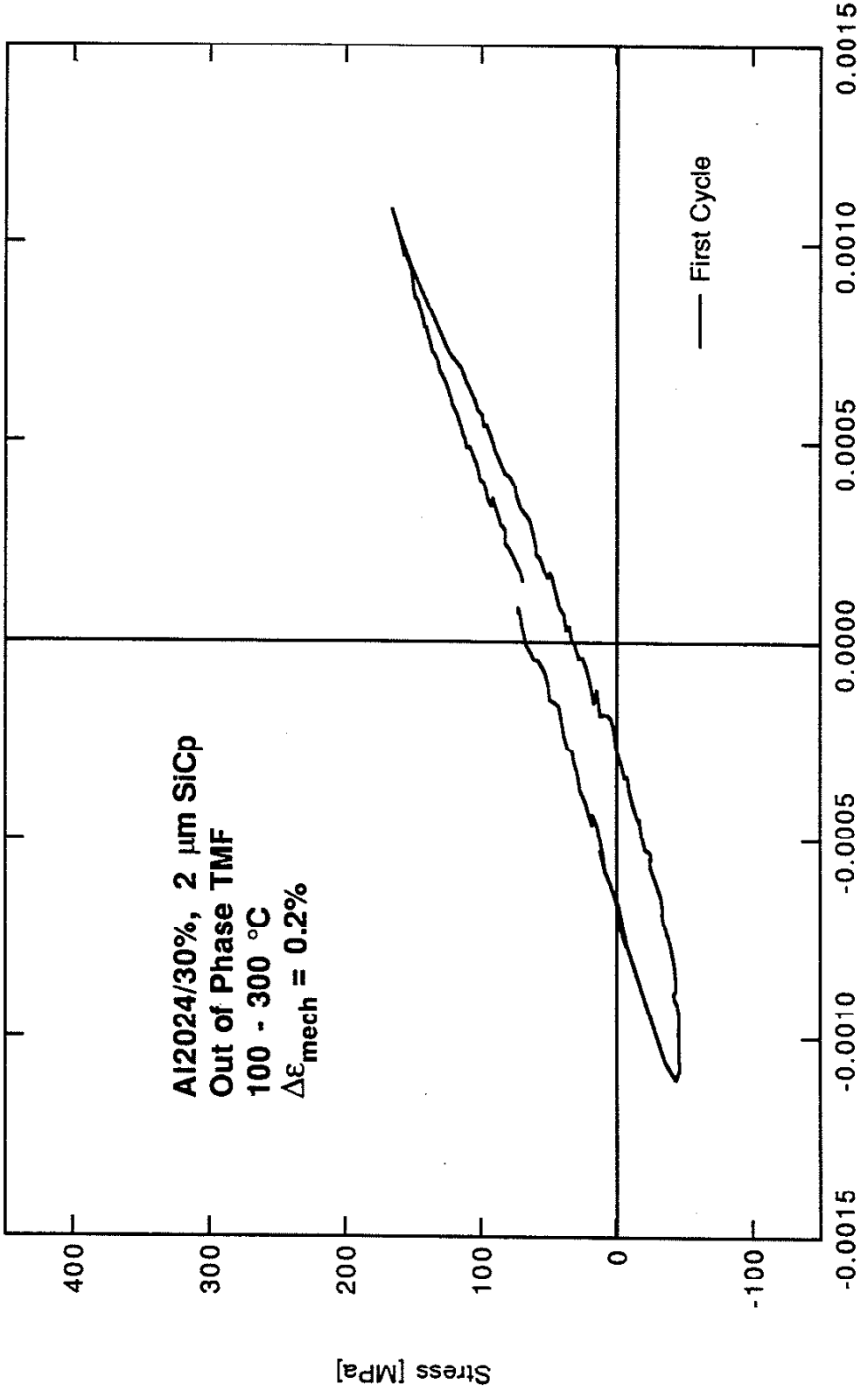

Figure B.12: Out-of-Phase TMF stress-strain behavior of Al2024/30%, 2 μm SiCp

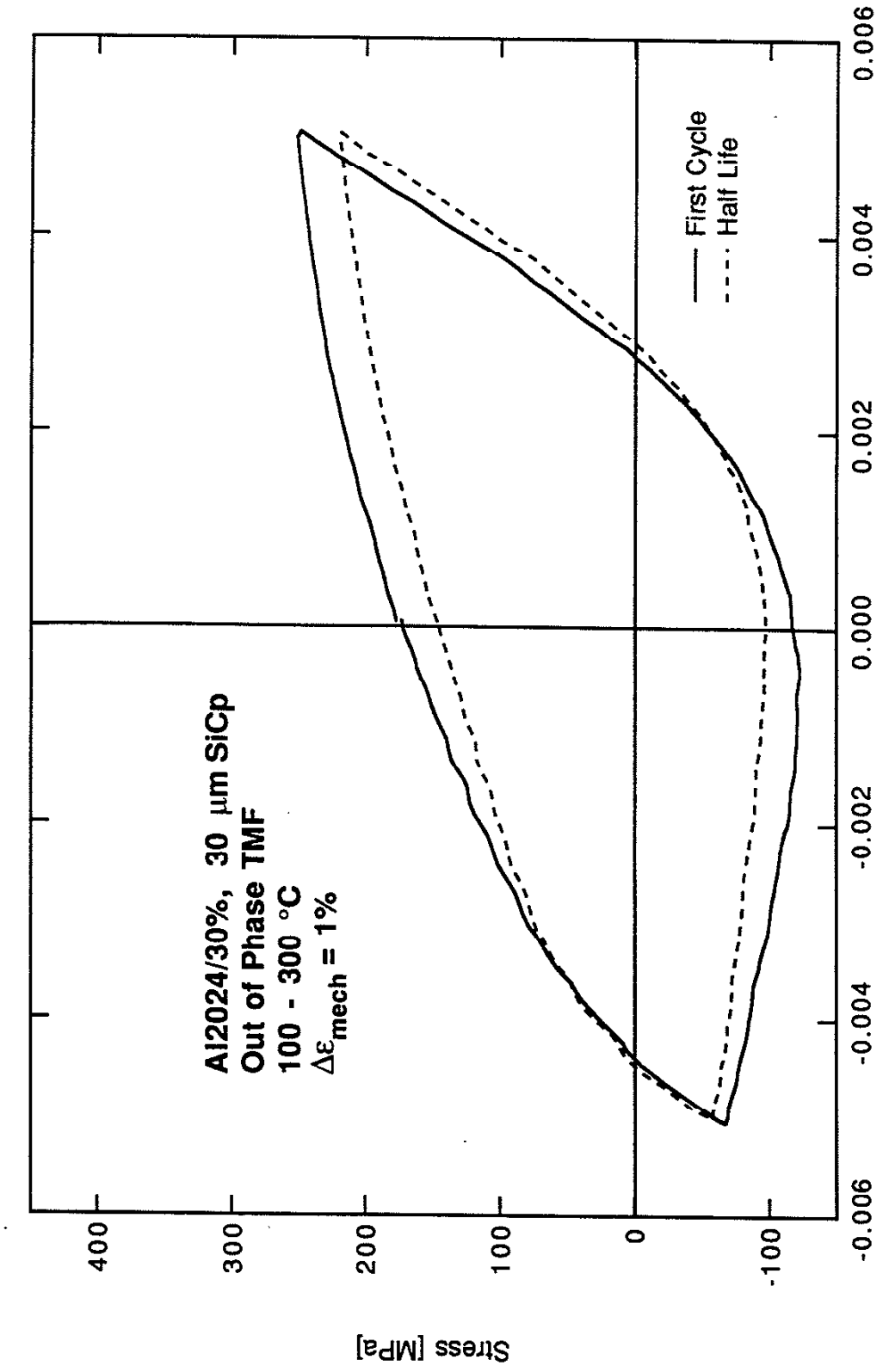

Figure B.13: Out-of-Phase TMF stress-strain behavior of Al2024/30%, 30 μm SiCp

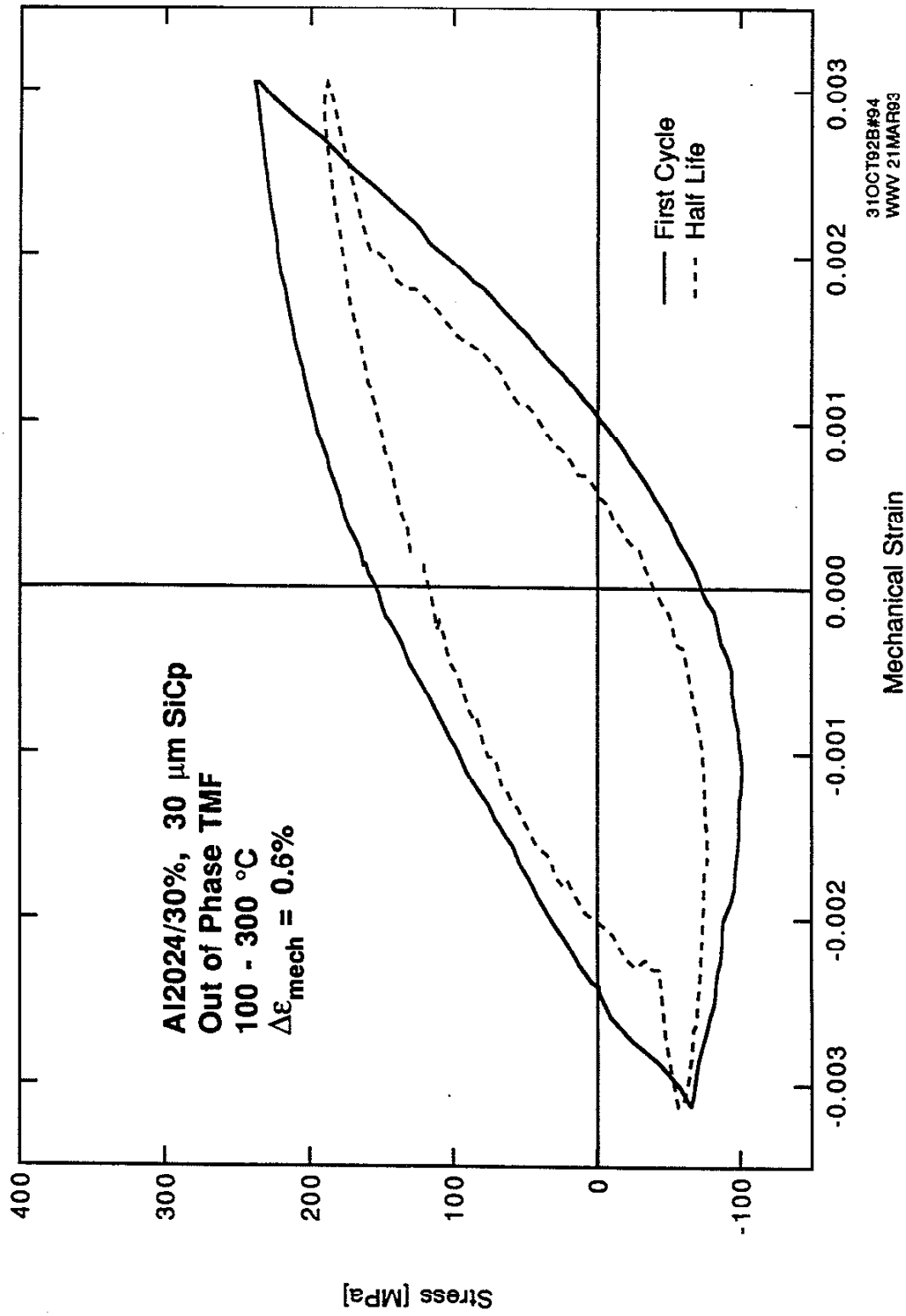

Figure B.14: Out-of-Phase TMF stress-strain behavior of Al2024/30%, 30 μm SiCp

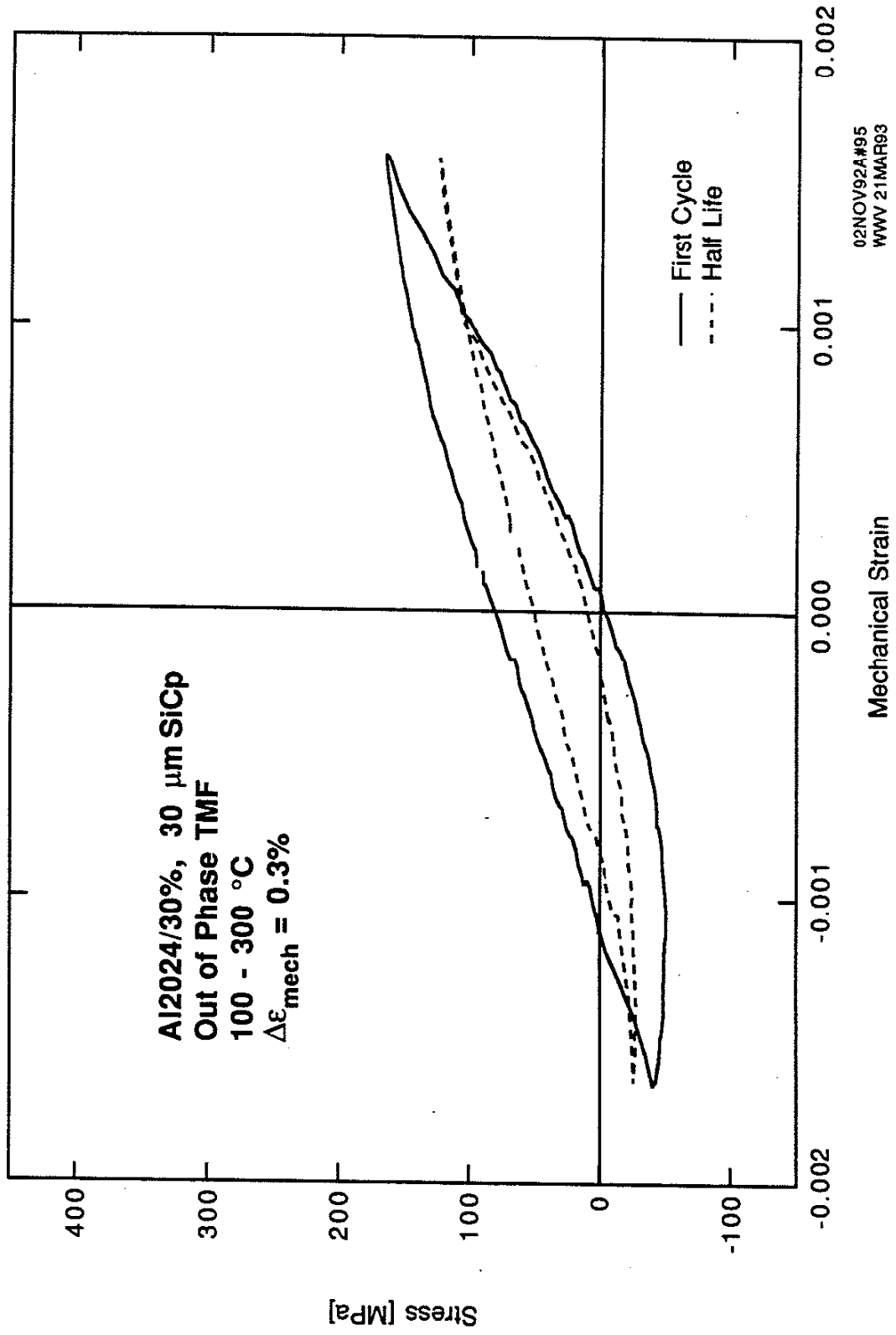

Figure B.15: Out-of-Phase TMF stress-strain behavior of Al2024/30%, 30 μm SiCp